Tetrazole-containing STAT5 Inhibitors Derived from Furazan-based Phosphate Mimetics

Inaugural-Dissertation

to obtain the academic degree

Doctor rerum naturalium (Dr. rer. nat.)

submitted to the Department of Biology, Chemistry, Pharmacy

of Freie Universität Berlin

by

XINNING WANG

2020

Declaration

I hereby declare that I have completed the present work myself and have used no tools other than those listed here.

The doctorate project was conducted from November 2015 until November 2019 under the supervision of Prof. Dr. Jörg Rademann at the Institute of Pharmacy of the Freie Universität Berlin.

1st Reviewer: Prof. Dr. Jörg Rademann

2nd Reviewer: Prof. Dr. Gerhard Wolber

Date of defense: 06.07.2020

Acknowledgements

I would like to express my sincere gratitude to my supervisor, Prof. Dr. Jörg Rademann, for providing me this opportunity to conduct doctoral study in his research group. Without his patient guidance and continuous encouragement, this work would not have been possible. I also want to thank Prof. Dr. Gerhard Wolber for accepting the request to be the 2nd reviewer of this dissertation and the discussion about docking results.

My sincere thanks also go to Dr. Christoph Arkona for protein expression and purification, to Dr. Ee Lin Wong for the assistance in binding assays and cellular assays, to Matteo Accorsi for peptide synthesis, to Silke Bergemann for supporting cellular assays, and to Lihua Deng for docking suggestions.

I acknowledge all the former and current members of the Rademann group, with whom I shared great time during and after work, in particular Dr. Christina Fischer, Damian Klemczak, Dr. Mike Jaegle, Rebekka Wamser, Dr. Sebastian Köhling, and Yuwen Jia.

I thank all my friends who enriched my life through the years.

Finally, I would like to express my deepest gratitude to my loving family. I thank my parents, my grandparents, and my uncle's family for their selfless support over the years. I especially thank my wife Lina for the love she keeps giving me.

Table of Contents

iii

List of Abbreviations

ABL	Abelson murine leukemia viral oncogene homolog 1
AcOH	acetic acid
AML	acute myeloid leukemia
Ar	aromatic ring
BCR	breakpoint cluster region protein
Bn	benzyl
CML	chronic myeloid leukemia
d	doublet
DAD	diode array detector
DIC	N,N'-diisopropylcarbodiimide
DCM	dichloromethane
DIPEA	N,N-diisopropylethylamine
DMF	dimethylformamide
DMSO	dimethyl sulfoxide
EDTA	ethylenediaminetetraacetic acid
eq	equivalent

ESI	electrospray ionization
FLT3	FMS-like tyrosine kinase 3
Fmoc	9-fluorenylmethoxycarbonyl
FP	fluorescence polarization
HEPES	2-(4-(2-hydroxyethyl)piperazin-1-yl)ethanesulfonic acid
HOBt	hydroxybenzotriazole
HPLC	high-performance liquid chromatography
HRMS	high-resolution mass spectrometry
ITD	internal tandem duplication
JAK	Janus kinase
LC-MS	liquid chromatography–mass spectrometry
m	multiplet
mAU	milli-absorbance units
mP	milli-polarization
MBP	maltose-binding protein
MeCN	acetonitrile
MOPS	3-(N-morpholino)propanesulfonic acid
MPLC	medium pressure liquid chromatography
MV	microwave
NMR	nuclear magnetic resonance
O/N	overnight
PCR	polymerase chain reaction

PDB	protein data bank
Ph	phenyl
py	pyridine
pY	phosphotyrosine
q	quartet
QTOF	quadrupole time-of-flight
RFU	relative fluorescence units
RT	room temperature
s	singlet
SH2	src homology 2
STAT	**s**ignal transducer and activator of transcription
t	triplet
TBTU	*O*-(benzotriazol-1-yl)-*N*,*N*,*N*',*N*'-tetramethyluronium tetrafluoroborate
TFA	trifluoroacetic acid
THF	tetrahydrofuran
TLC	thin-layer chromatography
Tm	melting temperature
TSA	thermal shift assay
UV	ultraviolet

Abstract

Signal transducers and activators of transcription (STAT) are a family of proteins that regulate gene transcription. Seven members (STAT1, STAT2, STAT3, STAT4, STAT5a, STAT5b, STAT6) have been identified in human STAT family since two decades ago. As a member of the STAT family, STAT5 plays a central role in transmitting signals from transmembrane receptors such as cytokine receptors and growth factor receptors to the nucleus. It has been found that STAT5 is constitutively phosphorylated at a conserved tyrosine residue located at the end of SH2 domain by various activated tyrosine kinases in a broad range of human cancer cells. Inhibiting STAT5 has been considered as a promising approach for cancer therapy. However, STATs have been described as difficult pharmacological targets and small-molecule inhibitors of STAT5 are poorly investigated.

The subject of this work is the investigation of small-molecule inhibitors targeting STAT5b-SH2. The tetrazole-containing active compounds discovered in this work are derived from the furazan-based phosphate mimetics. In the first section of this work, a structurally stable scaffold was designed. The aim is to improve the binding affinity of the existing inhibitors and to avoid the instability. For this purpose, four different methods were tried to synthesize the new structures. The main problem, low reactivity of the amino group in fragment **1** in the formation of a linkage between the furazan ring and the 5-position in the tetrazole ring, was solved in the *N*-cyanomethyl amine synthetic method. The obtained compounds showed expected

stability under acidic conditions. However, these compounds were surprisingly inactive in a FP binding assay.

In the second section of this work, a series of 1-aminomethyl tetrazoles based on the structures with different substituents at the 5-position of the tetrazole ring was synthesized via Mannich ligation reaction. Most of them displayed binding affinity to STAT5b-SH2 in low micromolar range in the FP-based competitive binding assay, in which compound **24** was the most active one with a K_i value of 1.8 μM. To investigate how different substituents at the 5-position of the tetrazole ring influence the stability of the scaffold, a systematic stability analysis was carried out on LC-MS and compounds **19**, **22**, **24**, and **25** were found to possess better stability in contrast with the lead compounds **2** and **3**. Furthermore, the binding of compound **24** to STAT5b-SH2 and the pivotal role of Asn642 were proven in the binding assays. Finally, the inhibitory activity of compounds **3** and **24** on leukemic cell proliferation was determined by the Alamar Blue assay.

I. General Part

1. Introduction

1.1. STAT5 protein

Signal transducers and activators of transcription (STAT) are a family of proteins that regulate gene transcription. They were first identified over two decades ago as transcription factors in the context of interferon signaling[1-3]. There are seven members (STAT1, STAT2, STAT3, STAT4, STAT5a, STAT5b, STAT6) in the human STAT family that have been identified. In cytoplasm these proteins play a role as cytosolic signaling proteins while in the nucleus they mediate expression of genes regarding proliferation, apoptosis, differentiation and inflammation[4-6]. STAT proteins have essential roles in a variety of human cells, particularly in immune and blood cells[7-9].

As a member of the STAT family, STAT5 is involved in a broad range of human cancers and has been considered as a high value target for cancer therapy[10-14]. It is expressed in two forms of STAT5a and STAT5b, showing around 94% sequence identity at the amino acid level[15]. STAT5a and STAT5b are often referred to collectively as STAT5. Apart from the N-terminal domain and the C-terminal transactivation domain, the core fragment of STAT5 structure comprises of four parts (**Figure 1.1**): a coiled-coil domain, a DNA binding domain, a linker domain and an SRC-homology type 2 (SH2) domain[16, 17]. The coiled-coil domain is involved in various early events in STAT5 activation and function, the DNA binding domain regulates recognition of specific DNA sequences for binding, the linker domain is responsible for keeping the appropriate structure for DNA binding as well as nuclear export, and the SH2 domain plays a critical role in STAT5 activation and dimerization through its phosphotyrosine recognition area to regulate gene transcription. Besides, a conserved tyrosine residue (residue 694 and 699 for STAT5a and STAT5b, respectively[18]), which is crucial for STAT5 functionalization, located at the C-terminal end of SH2 domain[18, 19].
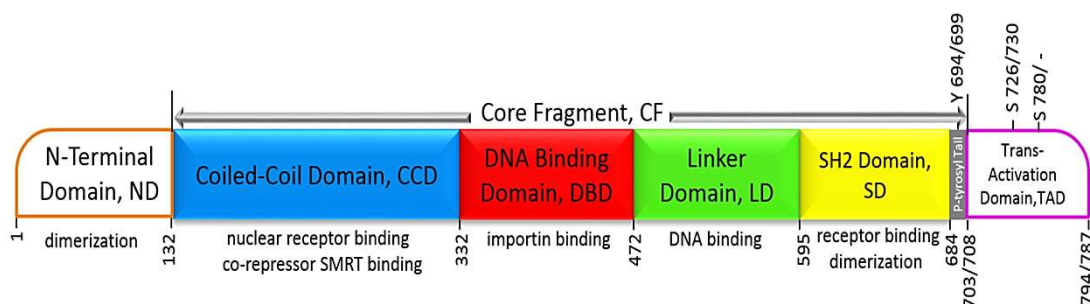
Figure 1.1. The structure of STAT5 protein, in which the SH2 domain (in yellow) plays a critical role in STAT5 activation and dimerization[19].

The crystal structure of unphosphorylated mouse STAT5a core fragment (PDB: 1Y1U)[20], lacking both the N-terminal and the C-terminal transactivation domains was published in 2005, which has allowed for a number of computational studies of STAT5 to be performed in the past years[21-25], leading to a better understanding of the protein structure and relevant molecular mechanisms. Most recently, the core fragment of unphosphorylated human STAT5b was crystallized (PDB 6MBW) and the structure was solved via molecular replacement with mouse STAT5a[26].

1.2. STAT5 signaling

STAT5 plays a central role in transmitting signals from transmembrane receptors such as cytokine receptors[4, 27, 28] and growth factor receptors[29, 30] to the nucleus (**Figure 1.2**). It is responsible for activation of genes that are involved in essential cellular functions[10, 31]. In normal cells, the signaling cascade begins at the cell surface. When ligands bind to the extracellular pockets of the upstream receptors, kinases are activated to phosphorylate specific tyrosine residues on the receptor's cytoplasmic domains. STAT5 proteins are recruited to bind to the phosphotyrosine residues of these receptors via SH2 domain. There, each of the bound STAT5 proteins is phosphorylated by tyrosine kinases such as JAK2[32-34] at the conserved tyrosine residue 694/699[18] and then released from the receptors. The subsequent phosphotyrosine–SH2 domain interactions between phosphor-STAT5 monomers in the

cytoplasm generates phospho-STAT5 dimers[35]. The phosphorylated dimers are able to translocate into the nucleus where they bind to target DNA sequences to regulate gene transcription and expression, although they are rapidly deactivated by a number of intracellular mechanisms, including cytosolic and nuclear phosphatase[19, 36].
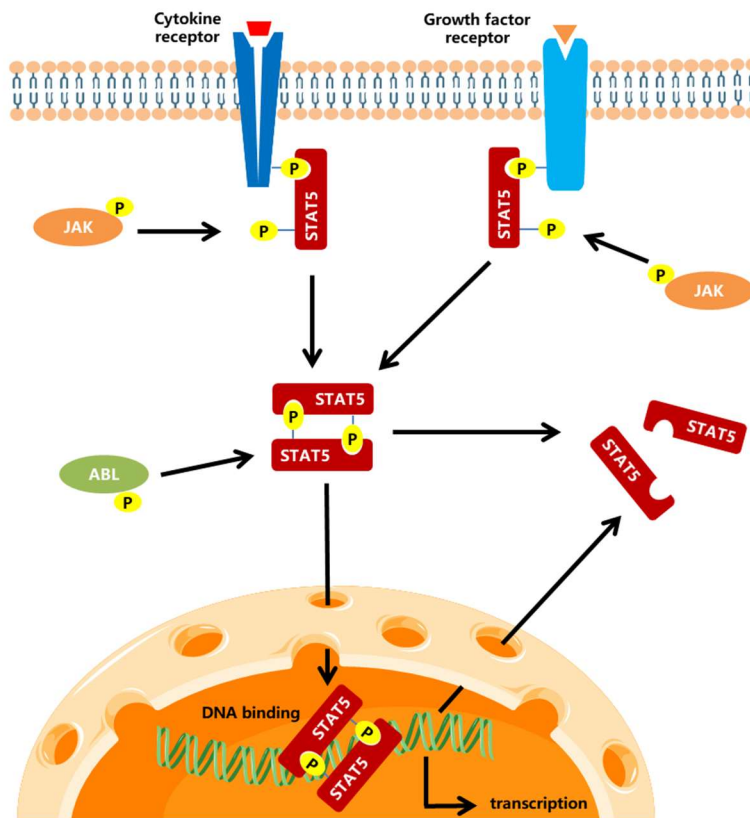

Figure 1.2. STAT5 signaling induced by activated transmembrane receptors and cytoplasmic tyrosine kinases.

In cancer cells, however, STAT5 is constitutively phosphorylated by activated upstream kinases[37-39] even without ligand-induced receptor stimulation due to numerous reasons such as receptor mutations[40-42] and altered expression and activity of cytoplasmic tyrosine kinases[32, 43, 44], leading to elevated expression levels of the target genes including Pim1 with pro-proliferative function, Bcl-xl with anti-apoptotic function, and Cis with negative regulatory function[45-47]. Constitutive phosphorylation of STAT5 has been proved to be a crucial role in various cancer types including acute myeloid leukemia, chronic myeloid leukemia, breast cancer, and prostate cancer[48]. Many tyrosine kinase inhibitors targeting

upstream STAT5 inducers to block STAT5 signaling have been reported[49-54]. However, the upstream tyrosine kinases usually are involved in many other downstream pathways except for STAT5 signaling. As a result, indirect strategies inhibiting STAT5 signaling could also generate strong undesirable effects. For example, it is common for cancer cells to develop resistance to tyrosine kinase inhibitors that specifically target FLT3[55, 56], which is a constitutively active tyrosine kinase that drives the pathogenesis of acute myeloid leukemia. On the other hand, it is unrealistic to inhibit all the upstream STAT5 inducers at one time[57] or with a single inhibitor. Thus, investigating inhibitors that are capable to directly block STAT5 phosphorylation and dimerization is of great meaning for anti-cancer drug discovery.

1.3. Phosphate mimetics

As mentioned before, inactive STAT5 monomers becomes capable of triggering downstream signaling pathways when they are phosphorylated at the conserved tyrosine residues by kinases after binding to phosphotyrosine-containing receptors via phosphoryrosine recognition area in SH2 domain. Afterwards, posphorylated STAT5 monomers dissociate from the receptors to form dimers by mutual binding of individual phosphorylated tyrosine sequences to the binding pockets within paired SH2 domains. In consequence, the SH2 domain serves as the binding target of phosphotyrosine residues of upstream receptors as well as those of phosphorylated STAT5 monomers. To inhibit the aberrant activation and transcriptional influences of STAT5 proteins in cancer cells, phosphate mimetics that occupy the phosphotyrosine recognition area[24, 35] in the SH2 domain to block phosphorylation and dimerization of STAT5 proteins could be potential anti-cancer drugs. Indeed, highly potent peptide-based phosphotyrosine mimetics has been reported[58, 59], although they usually fail to exhibit significant cellular activity. Meanwhile, active small-molecule inhibitors directly targeting on the phosphotyrosine binding pocket have been discovered successively in recent years[36, 60-64]. However, many of them didn't show enough target specificity for further development.

1.4. 4-Amino-furazan-3-carboxylic acid

In the previous work of Wong and coworkers[65], a fluorescence polarization (FP) screening utilizing a fragment library to discover phosphate mimetics was performed. The protein used in the FP assay was a recombinant MBP-fusion STAT5b-SH2 domain. One active fragment, a furazan derivative **1** with a K_D value of 420 μM and high ligand efficiency[66] of 2.1 kJ mol⁻¹ per non-hydrogen atom was selected as a promising phosphate mimetic for further optimization. In a thermal shift assay the melting point of STAT5 protein was increased by 3 °C after treatment of **1**, implying binding events existed between **1** and STAT5. Molecular docking of **1** into homology model of human STAT5-SH2 phosphotyrosine binding site indicated that the binding mode consisted of interaction between the carboxylate anion and the protonated Arg618 and several hydrogen bonds involving Arg618, Ser622 and Asn642. Interestingly, N642H was found to be a driver mutation for T-cell leukemia[26, 67-69].
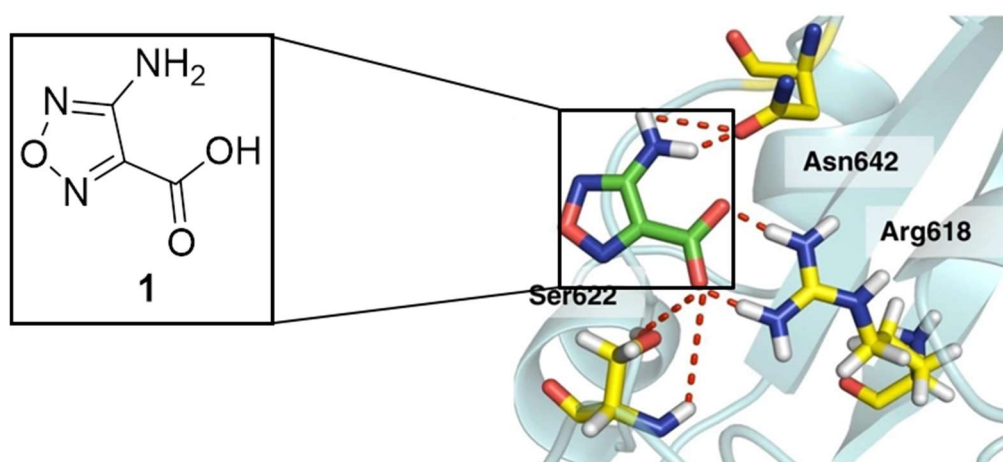

Figure 1.3. Molecular docking of phosphate mimetic **1** into the homology model of human STAT5-SH2 phosphotyrosine binding pocket (generated from the published structure of STAT5a, PDB 1Y1U). Arg618, Ser622 and Asn642 were suggested to be important binding sites[65].

1.5. Protein-induced fragment ligation products

Protein-induced fragment ligation has been described as a powerful method for protein ligands discovery[70-72]. This method based on the theory that a protein has the potential to serve as a binding template to catalyze specific multi-component reactions to form more active ligands by linking less active fragments together. The fragments usually have low binding affinities respectively to several adjacent binding pockets in the protein. The range of applicable reaction types has been expended in recent years[73-77]. In order to expand the structure of phosphate mimetic **1** and increase the possibility of discovering more active molecules, protein-induced fragment ligation methods were carried out by Wong[65]. At first, amidation of the amino group with different acyl chlorides, which is an effective method in fragment-based drug discovery[78] was introduced, resulting in several amide derivatives. None of them, however, were active in the FP assay. One possible reason was that the carbonyl linker couldn't make the molecule flexible enough to fit the phosphotyrosine binding pocket in the STAT5-SH2 domain. Thus, an alternative featured with Mannich ligation reactions was investigated. Fragment **1** was able to react with formaldehyde and some *N*-containing heteroaryl nucleophiles at room temperature to give 1-aminomethyl tetrazole products. The three-component Mannich ligations generated the products in acidic condition, whereas no product was observed at pH 7.4. Taking the above findings and the theory of protein-induced fragment ligation into account, a reasonable assumption was that if STAT5 protein could catalyze a Mannich ligation reaction to happen at pH 7.4, then the corresponding product would very likely to be a ligand to STAT5. The assumption was verified in the following investigations involving thermal shift assay (TSA), FP assay and HPLC-QTOF-MS analysis, in which 1*H*-tetrazole was used as an *N*-containing heteroaryl nucleophile. To exclude the interferences from any other primary and secondary amines in the Mannich ligation, a MOPS buffer at pH 7.4 was used in the assays. In the TSA, an obvious shift of the MBP-STAT5-SH2 protein's melting point was recorded after incubation of **1**, formaldehyde and 1*H*- tetrazole at pH 7.4 in the presence of the protein. On the other hand, in the FP assay, fragment **1** and 1*H*-

tetrazole were incubated in a similar way at pH 7.4, the FP values decreased with the increase of formaldehyde concentration. These two binding assays suggested the protein-induced formation of an inhibitor. Furthermore, the product formation was detected and quantified by HPLC-QTOF-MS analysis. As anticipated, incubation with protein led to the formation of **2**, while incubation without protein didn't show any product formation. However, when the same assay was carried out at pH 5.0, the product was formed no matter there's protein in presence or not. Similar results were obtained when 1*H*-tetrazole was replaced by 5-benzyl-1*H*-tetrazole in the assay. And replacement of MBP-STAT5-SH2 protein by MBP and other proteins didn't induce the ligation in the same conditions. Both ligation products **2** and **3** were re-synthesized, purified and tested in the FP assay, showing low-micromolar affinities to STAT5-SH2 protein, which was a significant improvement compared with that of fragment **1**.
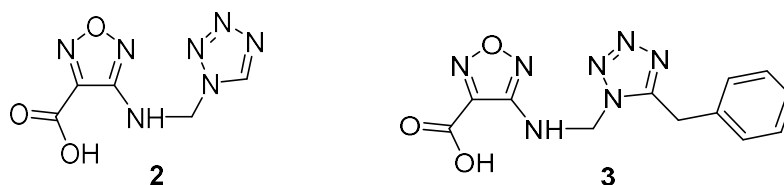

Figure 1.4. Derivatives **2** and **3** of lead compound **1** showed improved binding activity to STAT5-SH2.

The predicted binding mode of **2** to STAT5-SH2 indicated that the original interactions were retained and the expansion of structure introduced additional hydrophobic interactions to the adjacent pocket involving Trp641, Leu643, and Met639 residues. What's more, hydrogen bonds between the tetrazole ring and the amide-NH_2 of Asn642 could strengthen the binding. The crucial role of Asn642 in the increased affinity was further confirmed by a ligation assay with structurally related Asn642-lack GST-STAT3 protein. No Mannich ligation reaction was observed in that case.
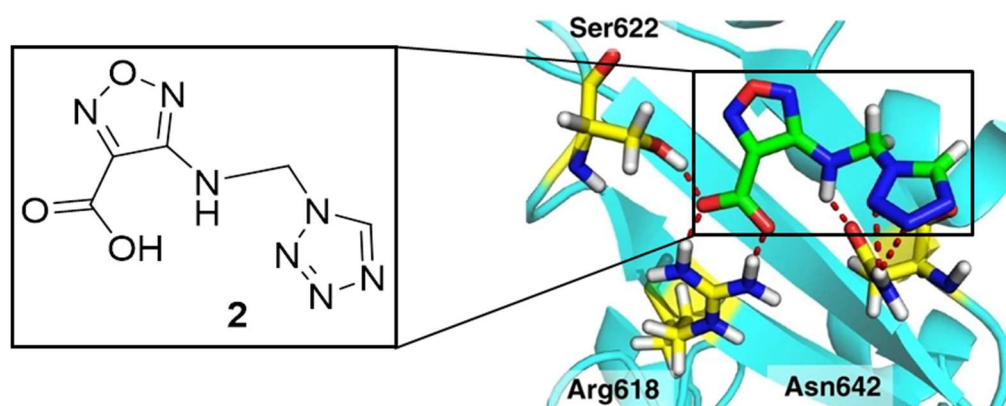
Figure 1.5. Predicted binding mode of compound **2** to the homology model of human STAT5-SH2. Additional hydrogen bonds between the tetrazole ring and Asn642 were suggested[65].

To investigate the specificity of these STAT5 inhibitors from Mannich ligation, various assays were performed. The ligation product **2** showed inhibition or binding specificity to STAT5 in comparison with SHP2 in enzyme assays and STAT3 in FP assay. Besides, **2** inhibited STAT5-DNA complex formation while the corresponding DNA complex formation of STAT1 and STAT3 were not suppressed. The inhibitors were further studied in living cells and animals. In BaF3 cells carrying FLT3-ITD mutation[79], a common AML model, STAT5 is constitutively phosphorylated. The cells were treated with re-synthesized Mannich ligation products and STAT5 phosphorylation level was determined using phosphotyrosine-specific antibodies afterwards. The results indicated **3** and the methyl ester derivative of **2** reduced STAT5 phosphorylation in BaF3 cells with FLT3-ITD mutation. What's more, transcription and protein expression of three important target genes of STAT5, Pim1 kinase, Bcl-xl and Cis, were also found significantly suppressed by analyzing mRNA in qRT-PCR study. In MV-4-11 leukemic cells inhibitor **3** showed synergistic effects with FLT3-inhibitor PKC412 in inhibition of reporter gene expression, STAT5 phosphorylation and cell proliferation. In a murine model of leukemia, tumor growth in nude mice with inoculated BaF3/FLT3-ITD cells after treatment with **3** was delayed compared with the control group.

All these findings suggest that the products of Mannich ligation reactions of fragment **1**, formaldehyde, and various 1*H*-tetrazoles are active and specific inhibitors of STAT5 with

promising anti-tumor efficacy. The furazan-based phosphate mimetics paved the way for further investigation of STAT5-SH2 inhibitors.

2. Objectives and planning

STAT proteins have been described as difficult pharmacological targets[9, 80, 81]. While many indirect inhibitors of other STAT family members are currently found at different stages of the pharmaceutical drug discovery process[49, 82, 83], the development of novel cancer therapeutics against STAT5 has been poorly investigated. To date only a few examples of chemical entities that specifically target this oncological protein have been published[84, 85]. In Wong's work, fragment **1** was proven as a phosphate mimetic to be able to form critical interactions with STAT5 SH2 in the phosphotyrosine binding area. With the help of a protein-templated drug discovery method utilizing Mannich ligation reactions[65], the tetrazole moiety was attached to fragment **1**, affording several active ligation products (1-aminomethyl tetrazoles) with STAT5 inhibitory activity. In the binding assays, the activity of these 1-aminomethyl tetrazoles was demonstrated to be significantly improved if compared with that of fragment **1**. However these compounds only showed limited activity in cellular assays. Besides, they were found not stable in aqueous solutions especially in acidic condition. For example, inhibitor **3** was decomposed in acidic mobile phase when analyzed by LC-MS. But the decomposition degree of these compounds could be very different due to different types of the substituents at the 5-position of the tetrazole ring. The instability of the existing 1-aminomethyl tetrazoles could have a negative impact on the results of further biological evaluations since fragment **1** only showed a binding activity of 420 μM to STAT5 protein and 5-substituted tetrazoles alone were not active towards the target protein. Furthermore, no inhibitor-protein complex was found in the protein mass experiment excluding an irreversible binding mode. If the compounds get decomposed easily, their inhibitory effect on STAT5 would very likely be weakened. Thus, the first aim of this work is to discover STAT5 inhibitors with improved stability and potency based on the existing structure. The second aim is to further understand the role of the tetrazole moiety in the binding to STAT5-SH2. The third aim is to clarify how

the acidity and the substituents on the tetrazole influence the scaffold's stability. To achieve these goals, structural modifications on the existing compounds were planned as follows.

To modify the structure of the 1-aminomethyl tetrazoles, one option is to change the scaffold itself. But the change should not be too extensive, so as not to generate unfavorable effects on the activity towards STAT5 protein. The plan is to exchange the positions of the two substituents on the tetrazole ring leading to the scaffold of 5-aminomethyl tetrazole, in which the connection between the furazan ring and the tetrazole ring should be more stable. And by comparing the activity of 5-aminomethyl tetrazoles with that of 1-aminomethyl tetrazoles, the ligand-protein interactions can be further understood. Another way of structural modification is to attach different substituents to the 5-position of the tetrazole ring. Because structure expansion could bring the possibility of binding to additional sites that were beyond reach previously. Besides, different substituents at the tetrazole ring could have diverse impacts on the stability of this scaffold.

II. Results and Discussion

3. Limitations of the existing compouds

In the previous work done by Wong[65], a number of fragment **1** based compounds were synthesized and tested. For example, amidation on the amino group of compound **1** with various acyl chlorides furnished *N*-acetyl derivatives. However, none of the amides were active in the binding assay probably because of the steric effect of the carbonyl linkage on ligand-protein interactions.
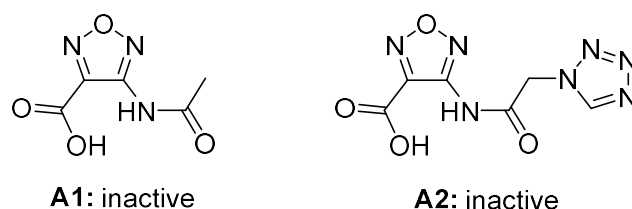

A1: inactive   **A2:** inactive

Figure 3.1. Examples of amidation products of fragment **1**.

In the Mannich ligation expansion of compound **1**, different *N*-heterocycles were used with formaldehyde to give various ligation products. It was discovered that products with five-membered *N*-heterocycles generally displayed enhanced inhibitory activity towards STAT5. For example, the compounds with 1,2,3-triazole ring (**B1** and **B2**) showed an increase of affinity in around 2 fold while the 1,2,4-triazole compound **B3** in over 9 fold. The pyrazole containing compound **B4** also showed an over 3 fold enhancement of binding affinity to STAT5. The most significant improvement of activity was found in the derivatives with 5-substituted tetrazoles (e.g. compounds **2** and **3**, mentioned in the introduction chapter), in which some of the them (**C3** and **C4**) even possessed submicromolar activity.
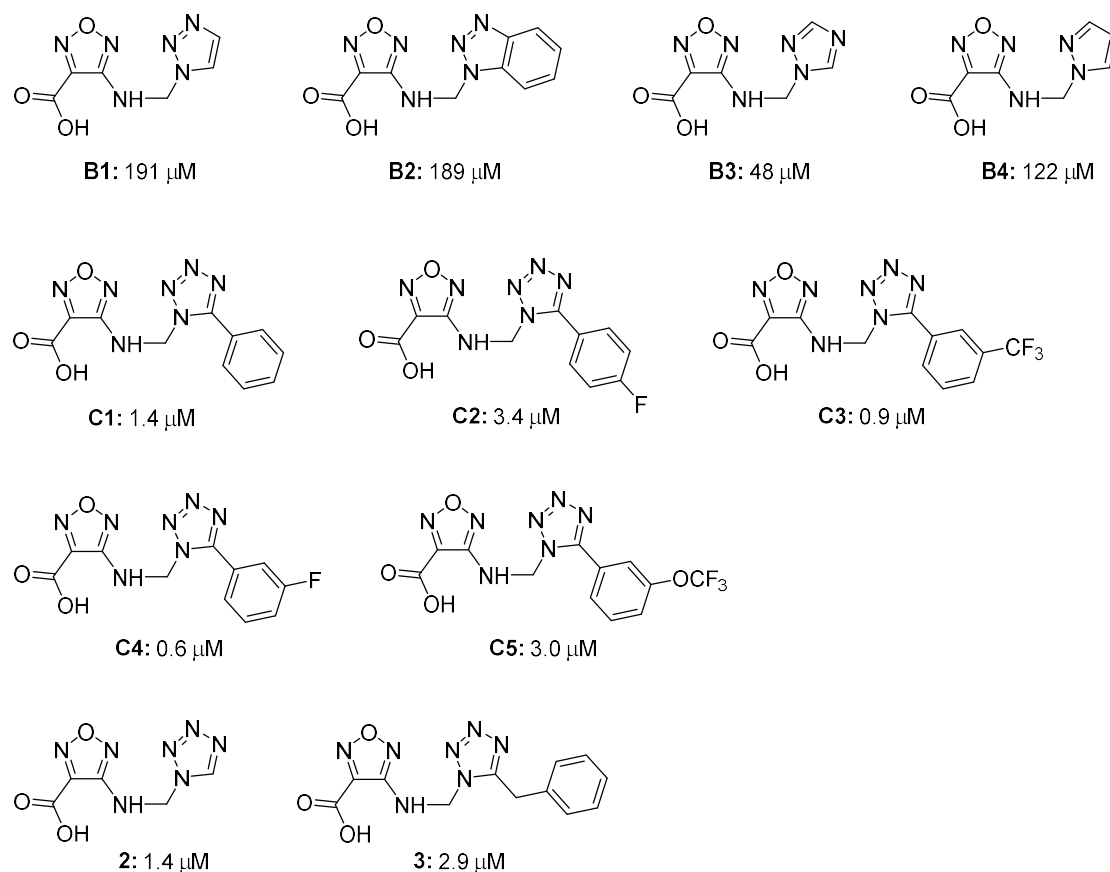
Figure 3.2. Examples of the active compounds derived from Mannich ligation reactions (with K_i values in the FP assay from Wong's work[65]).

Despite the improved activity of the tetrazole-containing ligation products showed in binding assays, several problems regarding the properties of the structures limited the further investigations. In cellular assays, compounds **C1**, **C3** and **C4** precipitated in buffer, resulting in failed tests. Other compounds that were soluble in DMSO and buffer, however, showed limited cellular activity. For example, compound **2** inhibited the phosphorylation of STAT5 in leukemic cells with an IC_{50} of only over 100 µM. The instability of these compounds could be a reason for the low cellular activity. The 1-aminomethyl tetrazoles were found to be decomposed into fragment **1** and corresponding 5-substituted tetrazoles in the process of chromatography (**Figure 3.3**), which will be discussed in detail in the following chapters.
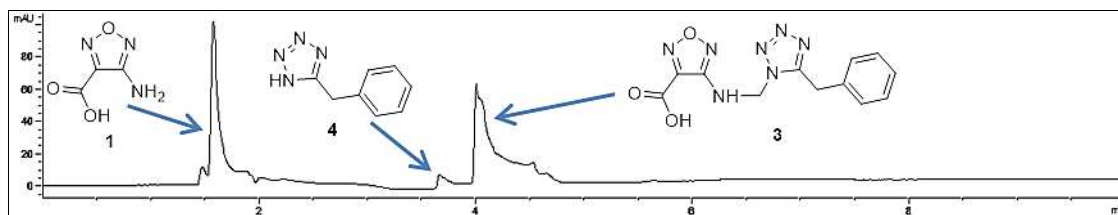
Figure 3.3. Compound **3** was decomposed in the process of chromatography using acidic mobile phase (wavelength = 254 nm).

Given the above limitations, optimization of the 1-aminomethyl tetrazoles is needed to discover potent and stable STAT5 inhibitors.

4. Study of 5-aminomethyl tetrazoles

4.1. Synthesis of 5-aminomethyl tetrazoles

The instability of 1-aminomethyl tetrazoles has a negative impact on subsequent activity studies. To overcome this problem, a modification on the structure is needed. The purpose of the modification is not only to find a stable scaffold but also to keep the existing activity. Thus, exchanging of the two substituents on the tetrazole ring, which leads to 5-aminomethyl tetrazoles, seems to be a reasonable way since the minimum extent to which the original structure to be changed. The key binding interactions between the ligand and the protein, involving residues such as Arg618, Ser622 and Asn642 were expected to be retained. In order to obtain the 5-aminomethyl tetrazole scaffold, different synthetic routes were designed and carried out (**Scheme 4.1**).
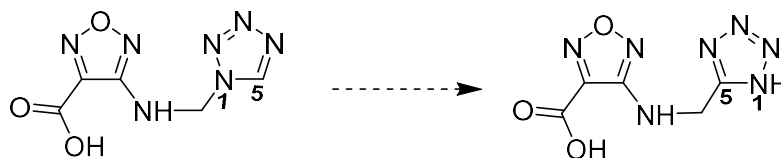
Figure 4.1. Structure modification from 1-aminomethyl tetrazole to 5-aminomethyl tetrazole.
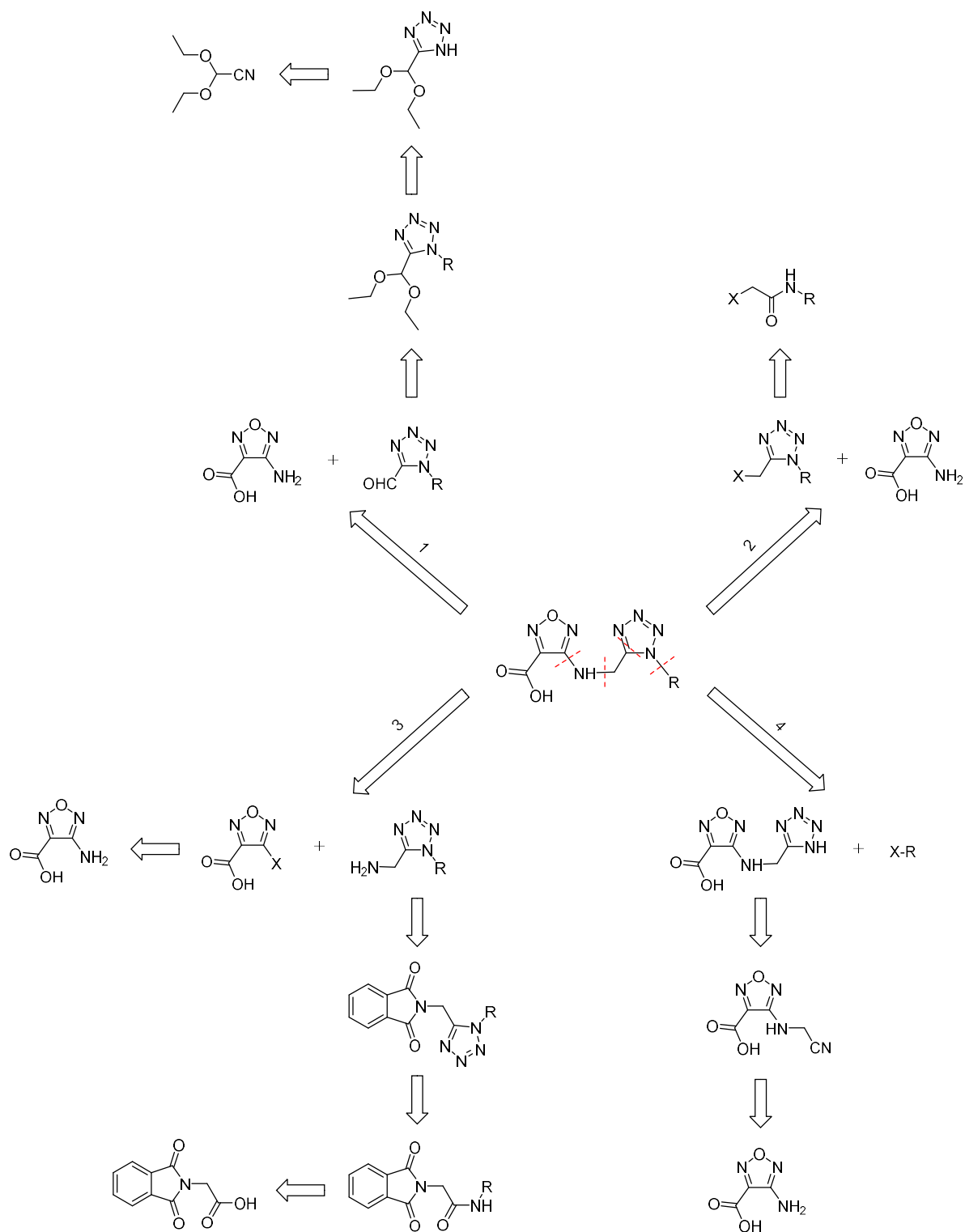
Scheme 4.1. Retrosynthetic analysis of 5-aminomethyl tetrazole compounds.

4.1.1. Reductive amination method

To synthesize the 5-aminomethyl tetrazole structure, a 4-step synthetic route starting from 2,2-diethoxyacetonitrile was designed (**Scheme 4.2**). In the conversion of 2,2-diethoxyacetonitrile to 5-(diethoxymethyl)-1*H*-tetrazole (**31**), sodium azide or trialkyltin azides[86-88] were first used as the azide source and the reaction mixture was stirred and heated under microwave irradiation. However, the yields were too low to proceed the following reaction. In the attempt to increase the yield, the azide source was changed to hydrazoic acid according to Pireto' work[89]. The hydrazoic acid solution was prepared in advance by addition of sulfuric acid into a suspension of sodium azide in chloroform under cooling. By use of hydrazoic acid solution, the yield was increased to 57%. Subsequent substitution of compound **31** at tetrazole's 1-position with a benzyl group was straightforward. The following hydrolysis to give the corresponding aldehyde compound **34** was achieved by use of hydrochloric acid.
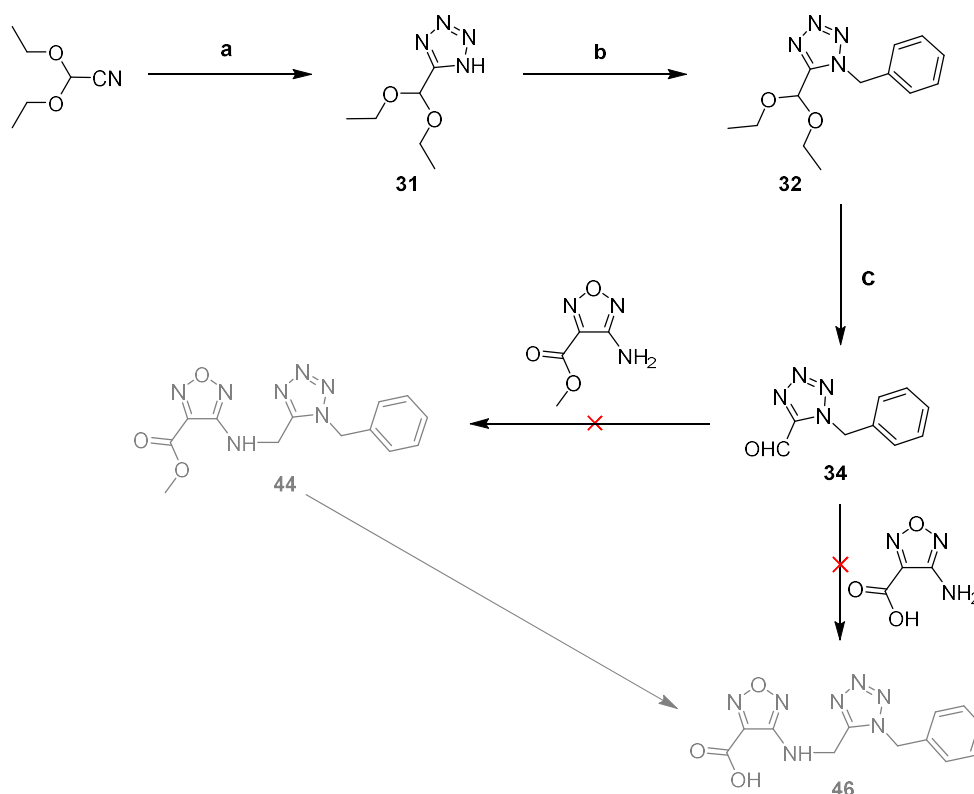
Scheme 4.2. Reductive amination method for the synthesis of compound **46**. Reagents and conditions: (a)

HN$_3$, pyridine, CHCl$_3$, RT, O/N, 57%; (b) PhCH$_2$Br, Cs$_2$CO$_3$, DMF, 100 °C, O/N, 67%; (c) HCl, H$_2$O, 50 °C, 2.5 h, 90%.

The final step was a reductive amination reaction involving either 4-amino-furazan-3-carboxylic acid **1** or the methyl ester compound and **34**. The amine and the aldehyde were first dissolved in methanol and stirred at room temperature. After 2 h, the mixture was treated with reducing agents such as sodium borohydride (NaBH$_4$), sodium cyanoborohydride (NaBH$_3$CN) and sodium triacetoxyborohydride (NaBH(OAc)$_3$). However, no product was found in either case. Various attempts including changing of different solvents (e.g., EtOH, i-PrOH, THF, DCM, MeCN, DMF), removal of water and increasing the reaction temperature were made but none of them was able to solve the problem. Actually, there was no obvious imine intermediate detected in the reaction process even sufficient time was given before introducing a reducing agent. The reason could be attributed to the low reactivity of the primary amino group of compound **1**. The strong electron-withdrawing effect of the furazan ring dramatically disperses the negative charge on the N atom of the amino group. As a result, the amine addition on the aldehyde carbonyl is difficult to proceed, which is the first step of the mechanism of reductive amination (**Scheme 4.3**). Consequently, there won't be enough imine or iminium ion to be reduced into the expected product in the following step.
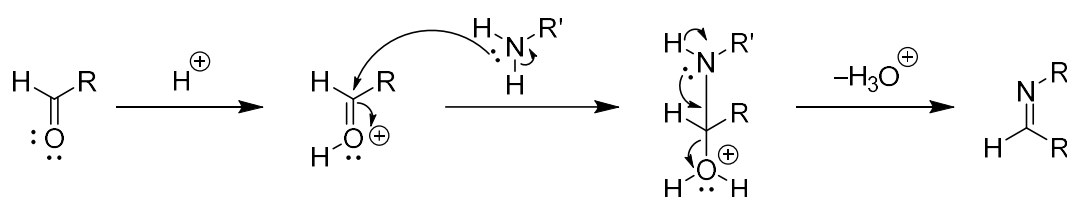

Scheme 4.3. Theoretical mechanism of imine formation in reductive amination.

4.1.2. *N*-Benzyl-2-chloroacetamide method

N-Benzyl-2-chloroacetamide is able to be transformed into 1-benzyl-5-(chloromethyl)-1*H*-tetrazole in a one-pot reaction involving chlorinating reagent phosphorus pentachloride (PCl$_5$) and azide source hydrazoic acid (HN$_3$) in toluene[90, 91]. In this tetrazole formation

process, the addition of PCl_5 on the carbonyl of *N*-benzyl-2-chloroacetamide happens at first. After cleavage of a $POCl_3$ and a chloride ion, the chloroimine intermediate forms. The subsequent conversion into the tetrazole compound after the attack of azide anion on the imine carbon is straightforward (**Scheme 4.4**). Thus, a synthetic route to furnish 5-aminomethyl tetrazoles was designed including a tetrazole formation step and an amine alkylation step. In theory, the order of these two steps could be interchanged (**Scheme 4.6**). DMF was used as solvent in the S_N2 alkylation reaction and different bases such as K_2CO_3, $NaHCO_3$, Cs_2CO_3, Et_3N were tried as additives in order to eliminate acid. However, the alkylation of the amino group in compound **1** was not successful in either route. The reason is that the 4-amino-furazan compound is a weak nucleophile under the influence of the furazan ring, and the chloride compounds are not active enough to promote the nucleophilic attack from the amine. So potassium iodide, a commonly used activating agent[92, 93], was added into the reaction leading to *in situ* formation of the corresponding iodide from the chloride compound (**Scheme 4.5**). Unfortunately, no product was found in the following nucleophilic substitution reaction either. The low reactivity of the 4-amino-furazan compound is still a key problem in this method.
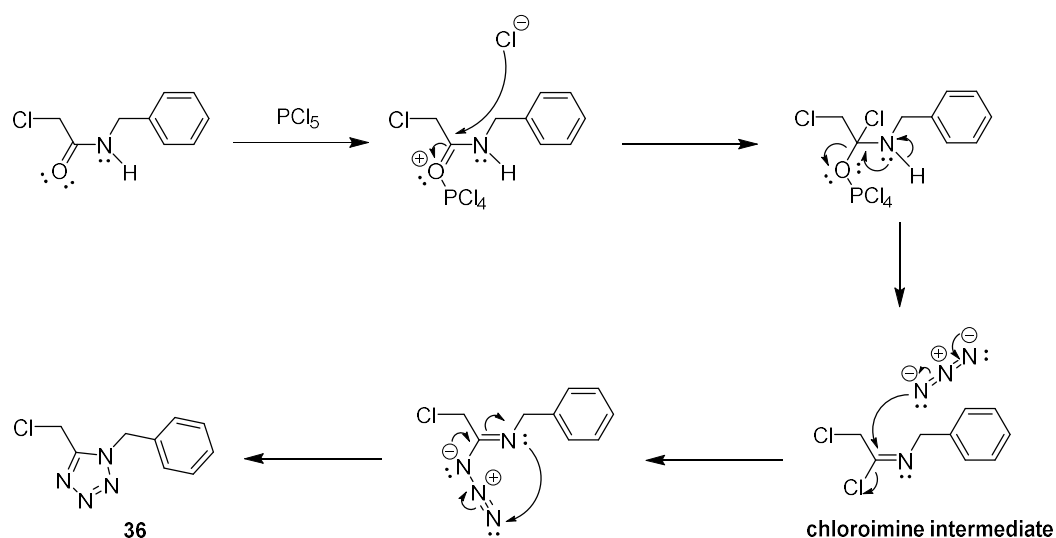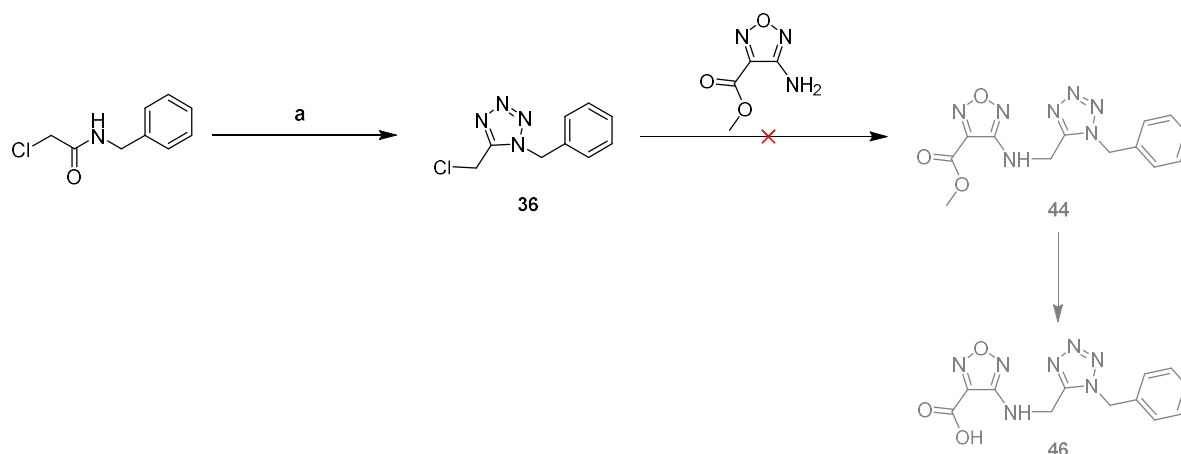

Scheme 4.4. Synthetic mechanism of compound **36** from *N*-benzyl-2-chloroacetamide using phosphorus pentachloride and hydrazoic acid.
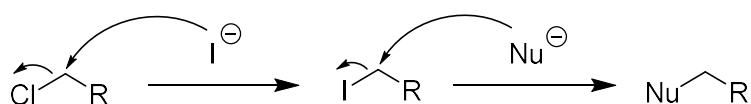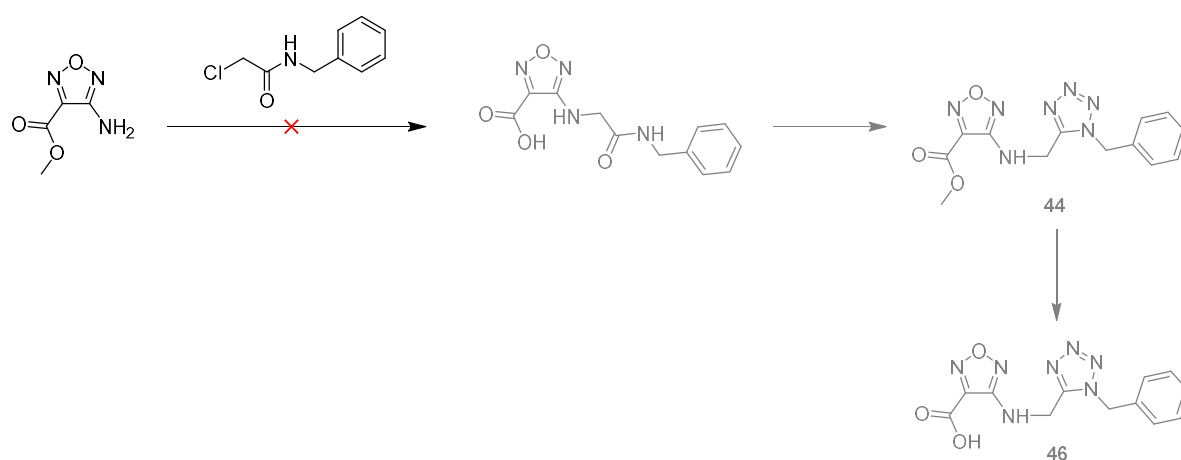
Scheme 4.5. Chlorides can be activated to corresponding iodides to undergo nucleophilic substitution from weak nucleophiles, as iodide ion is a better leaving group than chloride ion.

(**4.6-1**)

(**4.6-2**)

Scheme 4.6. *N*-benzyl-2-chloroacetamide methods for the synthesis of compound **46**. Reagents and conditions: (a) PCl$_5$, HN$_3$, toluene, 80 °C, O/N, 92%.

4.1.3. Sandmeyer reaction method

As previously mentioned, the amino group of 4-amino-furazan reactant was not active enough to react with **34**. Thus, an alternative way using (1-benzyl-1*H*-tetrazol-5-yl)methanamine (**39**)

as a nucleophile was designed (**Scheme 4.7**). *N*-benzyl-2-(1,3-dioxoisoindolin-2-yl)acetamide (**37**) was first synthesized from 2-(1,3-dioxoisoindolin-2-yl)acetic acid in a one-pot amidation reaction. The next step was tetrazole formation, in which hydrazoic acid and phosphorus pentachloride were used (the mechanism has been discussed in the previous method). Primary amine **39** was then released from the phthalimide compound **38** by reaction with hydrazine (**Scheme 4.8**). On the other hand, the amino group of 4-amino-furazan compound should be halogenated as a electrophile to react with compound **39**. To achieve this goal, Sandmeyer reaction was employed[94, 95]. Both sodium nitrite and tert-butyl nitrite were tried to form nitrosonium ion in acidic condition (**Scheme 4.9-1**), which theoretically acts as an electrophile to react with the heterocyclic amine to form corresponding diazonium salt (**Scheme 4.9-2**). The diazonium ion then reacts with CuBr through a radical mechanism to lose a nitrogen molecule, forming the brominated product (**Scheme 4.9-3**). However, no product formation was found under the above conditions when using the methyl ester of compound **1**. In this case, the nucleophilic attack of the amine on the nitrosonium ion probably didn't happen readily because of the low electron density on the nitrogen atom of the amino group.
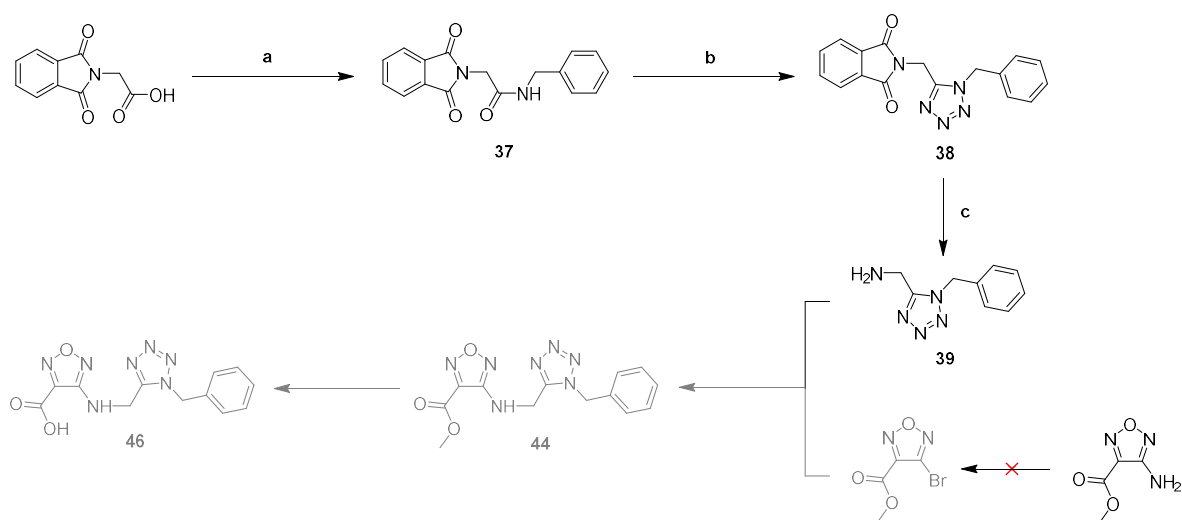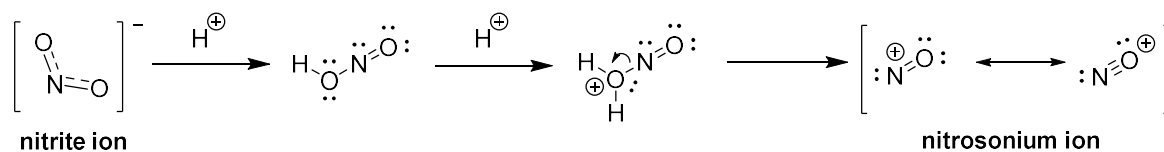

Scheme 4.7. Sandmeyer reaction method for the synthesis of compound **46**. Reagents and conditions: (a) (i) (COCl)$_2$, DMF, DCM, RT, 4h, (ii) BnNH$_2$, Et$_3$N, RT, 30 min. 98%; (b) PCl$_5$, HN$_3$, toluene, 80 °C, O/N, 78%; (c) N$_2$H$_4$, EtOH, reflux, 1.5 h, 85%.
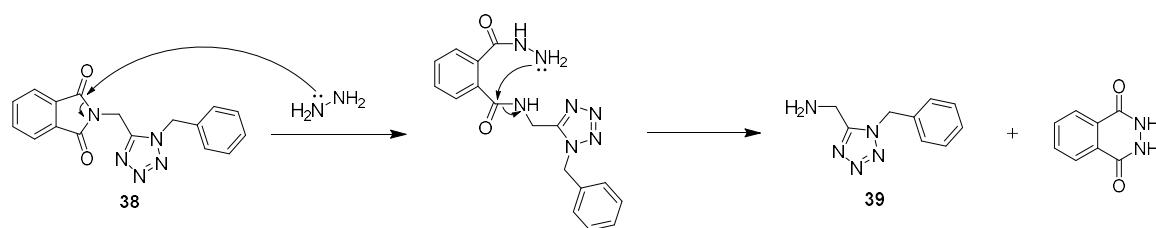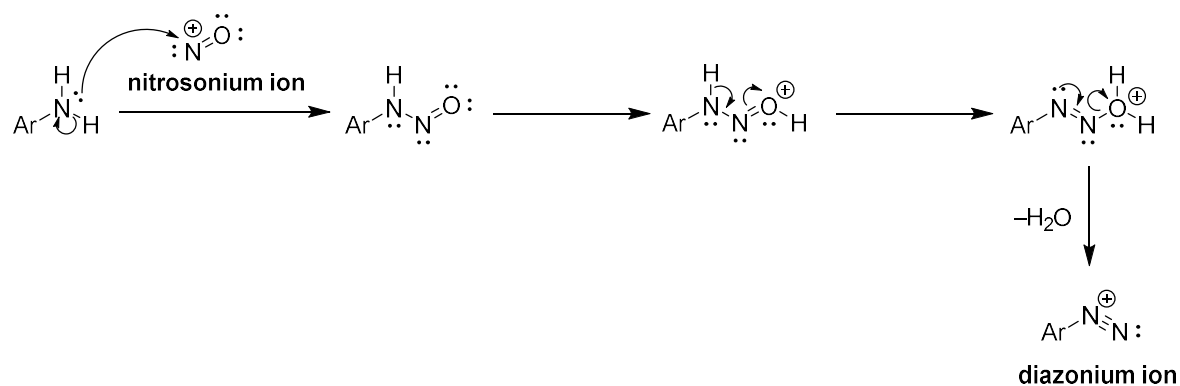
Scheme 4.8. Mechanism of compound **39** formation from compound **38** through hydrazinolysis.
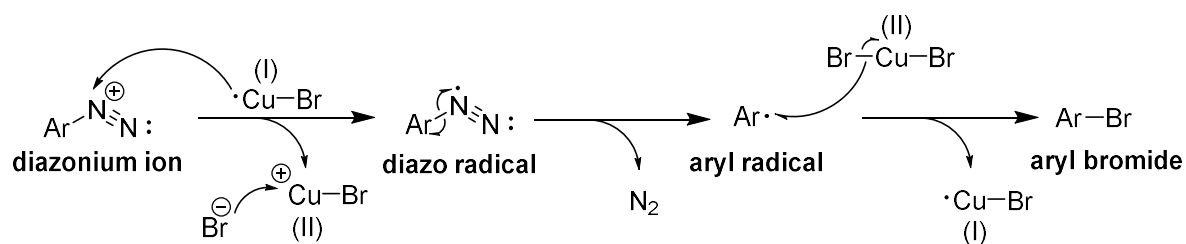
(4.9-1)

(4.9-2)

(4.9-3)

Scheme 4.9. Mechanism of Sandmeyer reaction to synthesize an aryl bromides from an aromatic amine.

Formations of nitrosonium ion (**4.9-1**), diazonium ion (**4.9-2**), and aryl bromide (**4.9-3**).

## 4.1.4. *N*-Cyanomethyl amine method

According to the previous reactions involving 4-amino-furazan compounds, formaldehyde seems to be a rare electrophile that is able to react with the amino group on the furazan ring. And considering the structure of 5-aminomethyl tetrazoles, a Strecker-type[96] nitrile intermediate (**40**) derived from 4-amino-furazan-3-carboxylic acid could be an alternative for tetrazole formation (**Scheme 4.10**). The synthesis of compound **40** involves imine formation and subsequent nucleophilic attack from a cyanide anion. At first, trimethylsilyl cyanide was used[96-98] in the reaction but no product was found. The categories of solvent used in this reaction were very limited. After a series of trials, DMSO was found to be the only feasible solvent to make the reaction happen. The reaction condition was mild and the workup went through column chromatography to obtain the nitrile compound **40** as a white solid. For the subsequent tetrazole formation reaction, the commonly used microwave-assisted reaction resulted in a very low yield. After study of related literatures and several trials, a method based on Sharpless' work[99-102] was applied. The nitrile compound was treated with sodium azide and catalyst zinc bromide in a mixture of water and isopropanol at room temperature to give corresponding tetrazole compound effectively. A possible mechanism is that, zinc cations play a coordination role by forming complex structures with nitrile nitrogen. This coordination increases the polarization of the nitrile moiety and lowers the energy barrier for nucleophilic attack by azide anion. The *N*-cyanomethyl amine compound **40** is able to react with sodium azide to produce the corresponding tetrazole compound **41**. Based on compound **41**, the following esterification, substitution and hydrolysis were carried out to give 5-aminomethyl tetrazoles (**45** and **46**) successfully.
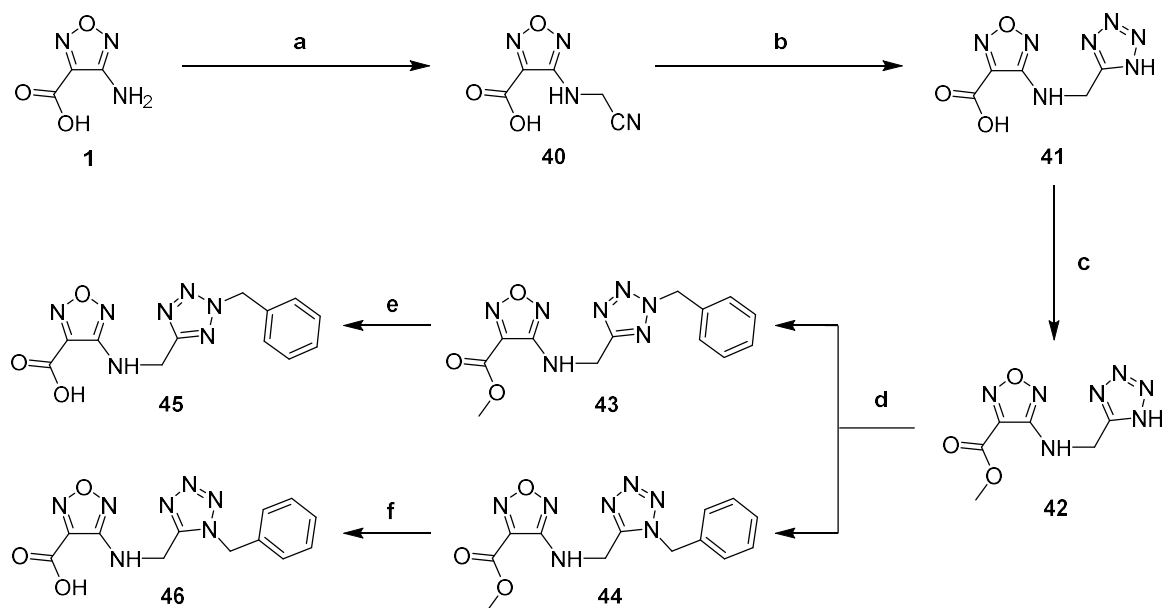
Scheme 4.10. Cyanomethyl amine method for the synthesis of compounds **45** and **46**. Reagents and conditions: (a) HCHO, KCN, DMSO, RT, 4 h, 67%; (b) NaN$_3$, ZnBr$_2$, H$_2$O/iPrOH, 80 °C, 7 h, 84%; (c) MeOH, reflux, 20 h, 91%; (d) PhCH$_2$Br, Et$_3$N, MeCN, RT, 24 h, 24% (**43**) and 21% (**44**); (e) NaOH, MeOH/H$_2$O, 1.5 h, 79%; (f) NaOH, MeOH/H$_2$O, 1 h, 76%.

Notably, in the substitution reaction a mixture of 1,5- and 2,5-disubstituted tetrazoles (**43** and **44**) were found as products with close yields. One possible reason of the isomeric products formation is that an unstable bimolecular intermediate generates in the process[103-106]. The negative charge of the tetrazolate ion is dispersed among the four nitrogen atoms, offering two different sites for the substitution to proceed (**Scheme 4.11**).
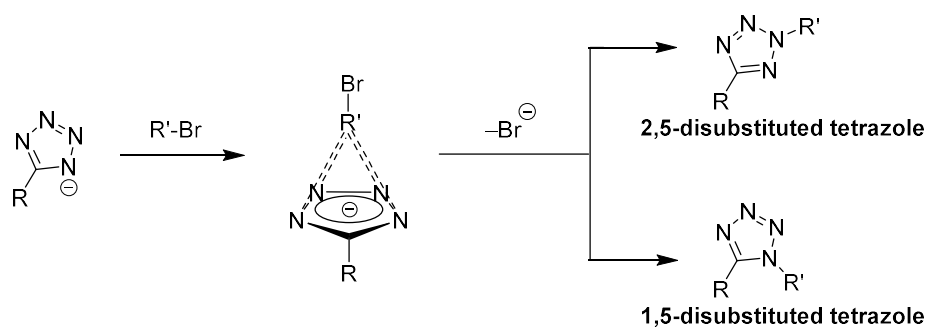
Scheme 4.11. Mechanism of the formation of 1,5- and 2,5-disubstituted tetrazole isomers in the reaction between a tetrazolate anion and an alkyl bromide.

4.2. Stability study of 5-aminomethyl tetrazoles

Stability study of compounds **45** and **46** was carried out on LC-MS (**Figure 4.2**). The compounds were first dissolved in 10 mM ammonium acetate buffers with pH values 1, 3, 5 and 7. After 30 min the solutions were analyzed by LC-MS at 254 nm wavelength with a 10 mM ammonium acetate mobile phase at physiological pH. As anticipated, all the eight chromatograms showed only one peak respectively. This means no decomposition has happened and the two molecules are stable in acidic conditions.
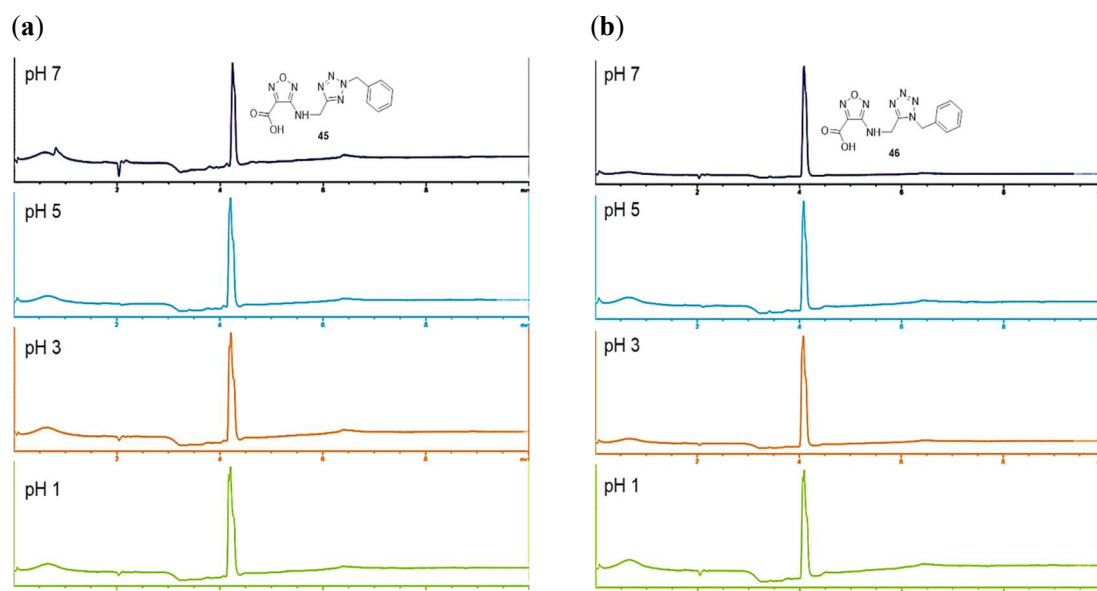
Figure 4.2. Stability of compounds **45** (**a**) and **46** (**b**) detected by LC-MS (DAD 254 nm). The two molecules are stable in acidic conditions.

4.3. FP assays with STAT5b-SH2

To determine the activity of the stable 5-aminomethyl tetrazoles, a competitive fluorescence polarization (FP) assay was applied[107-109] (**Figure 4.3**). In this assay, a potent probe is excited by linearly polarized light and rotate rapidly, resulting in a low spatial orientation when fluorescence emission happens. It is recorded as a low degree of fluorescence polarization. Upon binding to the target protein the rotation of the probe is slowed down because of the

significantly increased molecular weight. Thus, the orientation becomes more uniform and the degree of fluorescence polarization is increased. If a small molecule possessing binding affinity to the protein is added to replace the probe from the binding pockets, a decrease of fluorescence polarization can be detected because the molecular weight is reduced and the rotation of the probe is speeded up again.
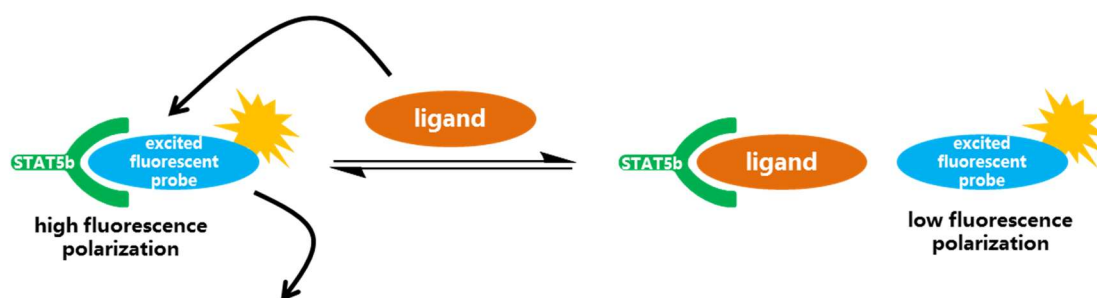

Figure 4.3. The mechanism of fluorescence polarization assay.

To conduct the competitive FP assay, the dissociation constant (K_D) between the protein and the probe is needed, on which the protein concentration used in the following experiments are dependent. The protein used in this work was a recombinantly expressed STAT5b-SH2 fused to maltose-binding protein (MBP) as affinity tag. A highly potent fluorophore-labeled peptide 5-CF-GpYLSLPPW-NH$_2$ was synthesized as the probe. Hence, a binding assay was first performed by treating 10 nM of the fluorophore-labeled peptide with varying concentrations of MBP-STAT5-SH2. The K_D value was determined by the protein concentration when 50% of the probe molecules were bound.
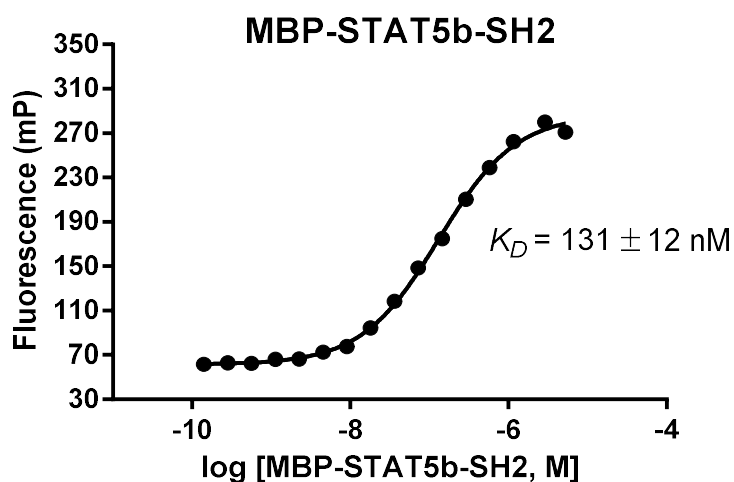
Figure 4.4. Binding of peptide 5-CF-GpYLSLPPW-NH$_2$ to MBP-STAT5b-SH2. (error bars denote mean ± SD, n = 2).

Then the competitive FP assays were conducted to test the known active compounds **2** and **3** (**Figure 4.5**), which are isomers of the synthesized 5-aminomethyl tetrazoles. Serial concentration of the compounds were added into the buffer to compete with the potent probe for the binding to STAT5 protein. By measuring the fluorescence at different concentrations of the compounds, the IC$_{50}$ values were determined.

Nevertheless, it is sometimes difficult to compare the IC$_{50}$ values measured under different experimental conditions and from different research groups[110]. A common practice is to convert them into inhibition constants (K_i), which is theoretically only dependent on the temperature. The conversion can be achieved by applying the Cheng–Prusoff equation[111, 112] (**Equation 4.1**), where [L] represents the concentration of free reference ligand (probe).

$$K_i = \frac{IC_{50}}{1 + \frac{[L]}{K_d}}$$

Equation 4.1. Cheng-Prusoff equation for the calculation of the K_i values in receptor-ligand binding assays[111, 112].

In a competitive binding assay, the concentration of the free probe usually cannot be measured directly. Accordingly, one solution is using the total concentration of the probe

instead of the free one. In the FP-based competitive binding assay, however, the experimental conditions are formulated to maximize the range of the mP shift. The concentration of the probe is lower than the K_D value and the concentration of the protein is higher than the K_D value (twice of the K_D value in this work) so that the polarization value before adding an inhibitor is close to the maximal mP. Since the majority of the probe is bound to the protein, the approximation of the free probe concentration to the total concentration must introduce a significant error. Besides, it was demonstrated that higher concentrations of the protein resulted in higher IC_{50} values for the same inhibitor in the competitive FP assays. Thus, all the IC_{50} values of the compounds in this work were converted to K_i values using a modified Cheng-Prusoff equation[113] (**Equation 4.2**) with a correction factor for the protein concentration, which is more precise than the original equation. Compound **2** and **3** showed K_i values of 2.2 μM and 3.8 μM respectively (**Figure 4.5**).

$$K_i = \frac{IC_{50}}{1 + \frac{[Probe]}{K_d} + \frac{[Protein]}{K_d}}$$

Equation 4.2. Modified Cheng-Prusoff equation containing a correction factor for the protein concentration[113].
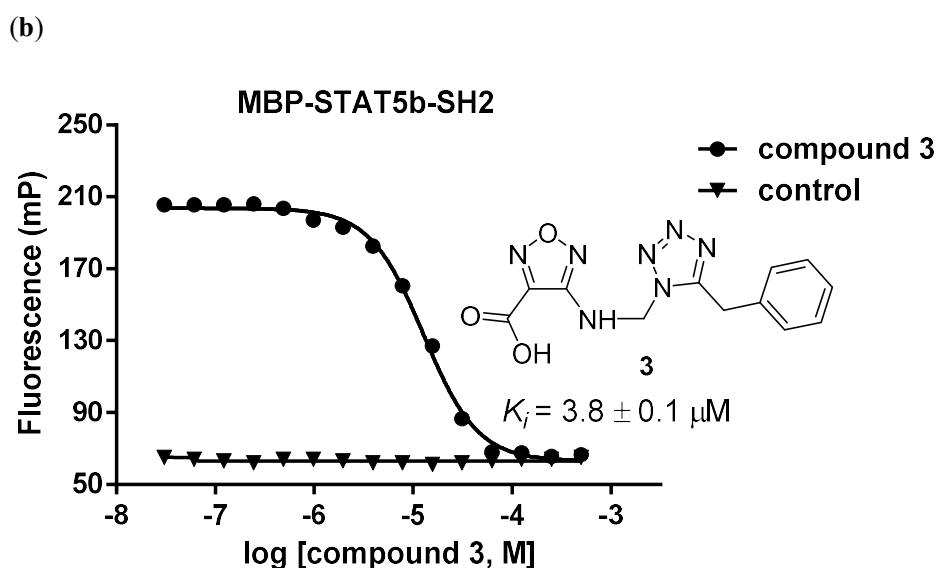
(a)

35

(b)
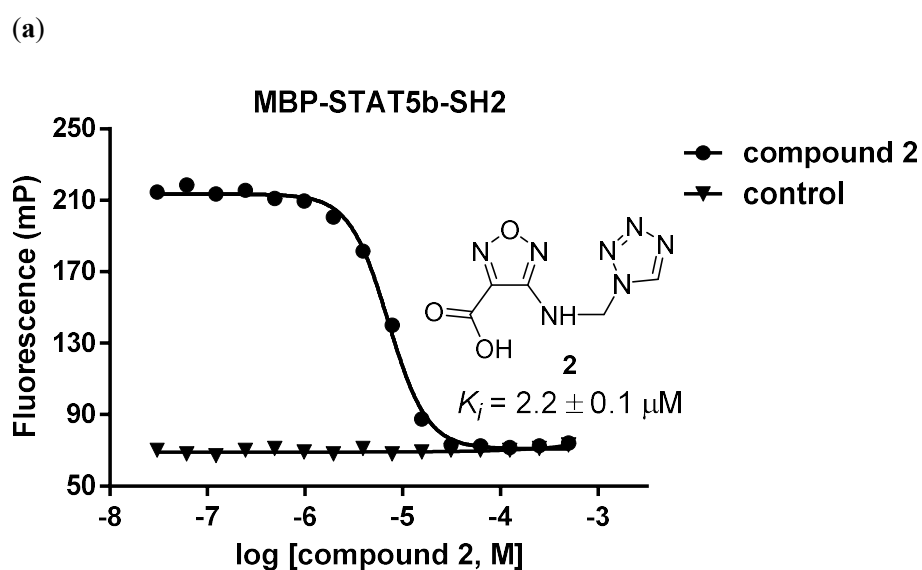
Figure 4.5. Competitive FP assay results of compounds **2** (**a**) and **3** (**b**), showing K_i values of 2.2 μM and 3.8 μM respectively (error bars denote mean ± SD, n = 2).

The stable 5-aminomethyl tetrazoles were also tested following the same protocol (**Figure 4.6**). First, compound **41** was measured in serial concentration ranging from 0.5 mM to 30 nM, however, it was inactive. While its 5-aminomethyl tetrazole isomer **2** possessed a K_i value of 2.2 μM (1.4 μM in Wong's work[65]). Next, compound **45** and compound **46** were tested in the same condition. The results showed that neither of them were active. In comparison, the isomer **3** had a K_i value of 3.8 μM (2.9 μM in Wong's work[65]).
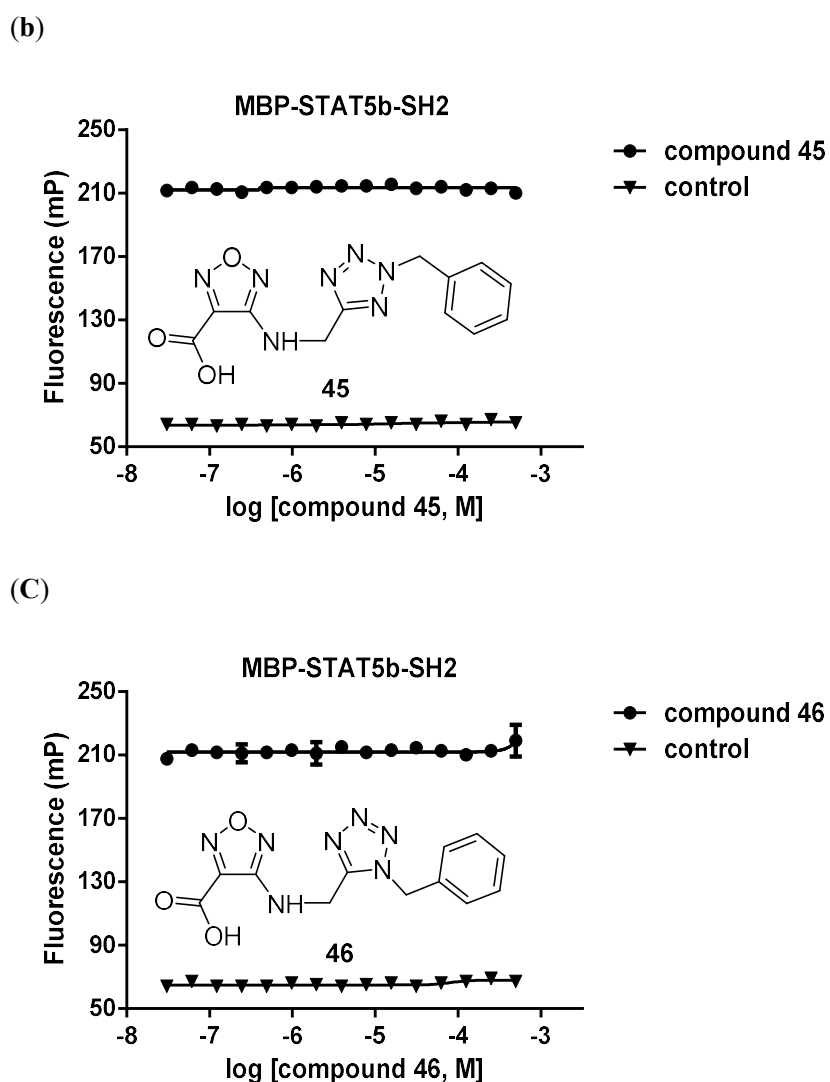
(a)

(b)

(C)
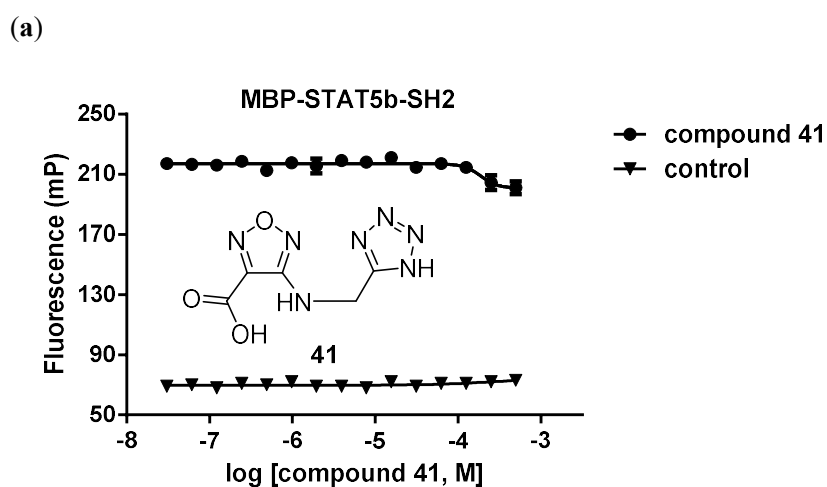
Figure 4.6. Competitive FP assays suggested 5-aminomethyl tetrazole compounds **41 (a)**, **45 (b)**, and **46 (c)** were inactive to MBP-STAT5b-SH2 (error bars denote mean ± SD, n = 2).

The unexpected results imply that some critical interactions between the inhibitor and STAT5 must be lost after the scaffold 1-aminomethyl tetrazole was transformed to 5-aminomethyl tetrazole. More specifically, the conversion of *C-N* bond to *C-C* bond between the aminomethyl group and the tetrazole ring results in the loss of binding activity to STAT5. According to the binding mode of 1-aminomethyl tetrazole to STAT5-SH2, Asn642 is a key residue in the neighboring area of the *C-N* bond within the phosphotyrosine binding site. The amide amino of Asn642 serves as hydrogen bond donor to attract the tetrazole ring to the pocket. The adjacent residues Trp641, Leu643, and Met639 make up an amphiphilic pocket

that can also form interactions with the tetrazole moiety. Compound **1** is not capable of forming these interactions with STAT5, which leads to a significant difference in binding affinity in contrast to the tetrazole-containing derivatives. This is a hint to explain the completely different affinities between **2** and **41**, **3** and **46**, although they are structurally similar. As the conversion of *C-N* bond to *C-C* bond could alter the tetrazole's energetically favorable pose, keeping the moiety away from Asn642 and the adjacent pocket, leading to its exposure to the solvent. Besides, the conformation change could in turn break the adjacent hydrogen bond between the secondary amino group and Asn642, resulting in a potential binding mode that is similar to that of the phosphotyrosine mimetic 4-formylphenyl phosphate reported in Wong's work[65] (**Figure 4.7**). Considering the phosphotyrosine binding site is a shallow pocket, it seems unlikely for the new conformation to generate extra interactions within this area.
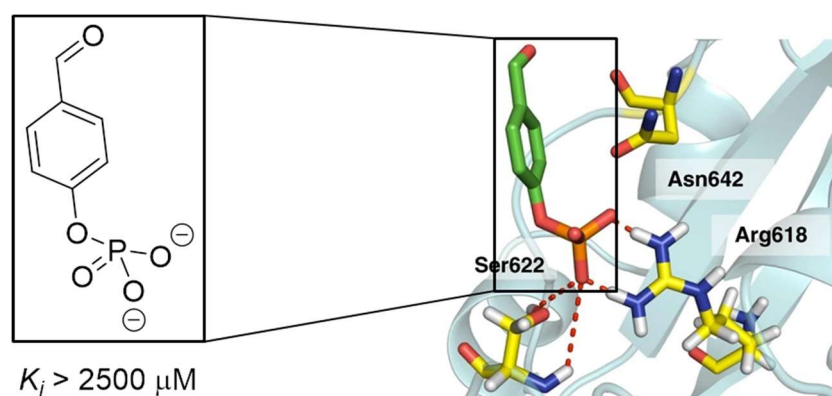

Figure 4.7. Molecular binding mode of phosphotyrosine mimetic 4-formylphenyl phosphate to STAT5 phosphotyrosine binding site. Hydrogen bonds are shown as red dashed lines[65].

Another possible reason for the activity difference was predicted in a new molecular docking experiment by using the homology model of human STAT5b-SH2. Five possible active sites of the SH2 domain were calculated by the software Molecular Operating Environment (MOE). One site that includes Lys600, Arg618, Asp621, Ser622, Asn642, and Met644 best matches the phosphotyrosine binding area was chosen as the docking pocket. Compounds **2** and **41** were then docked into the pocket respectively and 10 poses for each

compound were generated by GOLD. The preferred binding mode of active compound **2** is shown in **Figure 4.8** (**a**). The residues Arg618, Ser622, and Asn642 suggested by Wong's work are involved in the interactions within the new binding mode. However, the orientation of the molecule is reversed. In this binding mode, the tetrazole ring forms hydrogen bonds with Arg618 and Ser622 while the furazan carboxylate interacts with Asn642. As for the energetically favorable pose of inactive compound **41**, the interactions between the tetrazole and Arg618 are retained but the conformation of the furazan moiety has been different. As shown in **Figure 4.8** (**b**), the furazan carboxylate is exposed to the solvent, resulting in the loss of key interactions between the structure and Asn642.

(a)   **(b)**
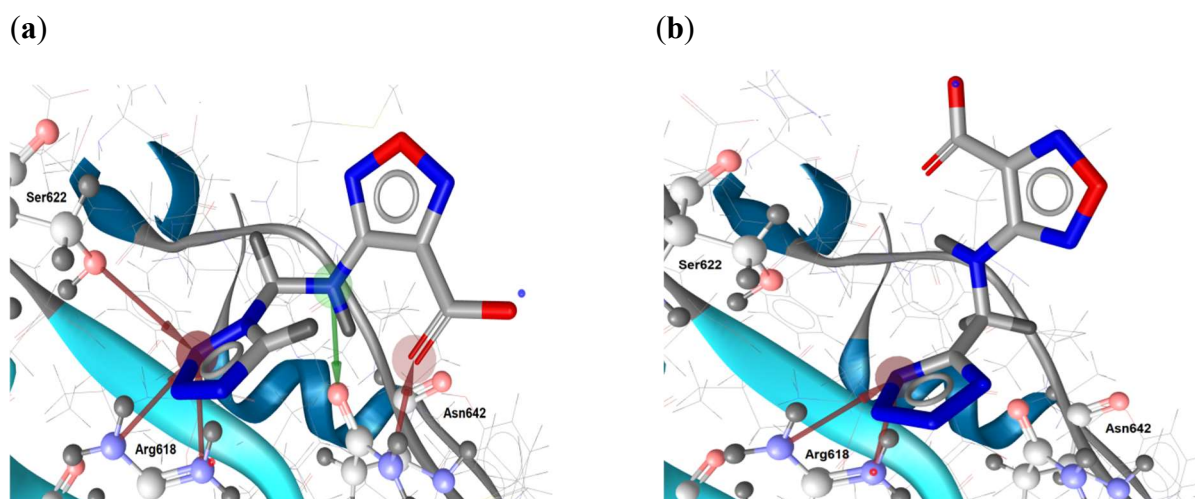
Figure 4.8. Preferred docking poses of compounds **2** (**a**) and **41** (**b**) in the binding cavity of STAT5-SH2. Hydrogen bonds are illustrated as arrows. Pictures were generated by ligandScout 4.2.

Both of the above speculations conclude the main cause for potency loss of 5-aminomethyl tetrazole scaffold could be conformation changes to the moiety that interacts with Asn642. However, the actual binding mode and the mechanism behind the possible conformation differences still need to be scrutinized computationally and crystallographically.

5. Study of 1-aminomethyl tetrazoles

5.1. Synthesis of 1-aminomethyl tetrazoles

In order to improve the activity and stability of the scaffold, another possible way is to attach different substituents to the 5-position of the tetrazole ring. Because structure extension could bring the possibility of binding to additional sites that were beyond reach previously. Besides, different substituents at the tetrazole ring could have diverse impacts on the stability of this scaffold. The following method was applied to synthesize theses derivatives.

5.1.1. Synthesis of 4-amino-furazan-3-carboxylic acid

The fragment 4-amino-furazan-3-carboxylic acid **1** is a necessary building block in the synthesis of 1-aminomethyl-5-substituted tetrazoles in this study. A one-pot method introduced by Sheremetev et al.[114, 115] was applied in the synthesis of compound **1**. The commercially available ethyl 2-cyanoacetate was used as the starting material.
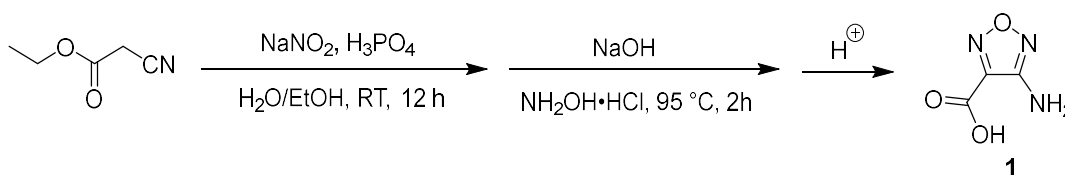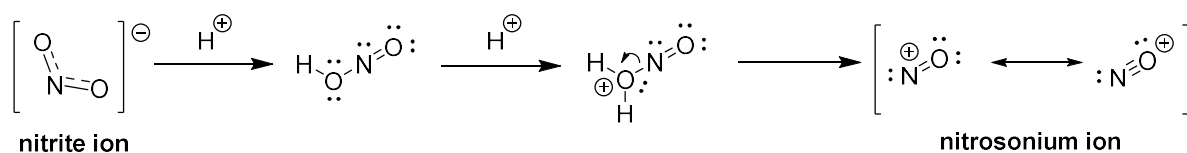

Scheme 5.1. One-pot synthesis of 4-amino-furazan-3-carboxylic acid **1**.

One potential explanation of the mechanism (**Scheme 5.3**) is that ethyl 2-cyanoacetate is first transformed into an enol intermediate in the presence of orthophosphoric acid. Meanwhile, in acidic condition, the nitrite ion is converted to nitrosonium ion (**Scheme 5.2**), which acts as a electrophile to react with the double bond of the enol to give a cyano oxime intermediate. The cyano oxime compound is subsequently converted to the dioxime

intermediate by treatment with hydroxylamine hydrochloride. Cyclization then happens under heating and vigorous stirring. After acidification, approximately two thirds of the amino acid product was obtained as white precipitation, which was pure enough for the following synthesis. The rest of the product was extracted from the filtrate with ethyl acetate.
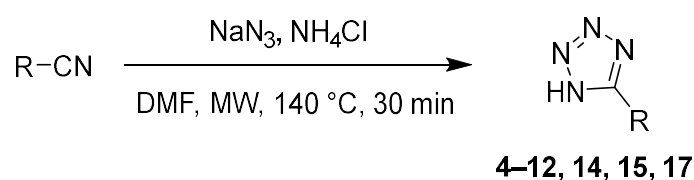

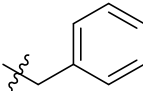**Scheme 5.2.** Mechanism of nitrosonium ion formation from nitrite ion in acidic condition.
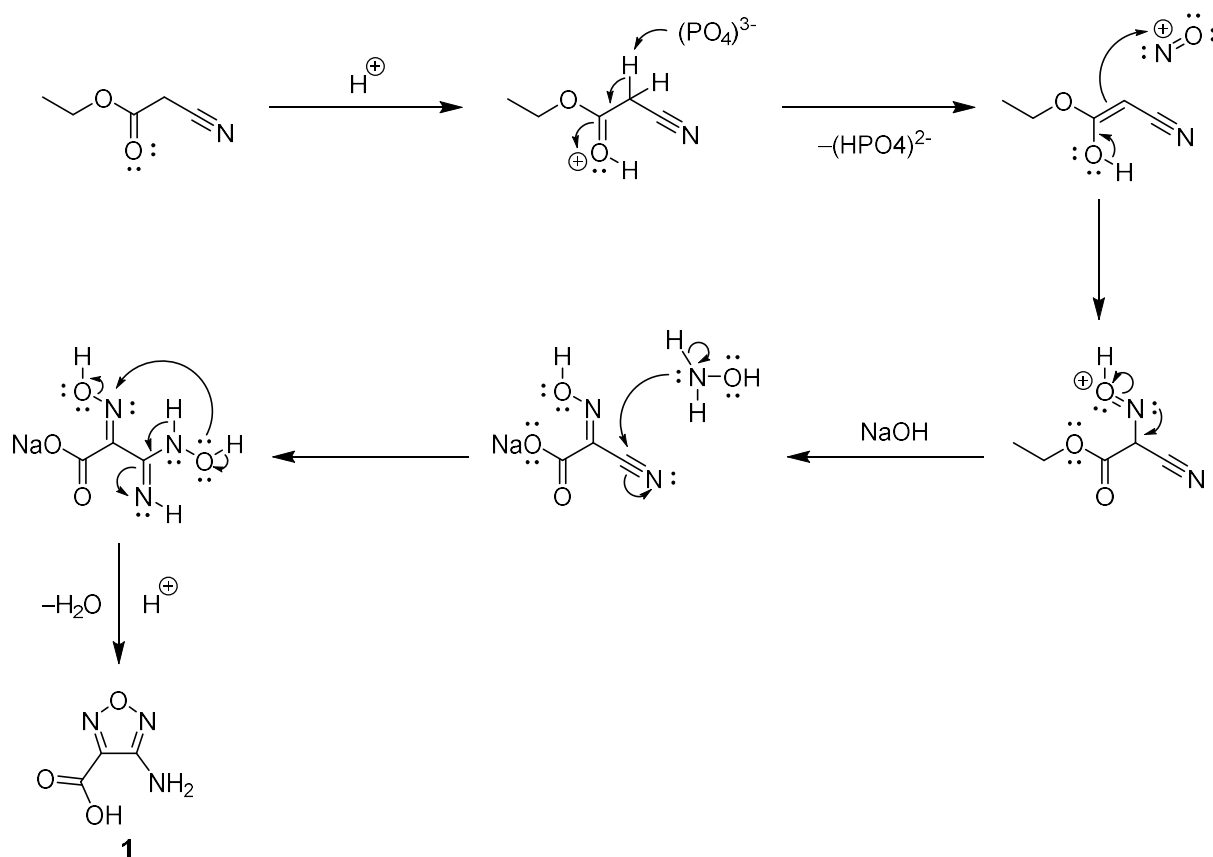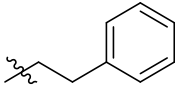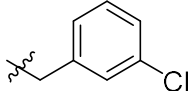

Scheme 5.3. A potential mechanism of 4-amino-furazan-3-carboxylic acid formation.
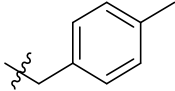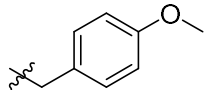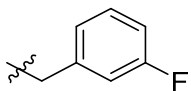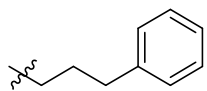
5.1.2. Synthesis of 5-substituted tetrazoles

The synthesis of 1-aminomethyl tetrazoles proceeded in two steps. A nitrile starting reactant was first converted to the corresponding 5-substituted tetrazole compound in the presence of 2 equivalent of sodium azide (NaN_3) and 1.1 equivalent of ammonium chloride. Previously, this 1,3-dipolar cycloaddition reaction was conducted under normal heating in DMF at 100 °C[116] with a reaction time of 3 h. By utilizing microwave reactor[117-119], the reaction time was decreased to 30 min. The yield of each compound varies depending on the R group at the 5-position of the tetrazole ring (**Table 5.1**).

$$R-CN \xrightarrow[\text{DMF, MW, 140 °C, 30 min}]{NaN_3, NH_4Cl}$$

4–12, 14, 15, 17

Compound	R	Yield (MW)
4		41%
5		46%
6		74%
7		65%
8		41%
9		66%
10		67%

43
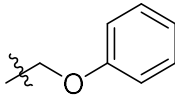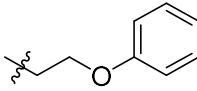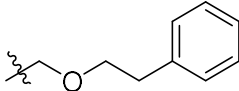
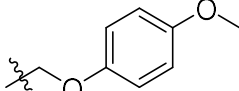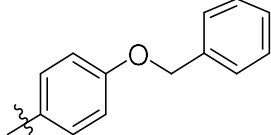| 11		91%
12		15%
14		98%
15		97%
17		99%

Table 5.1. Yields of 5-substituted tetrazole compounds in microwave-assisted reactions.

Remarkably, products with an *O*-containing linkage between the tetrazole ring and the phenyl group display high yields in the tetrazole formation reactions except for compound **12**. The reason could be the electron-withdrawing effect of *O*-containing linkage on the nitrile increases its reactivity in the reaction. As positive charge on the the nitrile group is favorable to the nucleophilic attack from the azide anion. While the substituents on the phenyl ring didn't show such big influence on the yields, which could attribute to the relatively long distance from the nitrile group, comparing that between the oxygen atom and the nitrile group.
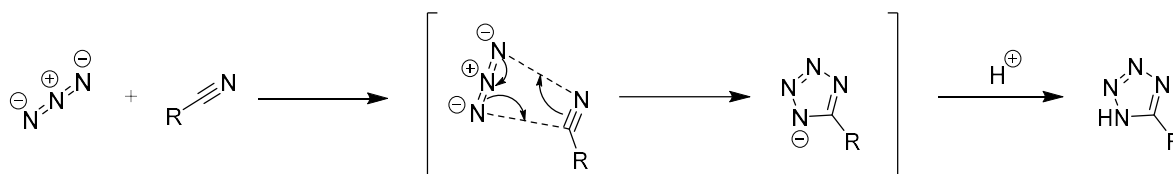
Scheme 5.4. Mechanism of 5-substituted tetrazole formation through concerted 1,3-dipolar cycloaddition.

5.1.3. Mannich ligations

The last step is the Mannich ligation reaction (**Scheme 5.5**). 4-amino-furazan-3-carboxylic acid (**1**), formaldehyde and a 5-substituted tetrazole were used in this three-component reaction. In the beginning compound **1** was not completely soluble in acetonitrile. After addition of formaldehyde the suspension gradually became a clear solution, indicating the formation of the imine intermediate. The 5-substituted tetrazole building block was then added into the solution and the resulting mixture was stirred for 16 h at room temperature. Afterwards, the product was isolated by column chromatography. The conversion of the starting materials was not complete even enough reaction time was given and the reaction temperature was increased, resulting in the low yield of this reaction. The incomplete conversion of the reaction could be due to the instability of the products in acidic condition, which will be discussed in the stability study section.
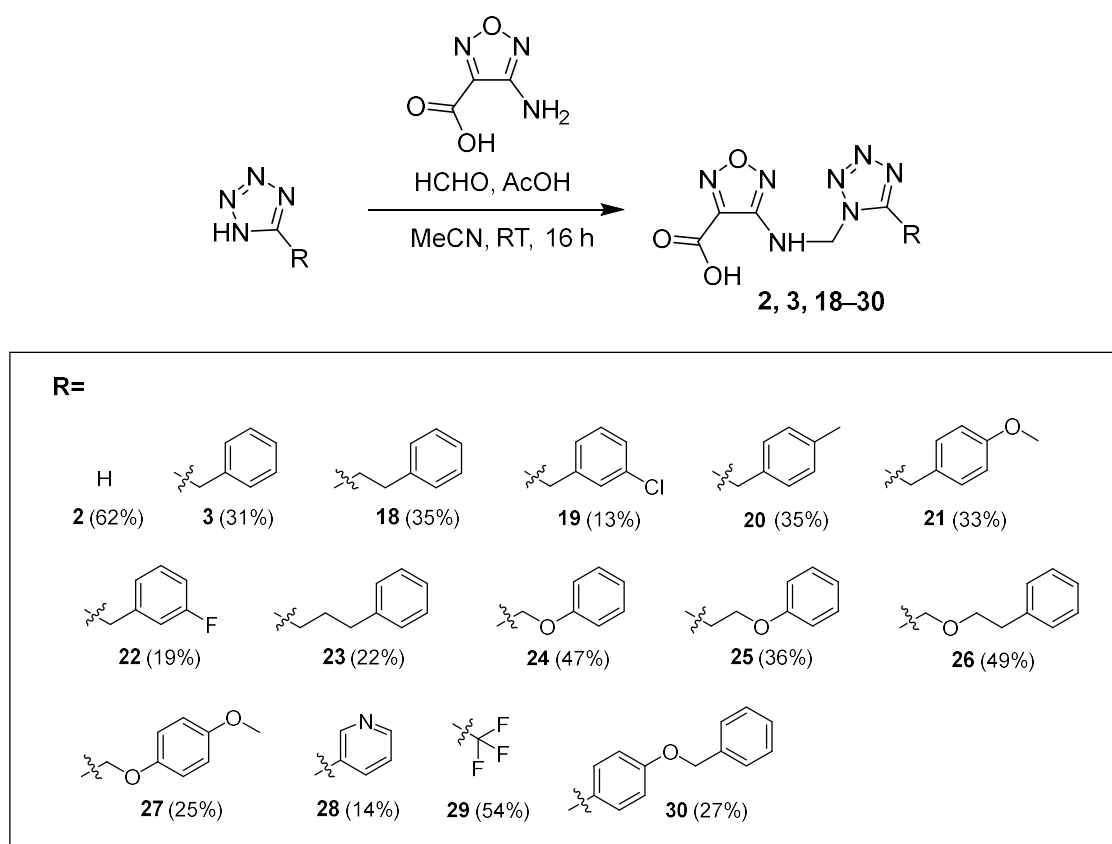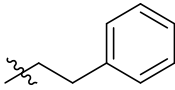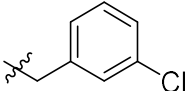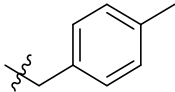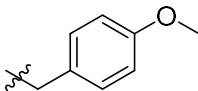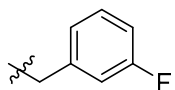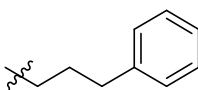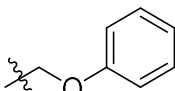
Scheme 5.5. Synthesis of 1-aminomethyl tetrazoles via Mannich ligation reactions.

5.2. Determination of binding activity

The binding activity of the 1-aminomethyl tetrazoles were measured in competitive FP assays using the same protocol introduced in the previous chapter. The IC$_{50}$ and K_i values of the compounds are summarized in **Table 5.2**. Most of them demonstrate a binding activity in low micromolar range, in which compound **24** is the most active with a K_i value of 1.8 μM (**Figure 5.1**).
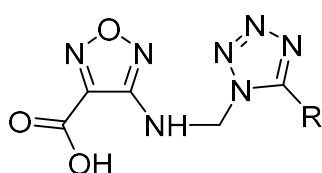
Compound	R	IC$_{50}$ (μM)	K_i (μM)
2	H	7.1	2.2
3	Bn	12.7	3.8
18		14.4	4.4
19		9.8	3.0
20		9.6	2.9
21		9.4	2.9
22		8.6	2.6
23		28.7	8.7
24		5.9	1.8

25		9.2	2.8
26		7.2	2.2
27		23.2	7.0
28		16.5	5.0
29		65.4	19.8
30		9.3	2.8

Table 5.2. Summary of the IC_{50} and K_i values of 1-aminomethyl tetrazoles in FP assays.
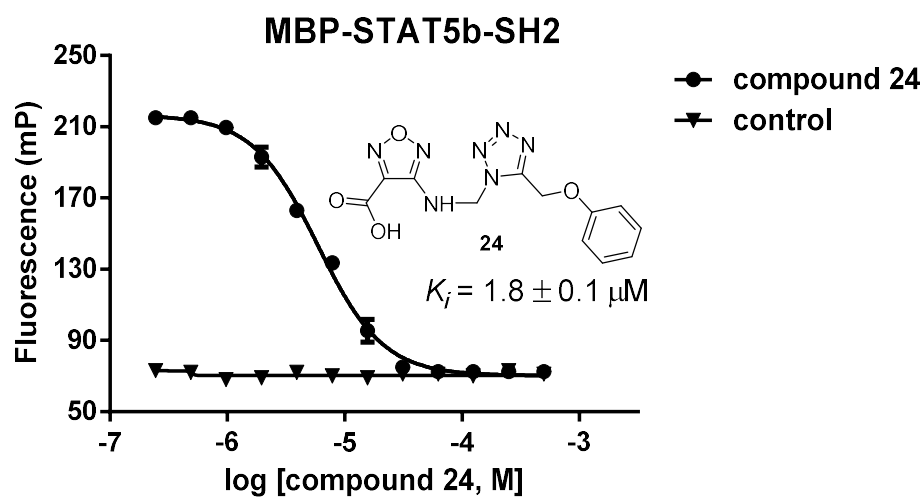
Figure 5.1. Binding activity of compound **24** to MBP-STAT5b-SH2 (error bars denote mean ± SD, n = 2).

5.3. Stability study of 1-aminomethyl tetrazoles

The 1-aminomethyl tetrazoles synthesized through Mannich ligation reactions showed good binding activity towards STAT5 protein in FP assays. However the scaffold was found unstable in aqueous medium with acidic pH. For example, after purification the above products were measured by LC-MS with acidic mobile phase (0.1% formic acid additive in acetonitrile/water), most of the resulting chromatograms displayed three main signals that belonged to the product, the corresponding 5-substituted tetrazole and the furazan compound **1** respectivly (**Figure 5.2**). This phenomenon indicated that the products were decomposed back into the starting materials of the corresponding ligation reactions. Only compounds **28** and **29** didn't show significant decomposition under the above condition. A possible mechanism is shown in **Scheme 5.6**. The break of the bond between aminomethyl and tetrazole ring gives iminium ion and 5-substituted tetrazolate ion intermediates. In the presence of enough acidity and water, they are transformed into fragment **1** and 5-substituted tetrazole respectively. The instability of the inhibitors could have a negative effect on their biological activity. Because in the HRMS measurement, the mass of the theoretical ligand-protein complex couldn't be found after sufficient incubation in the FP buffer, which excludes the possibility of irreversible binding mode.
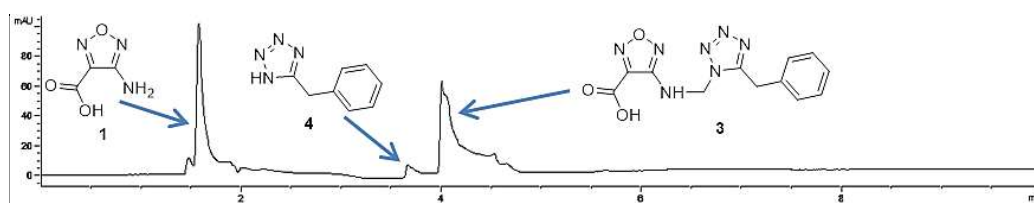
Figure 5.2. Compound **3** was decomposed in the process of chromatography using acidic mobile phase (wavelength = 254 nm).

To clarify how the environmental acidity and different substituents on the tetrazole influence the stability of the compounds and to find out possible stable molecules, an LC-MS based stability study was carried out. Compounds **27** and **30** were excluded because they precipitated in buffer. The testing compounds were first dissolved in a 20 mM ammonium

bicarbonate buffer at pH 7.4 to concentrations range from 0.5 mM to 1.5 mM (c_n). The resulting solutions were measured immediately by LC-MS at 254 nm wavelength with a 10 mM ammonium bicarbonate containing mobile phase (acetonitrile/water) at pH 7.4. No significant decompositions were found on the resulting chromatograms (e.g. compound **3**, **Figure 5.4**). The absorbance peaks of the testing compounds were then integrated and the nominal extinction coefficients (ε_n) of them under the above condition were calculated according to the Beer–Lambert law (**Equation 5.1**), which was used to reflect the decomposition degrees of the compounds in this work.
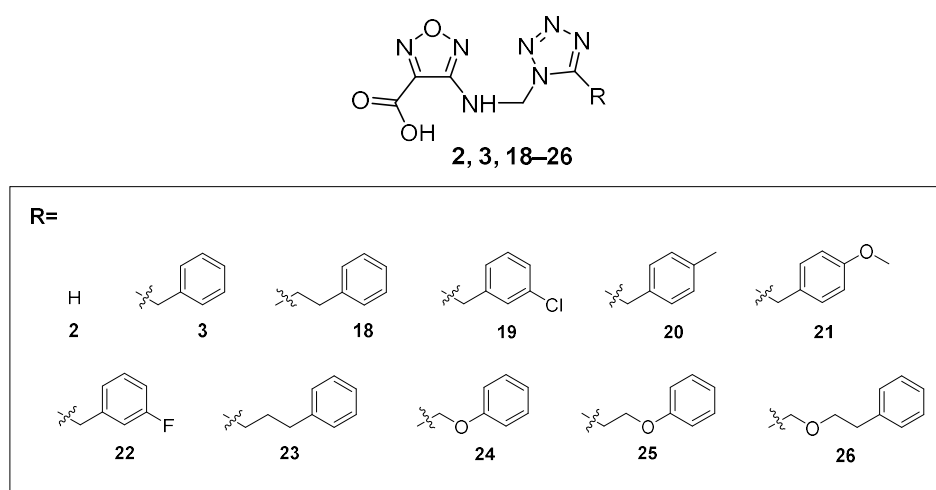
Figure 5.3. Structures of the testing compounds in the LC-MS based stability study.
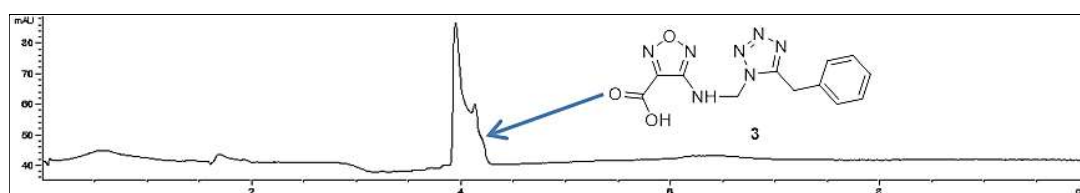
Figure 5.4. Chromatogram of compound **3** at 254 nm using acetonitrile/water mobile phase containing 10 mM ammonium bicarbonate at pH 7.4.

$$\varepsilon_n = \frac{A_I}{c_n l}$$

Equation 5.1. Calculation of the nominal extinction coefficients (ε_n) of the testing compounds at 254 nm according to the Beer-Lambert law, where A_I is the integrated absorbance of a testing compound, c_n is the nominal concentration of the compound, and l is the path length of the DAD flow cell in the LC system.

The next step was to investigate the influences of acidity and different substituents on the stability of these compounds. 20 mM ammonium acetate solution was chosen as the medium to dissolve the testing compounds as it has an acidic buffer range of pH 5.8 to 3.8, which best met the needs of this experiment[120]. 10 mM ammonium bicarbonate containing acetonitrile/water at pH 7.4 remained as the mobile phase of the LC system to minimize the possibility of compound decomposition in the process of chromatography. Each of the eleven compounds was first dissolved in DMSO to give a 20 mM stock solution, which was then diluted by four 20 mM ammonium acetate solutions at pH 5.8, 4.8, 3.8 and 2.8 respectively to the concentration of 1 mM (c_n). After 30 min, 3 µl of each solution was injected into the LC-MS system for measurement (e.g. compound **24**, **Figure 5.5**).
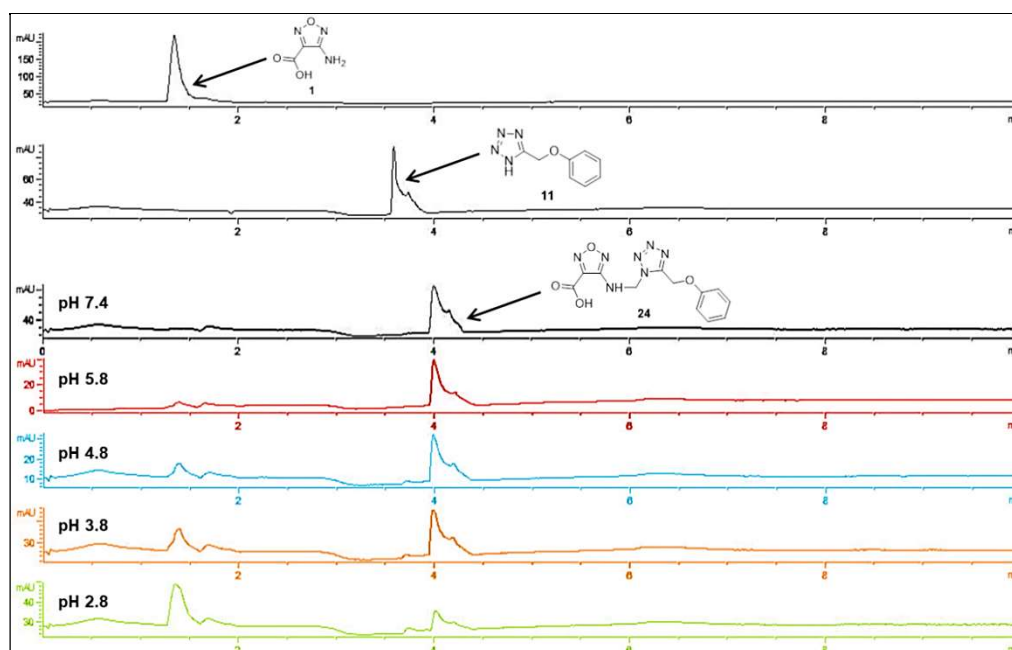
Figure 5.5. Chromatograms of compound **24** at 254 nm after dissolution in buffers with different pH values.

The absorbance peaks of the testing compounds on the resulting chromatograms were integrated and the nominal extinction coefficients (ε_n) of the compounds at different pH values were calculated using **Equation 5.1**. To reflect the decomposition degree more directly, the ε_n values of each compound under four acidic conditions were then divided by the corresponding ε_n at pH 7.4 to represent the relative absorbances (A_r), which are shown in **Figure 5.6**.
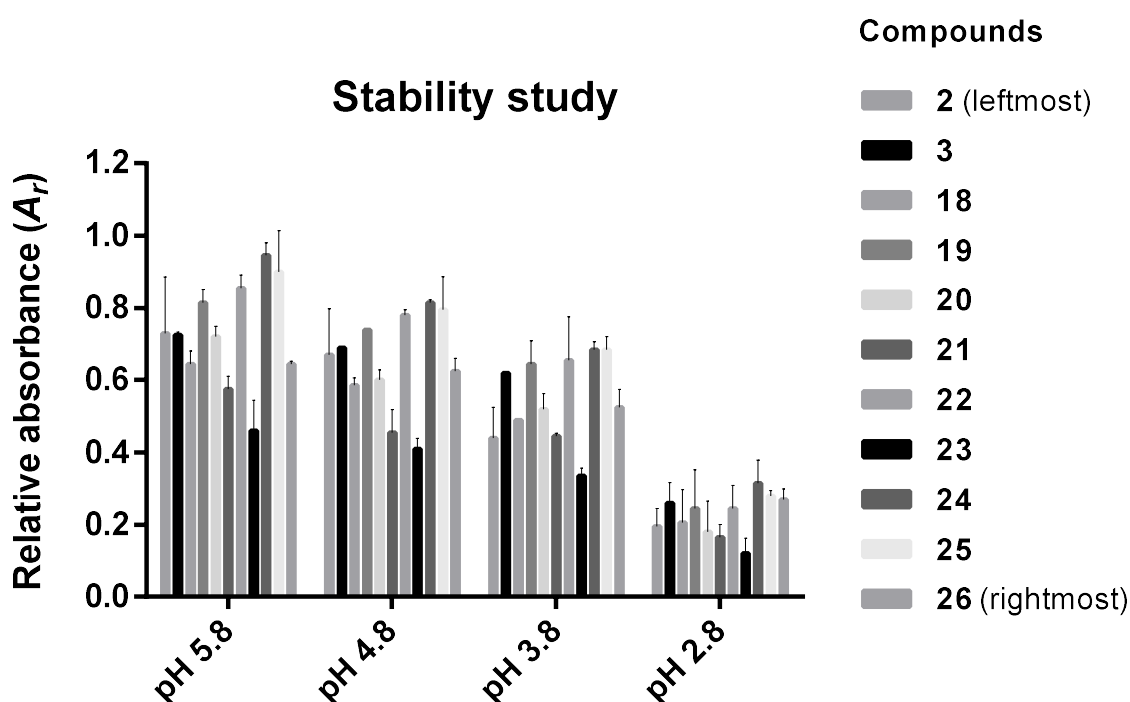
Figure 5.6. Decomposition degrees of compounds **2**, **3**, **18**–**26** in acidic buffer solutions with different pH values (error bars denote mean ± SD, n = 2).

In the above graph, a larger A_r value denotes that more molecules of a certain compound are intact, in other words, less decomposition has happened when compared with a smaller A_r. As the result shows, the acidity of the aqueous medium obviously has a negative effect on the stability of 1-aminomethyl tetrazoles. For each compound, the decomposition degree is extended as the acidity of the buffer increases. Among the eleven compounds, **24** and **25** are the most stable ones in all the four acidic conditions, indicating phenoxyalkyl substituents at

the 5-position of the tetrazole ring are favorable for the structure's stability. As for the benzyl-substituted compounds **3**, **19**, **20**, **21**, and **22**, electron-withdrawing groups on the phenyl ring are beneficial to the stability as **19** and **22** are generally more stable than **3**. While the decomposition degrees of **20** and **21** are greater than **3** suggesting that electron donating groups on the phenyl ring are unfavorable for maintaining the stability. When comparing the stability differences among compounds **3**, **18** ,and **23**, long aliphatic chain on the tetrazole ring is obviously a disadvantage. Because **23**, containing three methylene groups, is the least stable one in the three compounds and even is in the all eleven compounds. While **3**, which possesses only one methylene group, is more stable than **18** and **23**. This interpretation could also explain the reason that compound **26** is less stable than **24** and **25** in this experiment. To sum up, the substituent at the 5-position of the tetrazole ring has a remarkable influence on the stability of 1-aminomethyl tetrazoles. Electron-withdrawing effect is beneficial for the stability of the scaffold in acidic conditions while electron donating effect is a disadvantage. These findings are consistent with the facts that compounds **28** and **29** are stable in LC-MS measurements with acidic mobile phase and compound **2** without 5-substituent on the tetrazole ring generally possesses a stability extent between the consequences of the two opposite electronic effects.

In the chromatograms of this stability study, the absorbance peak of each substituted tetrazole compound is shown as a doublet, of which the two peaks have identical masses. The reason could be that 2,5-disubstituted regioisomers formed from the corresponding 1,5-disubstituted tetrazoles in the above buffer conditions. The possible mechanism (**Scheme 5.6**) of this isomerization could first follow the same step as that in the decomposition mechanism to give the iminium cation and the tetrazolate anion intermediates. The subsequent nucleophilic attack from the tetraolate anion on the iminium, which is not acid-driven, furnishes the corresponding 2,5-disubstituted regioisomer. This mechanism is consistent with the fact that decomposition and possible isomerization of the testing compounds exist simultaneously in the above acidic conditions according to the chromatograms.
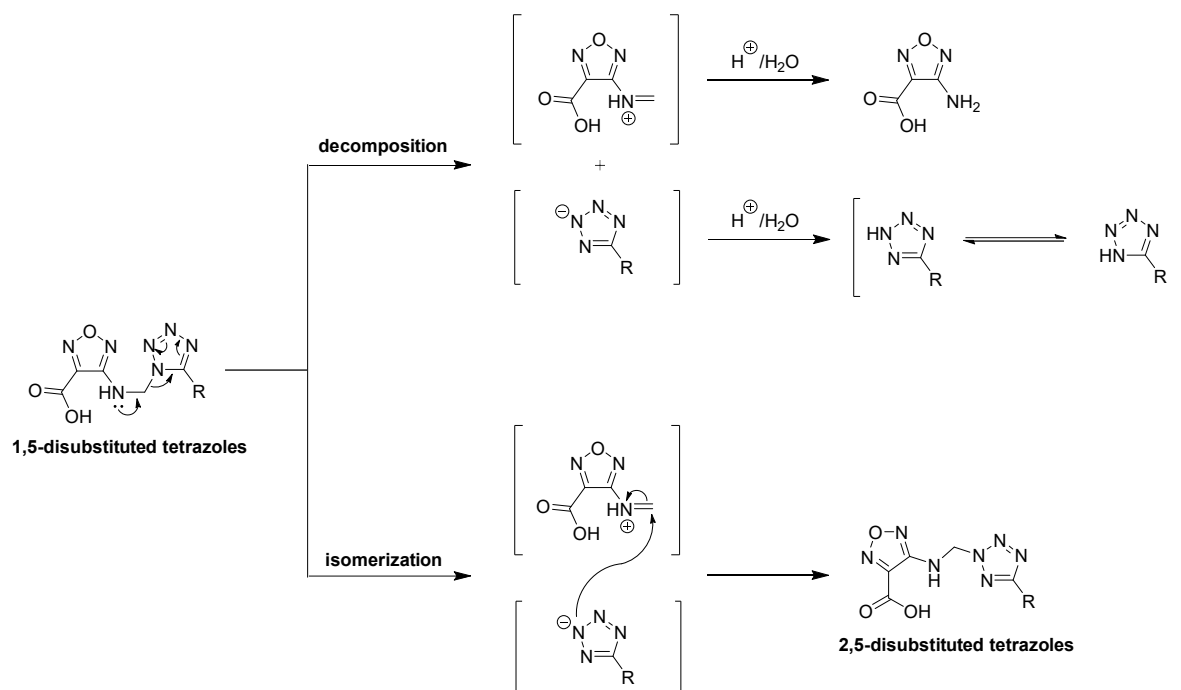
Scheme 5.6. Possible decomposition and isomerization mechanisms of 1,5-disubstituted tetrazoles

5.4. Validation of binding to STAT5b-SH2

Considering that compound **24** showed the best activity in FP binding assay, it was chosen for a thermal shift assay to validate the binding to STAT5-SH2. The mechanism of this assay is that the binding of a ligand can increase the thermal stability of its target protein, leading to a shift of melting temperature. Gradually increased temperature allows the protein to unfold and expose its hydrophobic surfaces. Fluorescent dye SYPRO Orange then is able to nonspecifically bind to the hydrophobic surfaces leading to an increase in fluorescence. By recording the variation of fluorescence with increased temperature, the denaturation midpoint (melting temperature, Tm) can be determined. An increase of Tm indicates enhancement of protein thermal stability due to ligand binding[121-124].

In the presence of SYPRO Orange, MBP-STAT5b-SH2 was treated with serial concentration of compound **24** or DMSO. The melting temperature of MBP-STAT5b-SH2 protein was 48 °C. In contrast, the addition of **24** increased the melting temperature to 58 °C (**Figure 5.7**). On the other hand, when the protein tag MBP was added instead of

MBP-STAT5b-SH2 protein in the same condition, the melting temperature of MBP didn't change after incubation with **24**. The results further validate that STAT5-SH2 is the binding target of **24** and the potential positive role of MBP in the binding event has been excluded.

(**a**)

(**b**)
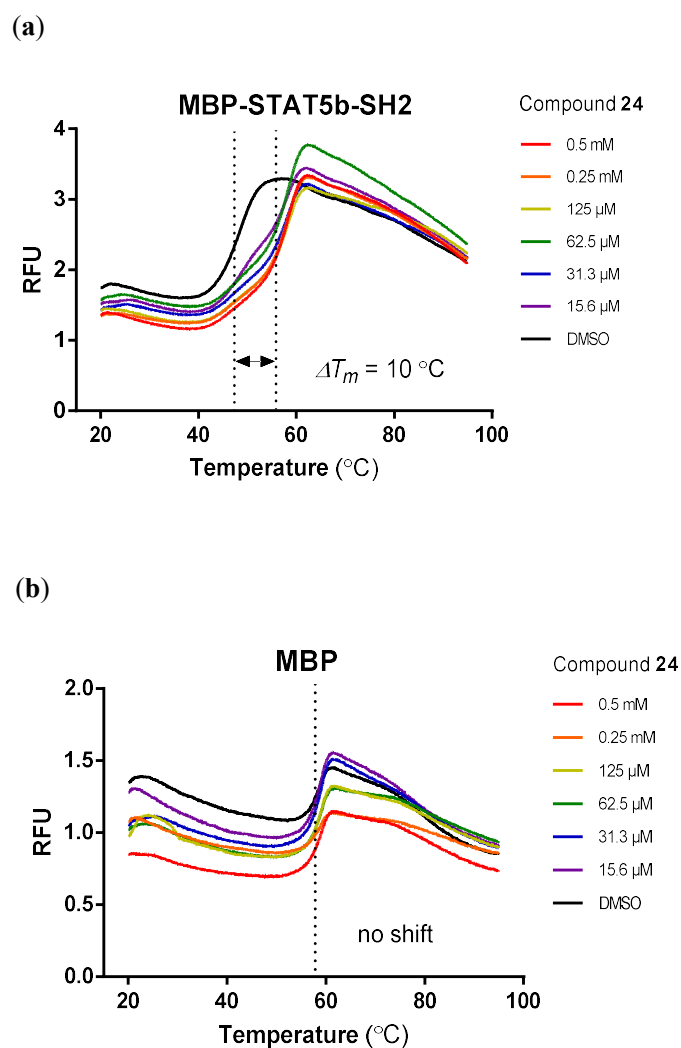
Figure 5.7. Thermal shift assay results of compound **24**. (**a**) Compound **24** bound to MBP-STAT5b-SH2 leading to an increase of protein melting temperature. (**b**) No thermal shift was observed indicating compound **24** did not bind to MBP.

5.5. Binding of compounds to STAT5b N642A

As mentioned before, Asn642 was crucial to the binding affinity between a ligand and STAT5b-SH2. Specifically to this work, the carbonyl and the amide-NH_2 of Asn642 were responsible for the formation of hydrogen bonds with the active compounds. To further confirm the importance of Asn642, the MBP-STAT5b-SH2 N642A protein was generated by site-directed mutagenesis. Binding of fluorophore-labeled peptide 5-CF-GpYLSLPPW-NH_2 to STAT5b N642A displayed a K_D value of ca. 5 μM[65], representing the binding affinity was significantly reduced.
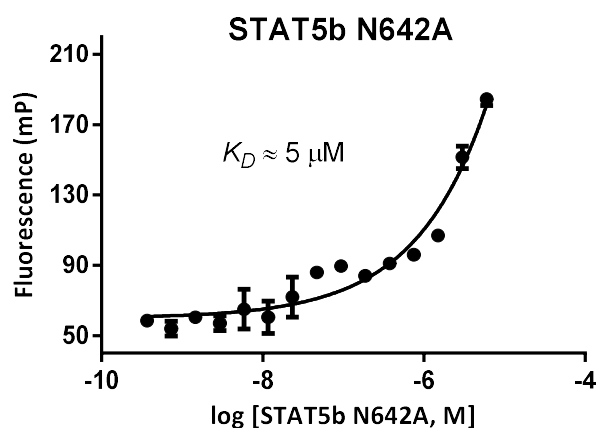
Figure 5.8. Binding of phosphopeptide 5-CF-GpYLSLPPW-NH_2 to MBP-STAT5b-SH2 N642A[65].

The binding affinity of compound **2** to MBP-STAT5b-SH2 N642A was determined by competitive FP assay. A K_i value of 31 μM suggested that the binding affinity of compound **2** to STAT5b N642A was in a 14 fold decrease in comparison with the activity against wild type STAT5b. Similar trend was found in the assay with compound **24**, where binding of compound **24** and mutant STAT5 protein resulted in a 12 fold decrease of affinity (**Figure 5.9**).

(a)

(b)
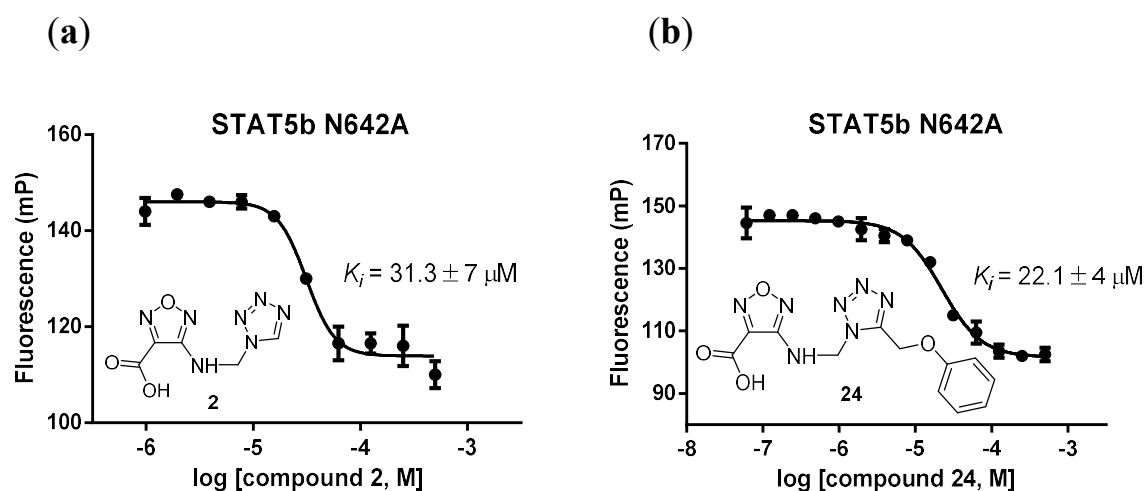
Figure 5.9. (**a**) Binding of compound **2** to MBP-STAT5b-SH2 N642A displayed a 14 fold decrease in the affinity. (**b**) Compound **24** showed a K_i value of 22 μM instead of 1.8 μM for the wild type protein.

These results validate that Asn642 in SH2 domain plays a pivotal role in the binding between ligands and STAT5 protein. Although the affinity of phosphopeptide 5-CF-GpYLSLPPW-NH$_2$ was strongly reduced, the importance of other possible binding sites should not be ignored, because compounds **2** and **24** still maintained K_i values of 31 μM and 22 μM respectively.

5.6. Inhibitory effect on leukemic cell proliferation

It has been well demonstrated that internal tandem duplication (ITD) mutation in FMS-like tyrosine kinase 3 (FLT3) gene is one of the most frequent genetic abnormalities in acute myeloid leukemia (AML) patients[40, 125-127]. The receptor tyrosine kinase FLT3 with the ITD mutation leads to the constitutive activation of STAT5, making it a key factor in the pathogenesis of AML. It would be interesting to examine the influence of STAT5 inhibitors on AML related cells' viability. Hence, the biological activity of compounds **3** and **24** were further studied in an Alamar Blue assay using human AML cell line MV-4-11, which carries the FLT3-ITD mutation. In this assay, the MV-4-11 cells in a 96-well microtiter plate were first treated with serial concentration of compounds. After 72 h of incubation, Alamar blue

solution was added and the proliferation of the cells was then determined by fluorescence spectrophotometry. The result validates the inhibitory effect of the 1-aminomethyl-5-substituted tetrazoles against the survival of AML cells (**Figure 5.10**).
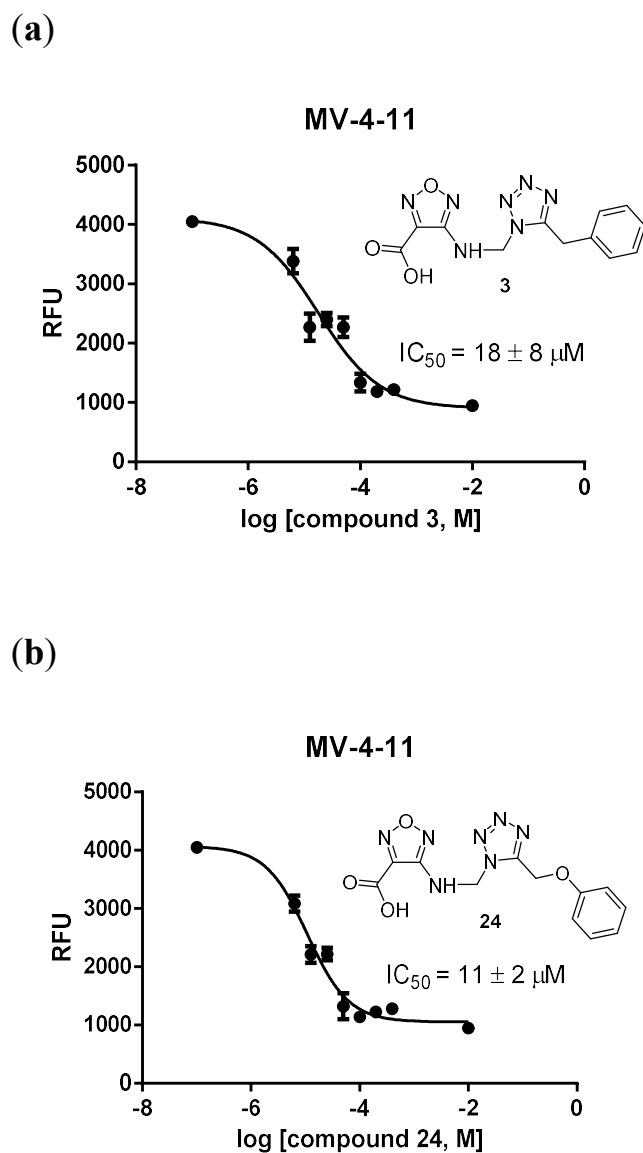
(a)

(b)

Figure 5.10. The proliferation of MV-4-11 cells was inhibited by compounds **3** (**a**) and **24** (**b**) in the Alamar Blue assay after 72 h of incubation (n=3).

6. Summary and outlook

This work has elaborated the investigation of the tetrazole-containing compounds derived from furazan-based phosphate mimetics to discover STAT5 inhibitors with improved potency and stability.

In the first section of this work, 5-aminomethyl tetrazoles were designed based on the scaffold of the lead compounds **2** and **3**, and four synthetic routes were planned. Due to the low reactivity of the amino group in fragment **1** as a nucleophile, the first three routes failed to give the expected products. In the fourth route, a Strecker-type reaction was used to first give the key intermediate **40**. The nitrile functional group in **40** was then used to form the tetrazole ring via 1,3-dipolar cycloaddition reaction. In this way, the 5-aminomethyl tetrazole scaffold was obtained. The synthesis of the stable 5-aminomethyl tetrzaole scaffold has been thoroughly studied and discussed although it is inactive to the expected target. The possible conformation reasons for the inactivation was speculated in docking experiments.

In the second section, efforts were made to investigate the 1-aminomethyl tetrazole scaffold. A series of 1-aminomethyl tetrazoles with different substituents at the 5-position of the tetrazole ring was synthesized. Most of the 1-aminomethyl-5-substituted tetrazoles have a binding activity to STAT5 SH2 domain in the low micromolar range, in which compound **24** is the most active one with a K_i value of 1.8 μM although the 5-substituent on the tetrazole ring has limited influence on the binding activity. To understand how the substituents on the tetrazole ring influence the scaffold's stability under acidic conditions, a systematic stability study was carried out on LC-MS. The electron-withdrawing 5-substituents were proved to be able to stabilize the scaffold and compounds **19**, **22**, **24**, and **25** were found more stable than the lead compounds. To further verify the binding to STAT5, a thermal shift assay was conducted. The melting temperature of MBP-STAT5b-SH2 was increased by 10 °C after addition of compound **24**, proving the binding to STAT5-SH2 exist. The importance of

Asn642 in STAT5-SH2 was also testified by using STAT5b N642A in the FP binding assay, in which the testing compounds **2** and **24** showed significant potency loss. It reveals the critical role of Asn642 in ligand-STAT5 interactions. Compounds **3** and **24** also showed inhibitory effect against the survival of human AML related cells in the cell proliferation assay.

Looking into the future, further studies on the molecular scaffolds elaborated in this work are still needed. For the 5-aminomethyl tetrazoles, strict computational and crystallographic methods can be reliable ways to reveal the cause for potency loss, which would be significant to the rational design of related STAT5 inhibitors. As for the 1-aminomethyl tetrazoles, efforts should be paid to the furazan moiety in order to discover more favorable STAT5 ligands. Because the 5-substituent on the tetrazole ring didn't show a significant effect on the activity and the space for modification on the tetrazole is already very limited. Thus, structure variations such as amidation on the furazan carboxylate and replacement of the furazan ring by other heterocycles are reasonable ways for further investigation.

III. Experimental Part

7. Materials and methods

7.1. Materials

All chemicals and reagents were purchased from standard suppliers like ABCR (Karlsruhe, Germany), Alfa Aeser (Karlsruhe, Germany), Bachem (Bubendorf, Switzerland), Carl Roth (Karlsruhe, Germany), Fisher Scientific (Schwerte, Germany), Merck (Darmstadt, Germany), Sigma-Aldrich (Taufkirchen, Germany), and VWR (Darmstadt, Germany) and were used without further purification. All reactions described and performed under dry conditions followed the conditions of Schlenk technology. The anhydrous solvents were purchased in HPLC grade from VWR and Merck (Darmstadt, Germany) and were further purified by a MB-SPS-800 solvent purification system from M. Braun (Garching, Germany). Water for HPLC purification and for MS analysis was obtained via a LaboStar ™ UV 2 ultrapure water system from Siemens (Barsbüttel, Germany). Deuterated solvents for NMR spectroscopy were purchased from Carl Roth (Kastellaun, Germany), Deutero (Kastellaun, Germany) and Sigma-Aldrich (Taufkirchen, Germany).

7.2. Used devices and methods

7.2.1. Microwave-assisted synthesis

Microwave-assisted syntheses were carried out on a Initiator$^+$ instrument from Biotage (Uppsala, Sweden). The volume of the septa-sealed, pressure-stable reaction vials used ranges from 5 mL to 20 mL.

7.2.2. TLC

Thin layer chromatograms were performed on silica gel 60 F254 coated aluminum plates from Merck. Compound visualizations were achieved by UV light with wavelengths of 254 nm and 366 nm.

7.2.3. Column chromatographic separation

Column chromatographic separations were carried out in MPLC system with automated fraction collections. Biotage Isolera One system and prepackaged Biotage SNAP cartridges were used.

7.2.4. Preparative HPLC

Purifications of the synthesized compounds by preparative HPLC were performed on an Agilent 1260 Infinity Binary LC System. A C18 HTec, 5 μm column from Macherey Nagel (Düren, Germany) was used for the separation. The eluent was a mixture of acetonitrile/water with a 0.1% trifluoroacetic acid additive. The compounds ($\leq$ 100 mg) to be purified were dissolved in a maximum of 10 mL acetonitrile/water (variable ratios depending on solubility, acetonitrile% $\leq$ 50%). The separations were carried out with linear gradients (5% $\rightarrow$ 95% acetonitrile over a period of 25–35 min at a flow rate of 30 mL/min).

7.2.5. NMR spectroscopy

The NMR spectra were recorded on an ECP500 (Jeol, Akishima, Japan) and an AVANCE III 700 (Bruker, Billerica, MA, USA). The values of chemical shift δ are given in ppm. The reference signals used were the deuterated solvents signal. The ^{13}C spectra were recorded by using 1H broadband decoupling. The multiplicities of signals were described as follows: s (singlet), d (doublet), t (triplet), q (quartet) and m (multiplet). Evaluations of the spectra were performed by *MestReNova 10* (Mestrelab Research, S. L., Santiago de Compostela, Spain).

7.2.6. LC-MS analysis

LC-MS analyses were carried out on an Agilent 1100 series system from Agilent (Santa Clara, CA, USA). The detections were carried out by a diode array detector (DAD) at different wavelengths. The coupled single quadrupole mass spectrometer used electrospray ionization (ESI) to ionize the molecules. The samples to be measured were dissolved in a mixture of acetonitrile/water (1: 1). The mobile phase was a mixture of acetonitrile/water with a 0.1% formic acid additive. The elutions were carried out with a linear gradient (5% → 99% acetonitrile) for 5.5 min, followed by a 4.5 min isocratic elution phase at a flow rate of 1 mL/min. A Phenomenex Luna-C18 (100 × 4.6 mm, 3 μm) column and an Agilent Pursuit XRs C8 (100 × 4.6 mm, 3 μm) column were used for separation.

In the stability study, the mobile phase used was a mixture of acetonitrile/water (pH 7.4), which contained 10 mM ammonium acetate or ammonium bicarbonate instead of formic acid additive. To change the acidic condition to physiological condition, acidic mobile phase was first replaced with neutral acetonitrile/water mixture. The bubbles generated in the storage bottles and pipelines during the replacement should be removed. After being disconnected from the DAD, the column to be used was washed with neutral mobile phase at a flow rate of 0.5 mL/min until a stable pressure was achieved. The column was washed for another 15 min at 1 mL/min. Then, the same procedures were carried out to replace the neutral mobile phase with the physiological one. The DAD should be connected to the column again before measurement.

7.2.7. LC-HRMS analysis

High resolution mass spectra were measured on an ESI-QTOF iFunnel Model 6550 spectrometer coupled with an HPLC system of the Series Infinity II 1290.

7.2.8. Melting point determination

The melting points of the synthesized compounds were determined by a Büch B-545 instrument.

7.2.9. Molecular docking

Molecular Operating Environment (MOE 2019.0102) was used to prepare the homology model of STAT5-SH2 and small molecules. The prepared protein file in PDB format and ligands file in SDF format were loaded into GOLD 5.7.0 for docking. LigandScout 4.2 was used to analyze the docking results.

7.3. Biochemical methods

7.3.1. Protein expression and purification

STAT5b and STAT5b N642A proteins were kindly expressed and purified by Dr. Arkona and Bergemann. Expression of the truncated version of STAT5b (aa 137-747) cloned into a modified pQE70, with N-terminal MBP-tag and C-terminal His-tag was conducted on autoinduction medium (overnight express/Novagen, cat. 71491, Merck, Germany). Cells were grown to an optical density (O.D.) of 0.3 at 37 °C, then the temperature was reduced to 20 °C for further 48 h of expression. Comparable soluble expression levels were obtained with Rosetta2 (DE3) (cat.71400, Novagen, Merck, Germany) and BL21 (DE3) pLysS (cat.69451, Novagen, Merck, Germany). The protein was purified by Ni-chelating chromatography followed by gel filtration (Superdex 200/10 mM HEPES pH 7.8, 100 mM NaCl, 1 mM EDTA, 1 mM DTT, 10% glycerol).A yield of 15 mg MBP-STAT5b-His per liter of culture was obtained and aliquots (200 µl of 3.2 mg ml-1) were quick-frozen and stored at –80 °C, ready for use. Site-directed mutagenesis was performed using PCR-based site directed mutagenesis with high fidelity PWO DNA polymerase (cat.11644947001, Roche, Germany) and confirmed

by Sanger sequencing (Supplementary Figure 9). The mutant proteins were expressed and purified as described above. Purified mutant proteins were further concentrated by ultrafiltration (Amicon 30-kDa MW cut-off; cat. UFC903024, Milipore Corporation, Billerica, MA).

7.3.2. Fluorophore-labeled peptide synthesis

The carboxyfluoresceine-labeled phosphotyrosine octapeptide 5-CF-GpYLSLPPW- NH_2 was kindly synthesized by coworker Accorsi. Peptide synthesis was conducted on Rink amide resin using Fmoc-strategy. PP/PE syringes equipped with a PE-frit were used as reaction vessels. Fmoc-amino acids and reagents were purchased from common suppliers. The coupling reactions were monitored using the Kaiser test and quantified via UV-photometric determination of the dibenzofulvene product following to Fmoc cleavage. The unnatural amino acid N-Fmoc-O-benzyl-phosphotyrosine was pre-activated with TBTU and DIPEA. First, N-Fmoc-O-benzyl-phosphotyrosine (4 eq) was dissolved in a minimal amount of DMF. Then, DIPEA (2 eq) was added and the solution was mixed for 2 min. Afterwards, TBTU (4 eq) was added, the solution was mixed for 3 min and pipetted to the resin. After 4 h the resin was washed and the conversion was analyzed with the Kaiser test.The first amino acid after incorporation of N-Fmoc-O-benzyl-phosphotyrosine was coupled with full conversion using the combination of Fmoc-AA-OH/TBTU/DIPEA (4 eq/4 eq/4 eq) for activation. Subsequent coupling steps were conducted with DIC/HOBt activation. The resin was washed after every coupling and cleavage procedure. First, the resin was washed with 5 syringe volumes of DMF, then with 5 volumes of THF, DCM and Et_2O. The Fmoc-group was cleaved by using a DBU/DMF (2:98 v/v) solution. The resin was suspended in the basic cocktail, shaken and washed. 5-carboxyfluorescein (10 eq.) was pre-activated with DIC/HOBt (10 eq/10 eq) for 2 min and pipetted to the resin. After 1 h, the resin was washed and DBU/DMF (2:98 v/v) was added to cleave formed CF-oligomers. After 15 min the resin was washed and again mixed with DBU/DMF. This procedure was repeated until the solution stayed clear. The phosphotyrosine-containing peptide was cleaved with 95% TFA/water and shaken for 2 h.

The cleaved peptide was filtered and the remaining resin was washed with TFA. The TFA was removed with a stream of dry nitrogen and the residue was dried in high vacuum. The peptide purified with the standard HPLC buffer (0.1% TFA in acetonitrile/water). The product fractions were directly lyophilized affording an orange powder which was dissolved in water and stirred over Amberlite resin (IR120 sodium form) for 1 h. The resin was filtered off and the filtrate was lyophilized to yield the sodium salt as a red-orange powder.

7.3.3. Fluorescence polarization assay

Fluorescence polarization experiments were performed on a Safire II microtiter plate reader from Tecan (Crailsheim, Germany). The final concentrations of buffer components were 50 mM MOPS (pH 7.4), 1 mM EDTA, 0.1% Igepal CA-630, 50 mM NaCl. The final concentration of STAT5b used was 190 nM. The final concentration of the fluorophore-labeled peptide 5-CF-GpYLSLPPW-NH$_2$ was 10 nM. To carry out the measurement, proteins were added to the black 384-well plates (Corning 4514) followed by treatment of peptides and varying concentrations of test compounds with a final concentration of 5% DMSO. Analysis was conducted after 20 min incubation at room temperature. The fluorescence polarization values were expressed in millipolarization units (mP) plotted against the logarithms of concentrations using GraphPad Prism 6 software and the IC$_{50}$ values were converted to K_i values using the modified Cheng-Prusoff equation.

7.3.4. Thermal shift assay

Thermal shift assays were performed on a real-time PCR setup (Light Cycler 480, Roche Diagnostics, Mannheim, Germany) using 96-well PCR plates (cat HSL9901 Bio-Rad Laboratories, Richmond, CA).The final concentrations of buffer components used were 300 mM HEPES (pH 7.4), 175 mM NaCl and 1% DMSO. The final concentration of STAT5 protein was 500 nM. STAT5 protein was treated with varying concentrations of test compounds in the presence of 20x Sypro Orange (cat.S6650, Thermo Scientific, Braunschweig, Germany). The PCR plates were sealed with optical seal, shaken for 15 min,

and centrifuged before measuring. The temperature was increased from 20 °C to 95 °C during the measuring process and the corresponding fluorescence intensity was recorded after every 0.3 s. The curve fitting and melting temperature calculation were performed using GraphPad Prism 6 software.

7.3.5. Cell proliferation assay

The cell proliferation assays were conducted by using a Resazurin based *In Vitro* Toxicology Assay Kit (TOX8-1KT, Sigma-Aldrich, Taufkirchen, Germany). MV-4-11 cells (ATCC CRL-9591, LGC Standards GmbH, Wesel, Germany) were first planted in triplicate in 96-well plates (5×10^3 and 1×10^4 per well for adherent and suspension cells respectively) and incubated in medium containing 10% FBS overnight. The complete medium of adherent cells should be replaced before treatment with compounds. After treated with serial concentration of compounds, the cells were incubated for 72 h. The unused wells were added with PBS to avoid evaporation effects. Alamar Blue solution was then add into each well and the cells were incubated overnight. The fluorescence values were read at an excitation wavelength of 560 nm and a emission wavelength of 590 nm.

8. Synthesis regulations

8.1. General synthetic methods

Method 1: 5-substituted-1*H*-tetrazole formation

To a solution of the corresponding nitrile compound (6 mmol, 1 eq) in DMF (10 mL) was added sodium azide (780 mg, 12 mmol, 2 eq) and ammonium chloride (353 mg, 6.6 mmol, 1.1 eq). The reaction mixture was stirred and heated under microwave at 140 °C for 30 min. After cooling to room temperature, the mixture was treated with water (50 mL), then acidified with concentrated HCl to pH 2. The resulting solution was extracted with ethyl acetate (3×30 mL). The combined organic phases were washed with brine, dried over Na_2SO_4, and concentrated under reduced pressure. The residue was purified by column chromatography (SiO_2, n-hexane/ethyl acetate, 40% $\rightarrow$ 70% ethyl acetate) to afford pure product.

Method 2: Mannich ligation reaction

To a stirred suspension of 4-amino-furazan-3-carboxylic acid (129 mg, 1 mmol, 1 eq) and the corresponding 5-substituted-1*H*-tetrazole (1.5 mmol, 1.5 eq) in acetonitrile (4 mL) was added 36% formaldehyde solution (154 µL) and glacial AcOH (300 µL). After stirring for 16 h at room temperature, the solvent was directly removed under reduced pressure. The residue was purified by column chromatography (SiO_2, n-hexane/ethyl acetate, 40% $\rightarrow$ 80% ethyl acetate).

Method 3: preparation of hydrazoic acid solution

A suspension of sodium azide (1.95 g, 30 mmol) in water (2 ml) was prepared, to which was added chloroform or toluene (12 mL) and the mixture was cooled to 0 °C. Concentrated

sulfuric acid (800 μL) was then added dropwise to this stirred mixture under cooling. After the addition of sulfuric acid, the organic layer was decanted and dried over anhydrous sodium sulfate.

8.2. Synthesized compounds

4-Amino-furazan-3-carboxylic acid 1
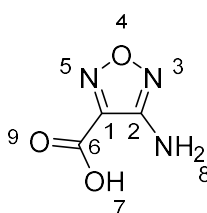
To a stirred suspension of ethyl cyanoacetate (14.2 g, 125 mmol, 1 eq) and sodium nitrite (8.7g, 125 mmol, 1 eq) in a mixture of absolute ethanol (8.5 mL) and water (100 mL) was added dropwise 85% H_3PO_4 (5 mL) at room temperature and stirred overnight. The reaction mixture was treated with NaOH (20 g, 500 mmol, 4 eq) and KOH (14 g, 250 mmol, 2 eq) afterwards. To the resulting solution was hydroxylamine hydrochloride (34.7 g, 500 mmol, 4 eq) slowly added at room temperature and heated up to 95 °C. After completion of the reaction (2 h), the mixture was cooled to room temperature, quenched with concentrated HCl to pH = 2 and a precipitate was formed. After filtration, the precipitate was dried to give a white powder as product **1**. And the filtrate was extracted with ethyl acetate, the combined organic phases were subsequently washed with brine and dried over Na_2SO_4. The solvent was removed under reduced pressure to give another portion of product **1** as an off-white powder.
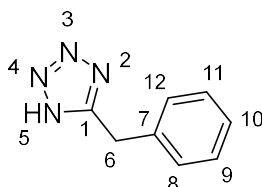
Yield: 10.0 g (62%)

¹H-NMR (500 MHz, DMSO-d_6): δ [ppm] = 6.33 (s, 2H, H-8).

¹³C-NMR (126 MHz, DMSO-d_6): δ [ppm] = 160.78 (C-6), 156.94 (C-2), 140.63 (C-1).

ESI-MS (*m/z*): [M-H]⁻ calcd for $C_3H_2N_3O_3^-$: 128.0 Da; found: 127.9 Da.

Melting point: 215 °C

5-Benzyl-1*H*-tetrazole 4

5-benzyl-1*H*-tetrazole **4** was synthesized from 2-phenylacetonitrile (693 µL, 6 mmol, 1 eq) according to Method 1 as a white solid.
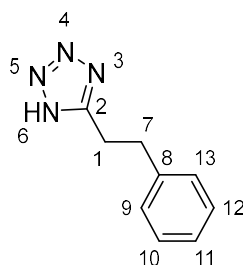
Yield: 390 mg (41%)

**¹H-NMR** (500 MHz, DMSO-d_6): δ [ppm] = 7.56 – 6.94 (m, 5H, H-12, H-8, H-9, H-11, H-10), 4.29 (s, 2H, H-6).

¹³C-NMR (126 MHz, DMSO-d_6): δ [ppm] = 146.95 (C-1), 136.51 (C-7), 129.28 (C-9, C-11), 129.22 (C-8, C-12), 127.57 (C-10), 29.47 (C-6).

ESI-MS (*m/z*): [M+H]$^+$ calcd for $C_8H_9N_4^+$: 161.1 Da; found: 161.0 Da.

Melting point: 125 °C

5-Phenethyl-1*H*-tetrazole 5

5-phenethyl-1*H*-tetrazole **5** was synthesized from 3-phenylpropanenitrile (786 µL, 6 mmol, 1 eq) according to Method 1 as a white solid.

Yield: 480 mg (46%)

^{1}H-NMR (500 MHz, DMSO-d_6): δ [ppm] = 7.41 – 7.15 (m, 5H, H-9, H-10, H-11, H-12, H-13), 3.19 (t, J = 7.8 Hz, 2H, H-7), 3.05 (t, J = 7.8 Hz, 2H, H-1).

^{13}C-NMR (126 MHz, DMSO-d_6): δ [ppm] = 155.97 (C-2), 140.53 (C-8), 128.97 (C-10, C-12), 128.82 (C-9, C-13), 126.84 (C-11), 33.28 (C-7), 25.15 (C-1).

ESI-MS (*m/z*): [M+H]$^+$ calcd for C$_9$H$_{11}$N$_4^+$: 175.1 Da; found: 175.3 Da.

Melting point: 102 °C

5-(3-Chlorobenzyl)-1*H*-tetrazole 6
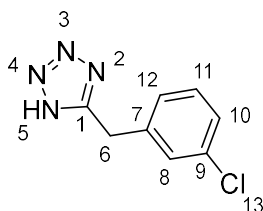
5-(3-chlorobenzyl)-1*H*-tetrazole **6** was synthesized from 2-(3-chlorophenyl)acetonitrile (709 µL, 6 mmol, 1 eq) according to Method 1 as a white solid.

Yield: 861 mg (74%)

^{1}H-NMR (500 MHz, DMSO-d_6): δ [ppm] = 7.54 – 7.30 (m, 3H, H-8, H-10, H-12), 7.24 (ddd, J = 7.3, 2.0, 1.3 Hz, 1H, H-11), 4.33 (s, 2H, H-6).

^{13}C-NMR (126 MHz, DMSO-d_6): δ [ppm] = 162.92 (C-1), 138.86 (C-7), 133.77 (C-9), 131.11 (C-11), 129.27 (C-10), 128.09 (C-8), 127.63 (C-12), 29.01 (C-6).

ESI-MS (*m/z*): [M+H]$^+$ calcd for C$_8$H$_8$ClN$_4^+$: 195.0 Da; found: 195.0 Da.

Melting point: 139 °C

5-(4-Methylbenzyl)-1*H*-tetrazole 7
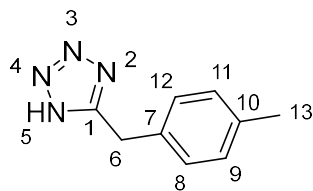
5-(4-methylbenzyl)-1*H*-tetrazole **7** was synthesized from 2-(*p*-tolyl)acetonitrile (810 μL, 6 mmol, 1 eq) according to Method 1 as a white solid.
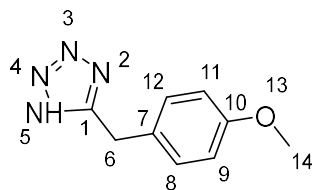
Yield: 683 mg (65%)

¹H-NMR (500 MHz, DMSO-d_6): δ [ppm] = 7.23 – 7.04 (m, 4H, H-8, H-9, H-11, H-12), 4.23 (s, 2H, H-6), 2.26 (s, 3H, H-13).

¹³C-NMR (126 MHz, DMSO-d_6): δ [ppm] = 152.70 (C-1), 136.69 (C-10), 133.41 (C-7), 129.81 (C-9, C-11), 129.08 (C-8, C-12), 29.06 (C-6), 21.16 (C-13).

ESI-MS (*m/z*): [M+H]⁺ calcd for $C_9H_{11}N_4^+$: 175.1 Da; found: 175.3 Da.

Melting point: 161 °C

5-(4-Methoxybenzyl)-1*H*-tetrazole 8

5-(4-methoxybenzyl)-1*H*-tetrazole **8** was synthesized from 2-(4-methoxyphenyl) acetonitrile (814 μL, 6 mmol, 1 eq) according to Method 1 as a white solid.

Yield: 470 mg (41%)

¹H-NMR (500 MHz, DMSO-d_6): δ [ppm] = 7.19 (d, J = 8.7 Hz, 2H, H-8, H-12), 6.90 (d, J = 8.7 Hz, 2H, H-9, H-11), 4.21 (s, 2H, H-6), 3.72 (s, 3H, H-14).
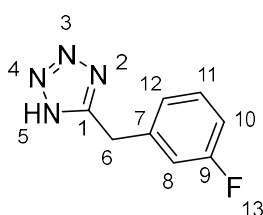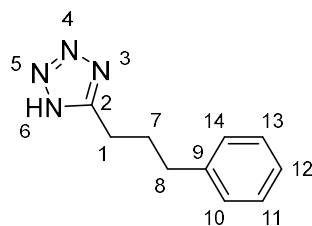
^{13}**C-NMR** (126 MHz, DMSO-d_6): δ [ppm] = 159.37, 158.85 (C-1), 130.31 (C-8, C-12), 128.31 (C-7), 114.68 (C-9, C-11), 55.64 (C-14), 28.61 (C-6).

ESI-MS (*m/z*): [M+H]$^+$ calcd for C$_9$H$_{11}$N$_4$O$^+$: 191.1 Da; found: 191.0 Da.

Melting point: 159 °C

5-(3-Fluorobenzyl)-1*H*-tetrazole 9

5-(3-fluorobenzyl)-1*H*-tetrazole **9** was synthesized from 2-(3-fluorophenyl)acetonitrile (697 μL, 6 mmol, 1 eq) according to Method 1 as a white solid.

Yield: 698 mg (66%)

^{1}**H-NMR** (500 MHz, DMSO-d_6): δ [ppm] = 7.38 (td, J = 7.9, 6.3 Hz, 1H, H-11), 7.25 – 6.98 (m, 3H, H-12, H-8, H-10), 4.33 (s, 2H, H-6).

^{13}**C-NMR** (126 MHz, DMSO-d_6): δ [ppm] = 163.73 (C-9), 161.79 (C-1), 139.17 (C-7), 131.20 (d, J = 8.3 Hz, C-11), 125.45 (d, J = 2.9 Hz, C-12), 116.22 (d, J = 21.8 Hz, C-8), 114.46 (d, J = 20.8 Hz, C-10), 29.12 (C-6).

ESI-MS (*m/z*): [M+H]$^+$ calcd for C$_8$H$_8$FN$_4$$^+$: 179.1 Da; found: 179.0 Da.

Melting point: 136 °C

5-(3-Phenylpropyl)-1*H*-tetrazole 10

5-(3-phenylpropyl)-1*H*-tetrazole **10** was synthesized from 4-phenylbutanenitrile (911 µL, 6 mmol, 1 eq) according to Method 1 as a white solid.
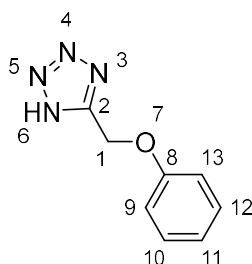
Yield: 760 mg (67%)

^{1}H-NMR (500 MHz, DMSO-d_6): δ [ppm] = 7.49 – 6.94 (m, 5H, H-11, H-13, H-12, H-14, H-10), 2.99 – 2.74 (m, 2H, H-8), 2.74 – 2.56 (m, 2H, H-1), 2.00 (p, J = 7.7 Hz, 2H, H-7).

^{13}C-NMR (126 MHz, DMSO-d_6): δ [ppm] = 155.89 (C-2), 141.70 (C-9), 128.94 (C-11, C-13), 128.93 (C-10, C-14), 126.51 (C-12), 34.83 (C-8), 29.24 (C-7), 22.78 (C-1).

ESI-MS (*m/z*): [M+H]$^+$ calcd for $C_{10}H_{13}N_4^+$: 189.1 Da; found: 189.0 Da.

Melting point: 92 °C

5-(Phenoxymethyl)-1*H*-tetrazole 11

5-(phenoxymethyl)-1*H*-tetrazole **11** was synthesized from 2-phenoxyacetonitrile (733 µL, 6 mmol, 1 eq) according to Method 1 as a white solid.
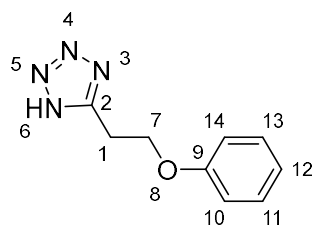
Yield: 961 mg (91%)

^{1}**H-NMR** (500 MHz, DMSO-d_6): δ [ppm] = 7.38 – 7.27 (m, 2H, H-10, H-12), 7.07 (dt, J = 7.8, 1.0 Hz, 2H, H-9, H-13), 7.04 – 6.96 (m, 1H, H-11), 5.49 (s, 2H, H-1).

^{13}**C-NMR** (126 MHz, DMSO-d_6): δ [ppm] = 157.98 (C-8), 154.14 (C-2), 130.21 (C-10, C-12), 122.23 (C-11), 115.39 (C-9, C-13), 59.82 (C-1).

ESI-MS (*m/z*): [M+H]$^+$ calcd for C$_8$H$_9$N$_4$O$^+$: 177.1 Da; found: 177.0 Da.

Melting point: 128 °C

5-(2-Phenoxyethyl)-1*H*-tetrazole 12

5-(2-phenoxyethyl)-1*H*-tetrazole **12** was synthesized from 3-phenoxypropanenitrile (883 mg, 6 mmol, 1 eq) according to Method 1 as a white solid.
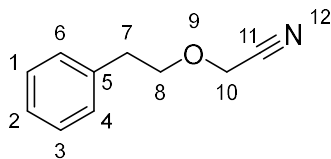
Yield: 173 mg (15%)

^{1}**H-NMR** (500 MHz, DMSO-d_6): δ [ppm] = 7.41 – 7.06 (m, 2H, H-11, H-13), 7.06 – 6.68 (m, 3H, H-10, H-12, H-14), 4.35 (t, J = 6.2 Hz, 2H, H-7), 3.37 (t, J = 6.2 Hz, 2H, H-1).

^{13}**C-NMR** (126 MHz, DMSO-d_6): δ [ppm] = 160.10 (C-9), 158.61 (C-2), 130.09 (C-11, C-13), 121.48 (C-12), 115.09 (C-10, C-14), 65.17 (C-7), 24.24 (C-1).

ESI-MS (*m/z*): [M+H]$^+$ calcd for C$_9$H$_{11}$N$_4$O$^+$: 191.1 Da; found: 191.0 Da.
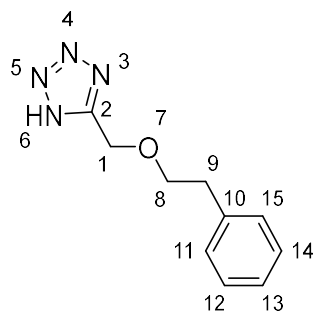
Melting point: 133 °C

2-Phenethoxyacetonitrile 13

To a solution of 2-phenylethanol (3.6 mL, 30 mmol, 1 eq) in dry THF (25 mL) was added 60% sodium hydride (1.32 g, 33 mmol, 1.1 eq) slowly at 0 °C. After 30 min of stirring 2-bromoacetonitrile (2.2 mL, 30 mmol, 1 eq) was added and the resulting mixture was stirred overnight. After completion of the reaction, the mixture was quenched and filtered. The filtrate was concentrated under reduced pressure and purified by column chromatography (SiO$_2$, n-hexane/ethyl acetate, 5% → 20% ethyl acetate) to give pure product **13** as a colorless oil.

Yield: 1.08 g (22%)

5-(Phenethoxymethyl)-1*H*-tetrazole 14

5-(phenethoxymethyl)-1*H*-tetrazole **14** was synthesized from 2-phenethoxyacetonitrile **13** (967 mg, 6 mmol, 1 eq) according to Method 1 as a white solid.

Yield: 718 mg (98%)

^{1}H-NMR (500 MHz, DMSO-d_6): δ [ppm] = 7.38 – 7.04 (m, 5H, H-12, H-14, H-13, H-11, H-15), 4.84 (s, 2H, H-1), 3.72 (t, J = 7.0 Hz, 2H, H-8), 2.87 (t, J = 7.0 Hz, 2H, H-9).
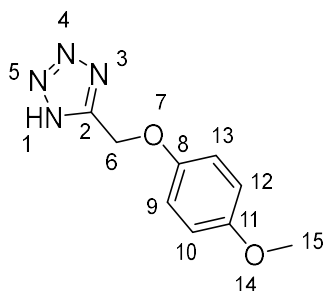
^{13}C-NMR (126 MHz, DMSO-d_6): δ [ppm] = 154.57 (C-2), 139.07 (C-10), 129.38 (C-11, C-15), 128.83 (C-12, C-14), 126.71 (C-13), 72.01 (C-8), 61.62 (C-1), 35.74 (C-9).

ESI-MS (*m/z*): [M+H]$^+$ calcd for C$_{10}$H$_{13}$N$_4$O$^+$: 205.1 Da; found: 205.3 Da.

Melting point: 76 °C

5-((4-Methoxyphenoxy)methyl)-1*H*-tetrazole 15

5-((4-methoxyphenoxy)methyl)-1*H*-tetrazole **15** was synthesized from 2-(4-methoxyphenoxy)acetonitrile (979 mg, 6 mmol, 1 eq) according to Method 1 as a white solid.
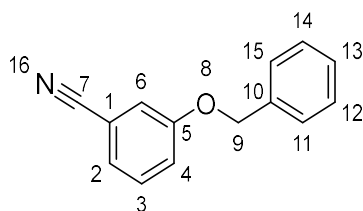
Yield: 1.20 g (97%)

^{1}H-NMR (500 MHz, DMSO-d_6): δ [ppm] = 7.08 – 6.94 (m, 2H, H-9, H-13), 6.94 – 6.78 (m, 2H, H-10, H-12), 5.41 (s, 2H, H-6), 3.70 (s, 3H, H-15).

^{13}C-NMR (126 MHz, DMSO-d_6): δ [ppm] = 155.99 (C-2), 154.74 (C-11), 151.95 (C-8), 116.62 (C-9, C-13), 115.26 (C-10, C-12), 60.54 (C-6), 55.95 (C-15).

ESI-MS (*m/z*): [M+H]$^+$ calcd for C$_9$H$_{11}$N$_4$O$_2^+$: 207.2 Da; found: 207.0 Da.

Melting point: 147 °C

3-(Benzyloxy)benzonitrile 16

To a solution of 3-hydroxybenzonitrile (360 mg, 3 mmol, 1 eq) in acetone (10 mL) was added benzyl bromide (535 µL, 4.5 mmol, 1.5 eq) and potassium carbonate (620 mg, 4.5 mmol, 1.5 eq). The resulting mixture was stirred at room temperature overnight. After completion of the reaction, the mixture was filtered. The filtrate was concentrated under reduced pressure and purified by column chromatography (SiO2, n-hexane/ethyl acetate, 2% → 20% ethyl acetate) to give pure product **16** as a white solid.

Yield: 579 mg (92%)

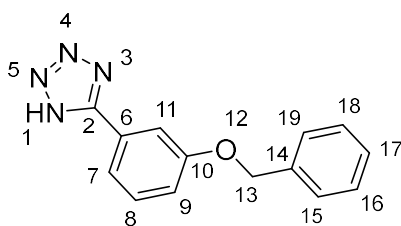**^{1}H-NMR** (500 MHz, DMSO-d_6): δ [ppm] = 7.73 – 7.07 (m, 9H, H-3, H-2, H-11, H-15, H-12, H-14, H-6, H-13, H-4), 5.17 (s, 2H, H-9).

^{13}C-NMR (126 MHz, DMSO-d_6): δ [ppm] = 159.04 (C-5), 136.90 (C-10), 131.44 (C-3), 129.07 (C-12, C-14), 128.64 (C-13), 128.45 (C-11, C-15), 125.26 (C-2), 121.20 (C-6), 119.22 (C-4), 118.33 (C-7), 112.82 (C-1), 70.26 (C-9).

ESI-MS (*m/z*): [M+H]$^+$ calcd for $C_{14}H_{12}NO^+$: 210.1 Da; found: 210.0 Da.

Melting point: 40 °C

5-(3-(Benzyloxy)phenyl)-1*H*-tetrazole 17

5-(3-(benzyloxy)phenyl)-1*H*-tetrazole **17** was synthesized from 3-(benzyloxy)-benzonitrile **16** (1.26 g, 6 mmol, 1 eq) according to Method 1 as a white solid.
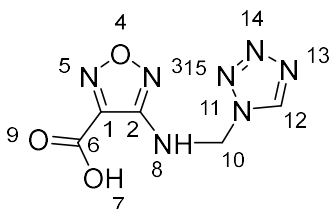
Yield: 1.51 g (99%)

¹H-NMR (500 MHz, DMSO-d_6): δ [ppm] = 7.96 – 6.97 (m, 9H, H-7, H-15, H-19, H-16, H-18, H-8, H-11, H-17, H-9), 5.21 (s, 2H, H-13).

¹³C-NMR (126 MHz, DMSO-d_6): δ [ppm] = 159.41 (C-10), 150.02 (C-2), 137.23 (C-14), 131.34 (C-8), 129.07 (C-16, C-18), 128.55 (C-17), 128.33 (C-15, C-19), 121.93 (C-6), 119.99 (C-7), 118.36 (C-9), 113.70 (C-11), 70.06 (C-13).

ESI-MS (*m/z*): [M+H]$^+$ calcd for $C_{14}H_{13}N_4O^+$: 253.1 Da; found: 253.0 Da.

Melting point: 213 °C

4-(((1*H*-Tetrazol-1-yl)methyl)amino)-furazan-3-carboxylic acid 2

4-(((1*H*-tetrazol-1-yl)methyl)amino)-furazan-3-carboxylic acid **2** was synthesized from 0.45 M 1*H*-tetrazole in acetonitrile (3.3 mL, 1.5 mmol, 1.5 eq) according to Method 2 as a white solid.
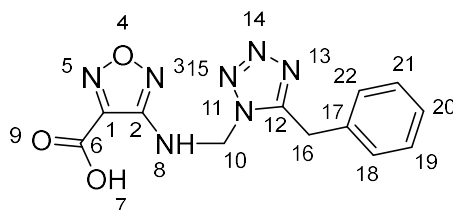
Yield: 130 mg (62%)

¹H-NMR (500 MHz, DMSO-d_6): δ [ppm] = 9.44 (s, 1H, H-12), 7.91 (t, J = 7.0 Hz, 1H, H-8), 5.91 (d, J = 7.0 Hz, 2H, H-10).

¹³C-NMR (126 MHz, DMSO-d_6): δ [ppm] = 169.84 (C-6), 160.16 (C-2), 155.80 (C-12), 144.58 (C-1), 57.19 (C-10).

ESI-MS (*m/z*): [M+Na]$^+$ calcd for $C_{10}H_{13}N_4O^+$: 234.0 Da; found: 234.0 Da.

Melting point: 154 °C

4-(((5-Benzyl-1*H*-tetrazol-1-yl)methyl)amino)-furazan-3-carboxylic acid 3

4-(((5-benzyl-1*H*-tetrazol-1-yl)methyl)amino)-furazan-3-carboxylic acid **3** was synthesized from 5-benzyl-1*H*-tetrazole **4** (240 mg, 1.5 mmol, 1.5 eq) according to Method 2 as a white solid.

Yield: 92 mg (31%)

¹H-NMR (500 MHz, DMSO-*d*$_6$): δ [ppm] = 7.89 (t, J = 6.6 Hz, 1H, H-8), 7.32 – 7.19 (m, 5H, H-18, H-22, H-19, H-21, H-20), 5.88 (d, J = 6.6 Hz, 2H, H-10), 4.48 (s, 2H, H-16).
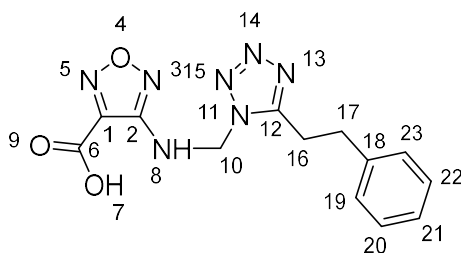
¹³C-NMR (126 MHz, DMSO-*d*$_6$): δ [ppm] = 160.11 (C-2), 155.55 (C-6), 155.03 (C-12), 140.46 (C-17), 135.77 (C-1), 129.29 (C-19, C-21), 129.05 (C-18, C-22), 127.45 (C-20), 56.47 (C-10), 28.68 (C-16).

ESI-MS (*m/z*): [M+Na]$^+$ calcd for $C_{12}H_{11}N_7O_3Na^+$: 324.1 Da; found: 324.0 Da.

Melting point: 159 °C

4-(((5-Phenethyl-1*H*-tetrazol-1-yl)methyl)amino)-furazan-3-carboxylic acid 18

4-(((5-phenethyl-1*H*-tetrazol-1-yl)methyl)amino)-furazan-3-carboxylic acid **18** was synthesized from 5-phenethyl-1*H*-tetrazole **5** (261 mg, 1.5 mmol, 1.5 eq) according to Method 2 as a white solid.
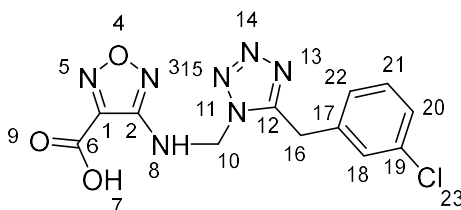
Yield: 111 mg (35%)

¹H-NMR (500 MHz, DMSO-*d₆*): δ [ppm] = 7.89 (t, J = 6.5 Hz, 1H, H-8), 7.52 – 6.99 (m, 5H, H-20, H-22, H-19, H-23, H-21), 5.75 (d, J = 6.5 Hz, 2H, H-10), 3.50 – 3.16 (m, 2H, H-16), 3.13 – 2.92 (m, 2H, H-17).

¹³C-NMR (126 MHz, DMSO-*d₆*): δ [ppm] = 160.21 (C-2), 155.68 (C-6), 155.58 (C-12), 140.71 (C-18), 140.56 (C-1), 129.00 (C-19, C-23), 128.92 (C-20, C-22), 126.86 (C-21), 56.03 (C-10), 32.91 (C-17), 24.73 (C-16).

ESI-HRMS (*m/z*): [M+H]⁺ calcd for $C_{13}H_{14}N_7O_3^+$: 316.1158 Da; found: 316.1151 Da.

Melting point: 177 °C

4-(((5-(3-Chlorobenzyl)-1*H*-tetrazol-1-yl)methyl)amino)-furazan-3-carboxylic acid 19

4-(((5-(3-chlorobenzyl)-1*H*-tetrazol-1-yl)methyl)amino)-furazan-3-carboxylic acid **19** was synthesized from 5-(3-chlorobenzyl)-1*H*-tetrazole **6** (240, 1.5 mmol, 1.5 eq) according to Method 2 as a white solid.
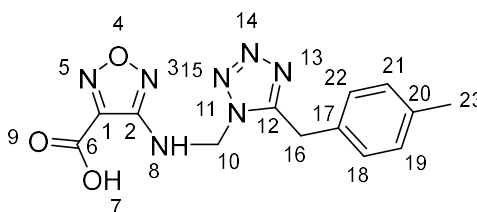
Yield: 42 mg (13%)

¹H-NMR (500 MHz, DMSO-*d₆*): δ [ppm] = 7.92 (t, J = 6.4 Hz, 1H, H-8), 7.33 – 7.26 (m, 3H, H-21, H-18, H-20), 7.20 (dd, J = 3.6, 1.7 Hz, 1H, H-22), 5.90 (d, J = 6.7 Hz, 2H, H-10), 4.49 (s, 2H, H-16).

¹³C-NMR (126 MHz, DMSO-*d₆*): δ [ppm] = 160.21 (C-6), 155.58 (C-2), 154.63 (C-12), 140.70 (C-17), 138.26 (C-1), 133.61 (C-19), 130.83 (C-21), 128.99 (C-20), 128.91 (C-22), 126.85 (C-18), 56.55 (C-10), 32.91 (C-16).

ESI-HRMS (*m/z*): [M+H]⁺ calcd for $C_{12}H_{11}ClN_7O_3^+$: 336.0612 Da; found: 336.0604 Da.

Melting point: 130 °C

4-(((5-(4-Methylbenzyl)-1*H*-tetrazol-1-yl)methyl)amino)-furazan-3-carboxylic acid 20

4-(((5-(4-methylbenzyl)-1*H*-tetrazol-1-yl)methyl)amino)-furazan-3-carboxylic acid **20** was synthesized from 5-(4-methylbenzyl)-1*H*-tetrazole **7** (261 mg, 1.5 mmol, 1.5 eq) according to Method 2 as a white solid.
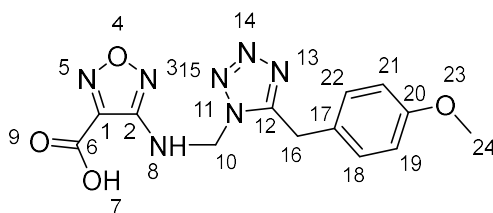
Yield: 112 mg (35%)

¹H-NMR (500 MHz, DMSO-d_6): δ [ppm] = 7.86 (t, J = 6.6 Hz, 1H, H-8), 7.18 – 6.96 (m, 4H, H-18, H-22, H-19, H-1), 5.86 (d, J = 6.6 Hz, 2H, H-10), 4.42 (s, 2H, H-16), 2.24 (s, 3H, H-23).

¹³C-NMR (126 MHz, DMSO-d_6): δ [ppm] = 160.12 (C-2), 155.49 (C-6), 155.11 (C-12), 140.35 (C-20), 136.56 (C-17), 132.66 (C-1), 129.60 (C-19, C-21), 129.10 (C-18, C-22), 56.44 (C-10), 28.27 (C-16), 21.16 (C-23).

ESI-HRMS (*m/z*): [M+H]$^+$ calcd for C$_{13}$H$_{14}$N$_7$O$_3{}^+$: 316.1158 Da; found: 316.1154 Da.

Melting point: 179 °C

4-(((5-(4-Methoxybenzyl)-1*H*-tetrazol-1-yl)methyl)amino)-furazan-3-carboxylic acid 21

4-(((5-(4-methoxybenzyl)-1*H*-tetrazol-1-yl)methyl)amino)-furazan-3-carboxylic acid **21** was synthesized from 5-(4-methoxybenzyl)-1*H*-tetrazole **8** (285 mg, 1.5 mmol, 1.5 eq) according to Method 2 as a white solid.
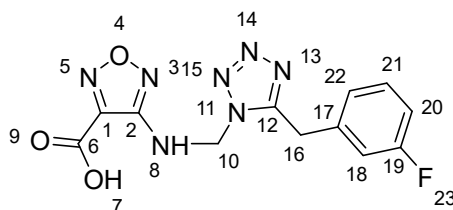
Yield: 109 mg (33%)

¹H-NMR (500 MHz, DMSO-d_6): δ [ppm] = 7.88 (t, J = 6.6 Hz, 1H, H-8), 7.14 (d, J = 8.8 Hz, 2H, H-18, H-22), 6.82 (d, J = 8.8 Hz, 2H, H-19, H-21), 5.86 (d, J = 6.6 Hz, 2H, H-10), 4.39 (s, 2H, H-16), 3.71 (s, 3H, H-24).

¹³C-NMR (126 MHz, DMSO-d_6): δ [ppm] = 160.13 (C-2), 158.73 (C-6), 155.53 (C-20), 155.31 (C-12), 140.47 (C-1), 130.35 (C-18, C-22), 127.52 (C-17), 114.49 (C-19, C-21), 56.41 (C-10), 55.59 (C-24), 27.83 (C-16).

ESI-HRMS (*m/z*): [M+H]$^+$ calcd for $C_{13}H_{14}N_7O_4^+$: 332.1107 Da; found: 332.1103 Da.

Melting point: 167 °C

4-(((5-(3-Fluorobenzyl)-1*H*-tetrazol-1-yl)methyl)amino)-furazan-3-carboxylic acid 22

4-(((5-(3-fluorobenzyl)-1*H*-tetrazol-1-yl)methyl)amino)-furazan-3-carboxylic acid **22** was synthesized from 5-(3-fluorobenzyl)-1*H*-tetrazole **9** (267 mg, 1.5 mmol, 1.5 eq) according to Method 2 as a white solid.
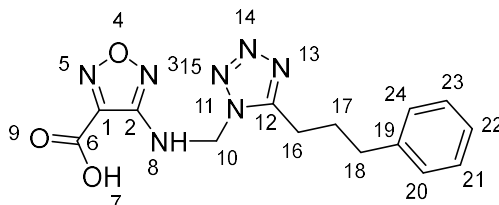
Yield: 60 mg (19%)

^{1}H-NMR (500 MHz, DMSO-d_6): δ [ppm] = 7.88 (t, J = 6.6 Hz, 1H, H-8), 7.42 – 6.93 (m, 4H, H-21, H-22, H-18, H-20), 5.86 (d, J = 6.6 Hz, 2H, H-10), 4.47 (s, 2H, H-16).

^{13}C-NMR (126 MHz, DMSO-d_6): δ [ppm] = 162.63 (d, J = 244.2 Hz, C-19), 160.09 (C-2), 155.52 (C-6), 154.62 (C-12), 140.39 (C-1), 138.51 (d, J = 7.5 Hz, C-17), 130.91 (d, J = 8.3 Hz, C-21), 125.42 (d, J = 2.6 Hz, C-22), 116.26 (d, J = 21.8 Hz, C-18), 114.32 (d, J = 21.0 Hz, C-20), 56.55 (C-10), 28.36 (C-16).

ESI-HRMS (*m/z*): [M+H]$^+$ calcd for $C_{12}H_{11}FN_7O_3^+$: 320.0907 Da; found: 320.0893 Da.

Melting point: 168 °C

4-(((5-(3-Phenylpropyl)-1*H*-tetrazol-1-yl)methyl)amino)-furazan-3-carboxylic acid 23

4-(((5-(3-phenylpropyl)-1*H*-tetrazol-1-yl)methyl)amino)-furazan-3-carboxylic acid **23** was synthesized from 5-(3-phenylpropyl)-1*H*-tetrazole **10** (282 mg, 1.5 mmol, 1.5 eq) according to Method 2 as a white solid.
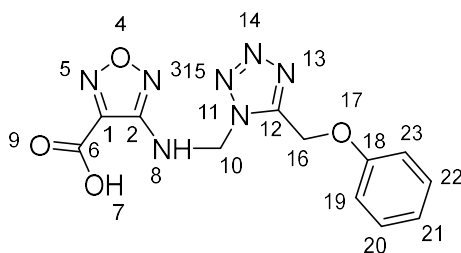
Yield: 72 mg (22%)

¹H-NMR (500 MHz, DMSO-*d₆*): δ [ppm] = 7.91 (t, J = 6.6 Hz, 1H, H-8), 7.46 – 7.12 (m, 5H, H-21, H-23, H-22, H-20, H-24), 5.80 (d, J = 6.6 Hz, 2H, H-10), 3.18 – 2.85 (m, 2H, H-18), 2.80 – 2.54 (m, 2H, H-16), 2.14 – 1.88 (m, 2H, H-17).

¹³C-NMR (126 MHz, DMSO-*d₆*): δ [ppm] = 13C NMR (126 MHz, DMSO-D6) δ 160.19 (C-6), 155.91 (C-2), 155.71 (C-12), 141.86 (C-19), 140.59 (C-1), 128.91 (C-20, C-24), 128.87 (C-21, C-23), 126.48 (C-22), 56.14 (C-10), 34.98 (C-18), 28.87 (C-16), 22.48 (C-17).

ESI-MS (*m/z*): [M+Na]⁺ calcd for $C_{14}H_{15}N_7O_3Na^+$: 352.1 Da; found: 351.8 Da.

Melting point: 149 °C

4-(((5-(Phenoxymethyl)-1*H*-tetrazol-1-yl)methyl)amino)-furazan-3-carboxylic acid 24

4-(((5-(phenoxymethyl)-1*H*-tetrazol-1-yl)methyl)amino)-furazan-3-carboxylic acid **24** was synthesized from 5-(phenoxymethyl)-1*H*-tetrazole **11** (264 mg, 1.5 mmol, 1.5 eq) according to Method 2 as a white solid.
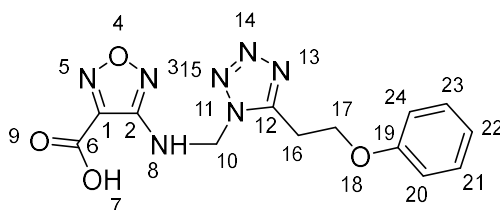
Yield: 146 mg (47%)

^{1}H-NMR (500 MHz, DMSO-d_6): δ [ppm] = 7.90 (t, J = 6.8 Hz, 1H, H-8), 7.33 (t, J = 8.0 Hz, 2H, H-20, H-22), 7.06 (d, J = 7.9 Hz, 2H, H-19, H-23), 7.01 (t, J = 7.3 Hz, 1H, H-21), 5.99 (d, J = 6.8 Hz, 2H, H-10), 5.63 (s, 2H, H-16).

^{13}C-NMR (126 MHz, DMSO-d_6): δ [ppm] = 160.22 (C-2), 157.89 (C-6), 155.75 (C-18), 152.27 (C-12), 140.63 (C-1), 130.13 (C-20, C-22), 122.27 (C-21), 115.40 (C-19, C-23), 58.85 (C-16), 56.99 (C-10).

ESI-HRMS (*m/z*): [M+Na]$^+$ calcd for $C_{12}H_1N_7O_4Na^+$: 340.0770 Da; found: 340.0772 Da.

Melting point: 164 °C

4-(((5-(2-Phenoxyethyl)-1*H*-tetrazol-1-yl)methyl)amino)-furazan-3-carboxylic acid 25

4-(((5-(2-phenoxyethyl)-1*H*-tetrazol-1-yl)methyl)amino)-furazan-3-carboxylic acid **25** was synthesized from 5-(2-phenoxyethyl)-1*H*-tetrazole **12** (285 mg, 1.5 mmol, 1.5 eq) according to Method 2 as a white solid.
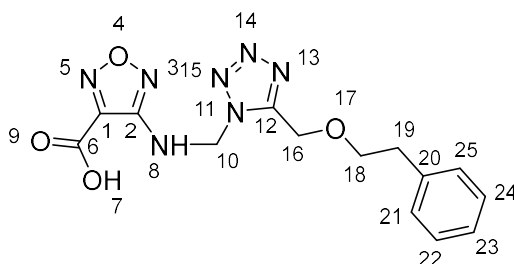
Yield: 120 mg (36%)

¹H-NMR (500 MHz, DMSO-d_6): δ [ppm] = 7.95 (t, J = 6.3 Hz, 1H, H-8), 7.28 (t, J = 7.7 Hz, 2H, H-21, H-23), 6.94 (dd, J = 11.7, 8.0 Hz, 3H, H-20, H-22, H-24), 5.90 (d, J = 6.5 Hz, 2H, H-10), 4.39 (t, J = 6.3 Hz, 2H, H-17), 3.58 (t, J = 6.3 Hz, 2H, H-16).

¹³C-NMR (126 MHz, DMSO-d_6): δ [ppm] = 160.20 (C-2), 158.59 (C-6), 155.75 (C-19), 153.86 (C-12), 138.47 (C-1), 130.11 (C-21, C-23), 121.47 (C-22), 115.00 (C-20, C-24), 65.08 (C-17), 56.35 (C-10), 23.72 (C-16).

ESI-HRMS (*m/z*): [2M+Na]$^+$ calcd for $C_{26}H_{26}N_{14}O_8Na^+$: 685.1956 Da; found: 685.1995 Da.

Melting point: 162 °C

4-(((5-(Phenethoxymethyl)-1*H*-tetrazol-1-yl)methyl)amino)-furazan-3-carboxylic acid 26

4-(((5-(phenethoxymethyl)-1*H*-tetrazol-1-yl)methyl)amino)-furazan-3-carboxylic acid **26** was synthesized from 5-(phenethoxymethyl)-1*H*-tetrazole **12** (306 mg, 1.5 mmol, 1.5 eq) according to Method 2 as a white solid.
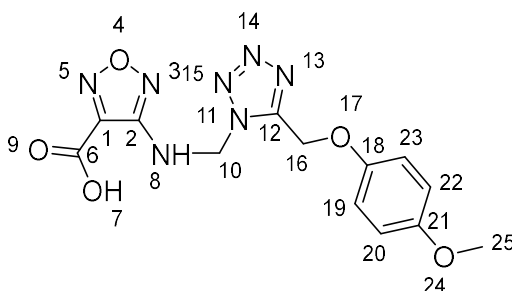
Yield: 169 mg (49%)

¹H-NMR (500 MHz, DMSO-d_6): δ [ppm] = 7.78 (t, J = 6.9 Hz, 1H, H-8), 7.35 – 7.15 (m, 5H, H-22, H-24, H-23, H-25, H-21), 5.79 (d, J = 6.9 Hz, 2H, H-10), 4.99 (s, 2H, H-16), 3.72 (t, J = 6.8 Hz, 2H, H-18), 2.84 (t, J = 6.8 Hz, 2H, H-19).

¹³C-NMR (126 MHz, DMSO-d_6): δ [ppm] = 163.63 (C-12), 160.23 (C-6), 155.71 (C-2), 152.92 (C-20), 139.09 (C-1), 129.33 (C-21, C-25), 128.81 (C-22, C-24), 126.72 (C-23), 71.89 (C-18), 60.86 (C-16), 56.61 (C-10), 35.71 (C-19).

ESI-HRMS (*m/z*): [M+H]$^+$ calcd for $C_{14}H_{16}N_7O_4^+$: 346.1264 Da; found: 346.1292 Da.

Melting point: 124 °C

4-(((5-((4-Methoxyphenoxy)methyl)-1*H*-tetrazol-1-yl)methyl)amino)-furazan-3-carboxylic acid 27

4-(((5-((4-methoxyphenoxy)methyl)-1*H*-tetrazol-1-yl)methyl)amino)-furazan-3-carboxylic acid **27** was synthesized from 5-((4-methoxyphenoxy)methyl)-1*H*-tetrazole **15** (309 mg, 1.5 mmol, 1.5 eq) according to Method 2 as a white solid.

Yield: 86 mg (25%)

¹H-NMR (500 MHz, DMSO-d_6): δ [ppm] =   7.96 – 7.82 (m, 1H, H-8), 7.06 – 6.96 (m, 2H, H-19, H-23), 6.96 – 6.84 (m, 2H, H-22, H-20), 5.98 (d, J = 6.7 Hz, 1H, H-10), 5.41 (s, 1H, H-16), 3.70 (s, 3H, H-25).
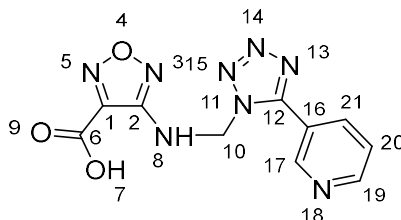
13C-NMR (126 MHz, DMSO-d_6): δ [ppm] = 160.22 (C-2), 155.76 (C-6), 154.75 (C-21), 152.37 (C-12), 151.95 (C-18), 120.00 (C-1), 116.62 (C-19, C-23), 115.26 (C-20, C-22), 60.54 (C-16), 59.59 (C-10), 55.95 (C-25).

ESI-HRMS (*m/z*): [M+H]$^+$ calcd for C$_{13}$H$_{14}$N$_7$O$_5$$^+$: 348.1056 Da; found: 348.1134 Da.

Melting point: 106 °C

4-(((5-(Pyridin-3-yl)-1*H*-tetrazol-1-yl)methyl)amino)-furazan-3-carboxylic acid 28

4-(((5-(pyridin-3-yl)-1*H*-tetrazol-1-yl)methyl)amino)-furazan-3-carboxylic   acid   **28**   was synthesized from 3-(1*H*-tetrazol-5-yl)pyridine (221 mg, 1.5 mmol, 1.5 eq) according to Method 2 as a white solid.
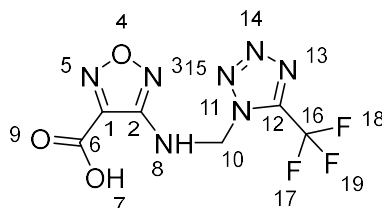
Yield: 40 mg (14%)

1H-NMR (500 MHz, DMSO-d_6): δ [ppm] = 9.22 (s, 1H, H-17), 8.75 (s, 1H, H-8), 8.40 (d, J = 8.1 Hz, 1H, H-19), 8.13 (t, J = 6.9 Hz, 1H, H-21), 7.61 (dd, J = 7.2, 4.8 Hz, 1H, H-20), 6.18 (d, J = 6.8 Hz, 2H, H-10).

13C-NMR (126 MHz, DMSO-d_6): δ [ppm] = 162.66 (C-2), 160.17 (C-6), 155.83 (C-17), 151.95 (C-12), 147.64 (C-19), 140.74 (C-21), 134.72 (C-1), 125.02 (C-16), 120.00 (C-20), 62.32 (C-10).

ESI-HRMS (*m/z*): [M+H]$^+$ calcd for C$_{10}$H$_9$N$_8$O$_3$$^+$: 289.0798 Da; found: 289.0795 Da.

Melting point: 186 °C

4-(((5-(Trifluoromethyl)-1*H*-tetrazol-1-yl)methyl)amino)-furazan-3-carboxylic acid 29

4-(((5-(trifluoromethyl)-1*H*-tetrazol-1-yl)methyl)amino)-furazan-3-carboxylic acid **29** was synthesized from 5-(Trifluoromethyl)-1*H*-tetrazole hydrate (170 mg, 1.5 mmol, 1.5 eq) according to Method 2 as a viscous oil.
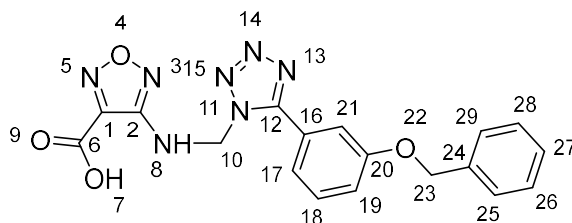
Yield: 146 mg (54%)

¹H-NMR (500 MHz, DMSO-d_6): δ [ppm] = 8.18 (t, J = 7.1 Hz, 1H, H-8), 6.23 (d, J = 7.1 Hz, 2H, H-10).

¹³C-NMR (126 MHz, DMSO-d_6): δ [ppm] = 160.09 (C-2), 155.72 (C-6), 151.69 (C-12), 140.66 (C-1), 120.12 (C-16), 63.53 (C-10).

ESI-MS (*m/z*): [M-H]⁻ calcd for $C_6H_3F_3N_7O_3^-$: 278.0 Da; found: 278.8 Da.

Melting point: < 50 °C

4-(((5-(3-(Benzyloxy)phenyl)-1*H*-tetrazol-1-yl)methyl)amino)-furazan-3-carboxylic acid 30

4-(((5-(3-(benzyloxy)phenyl)-1*H*-tetrazol-1-yl)methyl)amino)-furazan-3-carboxylic acid **30** was synthesized from 5-(3-(benzyloxy)phenyl)-1*H*-tetrazole **17** (378 mg, 1.5 mmol, 1.5 eq) according to Method 2 as a white solid.
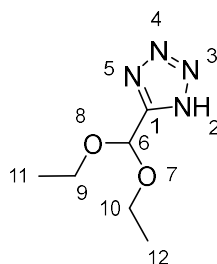
Yield: 108 mg (27%)

¹H-NMR (500 MHz, DMSO-d_6): δ [ppm] = 8.04 (t, J = 7.0 Hz, 1H, H-8), 7.69 – 7.14 (m, 9H, H-17, H-29, H-25, H-28, H-26, H-18, H-27, H-21, H-19), 6.10 (d, J = 7.0 Hz, 2H, H-10), 5.15 (s, 2H, H-23).

¹³C-NMR (126 MHz, DMSO-d_6): δ [ppm] = 164.02 (C-6), 159.61 (C-20), 158.82 (C-2), 155.29 (C-12), 136.81 (C-24), 130.60 (C-1), 128.50 (C-18), 128.47 (C-26, C-28), 127.89 (C-27), 127.76 (C-16), 127.67 (C-25, C-29), 118.94 (C-17), 117.36 (C-19), 112.30 (C-21), 69.37 (C-23), 62.55 (C-10).

ESI-HRMS (*m/z*): [M+H]$^+$ calcd for $C_{18}H_{16}N_7O_4^+$: 394.1311 Da; found: 394.1264 Da.

Melting point: 173 °C

5-(Diethoxymethyl)-1*H*-tetrazole 31

A solution of HN$_3$ in chloroform was first prepared according to Method 3.

To the solution of HN_3 (6 mL) was added 2,2-diethoxyacetonitrile (860 µL, 6 mmol, 1 eq) and pyridine (480 µL). The reaction solution was stirred at room temperature overnight. After completion of the reaction, the solvent was evaporated and saturated Na_2CO_3 solution (2 mL) was added. The resulting solution was washed with diethyl ether (3 × 3 mL). The aqueous phase was acidified with 4N HCl to pH = 2, followed by extraction with diethyl ether (6 × 3 mL). The combined organic phases were concentrated and lyophilized to give product **31** as a white solid.
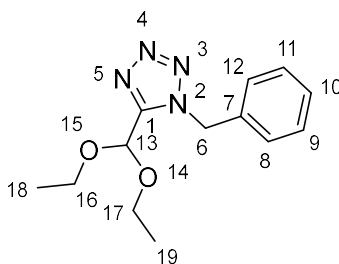
Yield: 295 mg (28%)

¹H-NMR (500 MHz, DMSO-d_6): δ [ppm] = 5.98 (s, 1H, H-6), 3.63 (q, J = 7.1 Hz, 4H, H-9, H-10), 1.17 (t, J = 7.1 Hz, 6H, H-11, H-12).

¹³C-NMR (126 MHz, DMSO-d_6): δ [ppm] = 158.98 (C-1), 94.60 (C-6), 62.60 (C-9, C-10), 15.49 (C-11, C-12).

ESI-MS (*m/z*): [M+H]$^+$ calcd for $C_6H_{13}N_4O_2^+$: 173.1 Da; found: 173.3 Da.

Melting point: 76 °C

1-Benzyl-5-(diethoxymethyl)-1*H*-tetrazole 32

To a solution of 5-(diethoxymethyl)-1*H*-tetrazole **31** (344 mg, 2 mmol, 1 eq) in DMF (5 mL) was added benzyl bromide (360 µL, 3 mmol, 1,5 eq) and cesium carbonate (800 mg, 2.4 mmol, 1.2 eq). The reaction mixture was heated at 100 °C and stirred overnight. After completion of the reaction, the mixture was allowed to cool to room temperature and water

(10 mL) was added. The resulting solution was extracted with ethyl acetate (5 × 5 mL) and the combined organic phases were concentrated under reduced pressure. The product 1-benzyl-5-(diethoxymethyl)-1*H*-tetrazole **32** and its isomer 2-benzyl-5-(diethoxymethyl)-2H-tetrazole **33** were separated by column chromatography (SiO$_2$, n-hexane/ethyl acetate, 0% → 20% ethyl acetate). After lyophilization, the product **32** was obtained as a colorless oil.

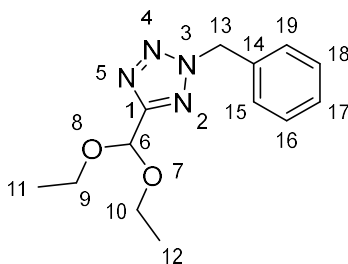Yield: 142 mg (27%)

^{1}H-NMR (500 MHz, DMSO-d_6): δ [ppm] = 7.48 – 7.31 (m, 5H, H-11, H-9, H-10, H-8, H-12), 5.95 (s, 2H, H-6), 5.86 (s, 1H, H-13), 3.77 – 3.49 (m, 4H, H-16, H-17), 1.13 (t, J = 7.1 Hz, 6H, H-18, H-19).

^{13}C-NMR (126 MHz, DMSO-d_6): δ [ppm] = 164.36 (C-1), 134.44 (C-7), 129.33 (C-8, C-12), 129.09 (C-9, C-11), 128.84 (C-10), 95.13 (C-13), 61.88 (C-16, C-17), 56.49 (C-6), 15.39 (C-18, C-19).

ESI-MS (*m/z*): [M+H]$^+$ calcd for C$_{13}$H$_{19}$N$_4$O$_2^+$: 263.2 Da; found: 263.0 Da.

2-Benzyl-5-(diethoxymethyl)-2*H*-tetrazole 33

2-benzyl-5-(diethoxymethyl)-2*H*-tetrazole **33** was obtained simultaneously with 1-benzyl-5-(diethoxymethyl)-1*H*-tetrazole **32** as a colorless oil.
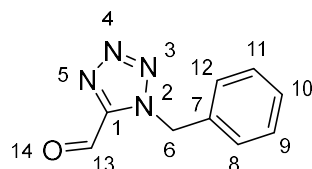
Yield: 210 mg (40%)

^{1}H-NMR (500 MHz, DMSO-d_6): δ [ppm] = 7.45 – 7.26 (m, 5H, H-16, H-18, H-19, H-15, H-17), 6.06 (s, 1H, H-6), 5.74 (s, 2H, H-13), 3.71 (dd, J = 9.6, 7.1 Hz, 2H, H-9', H-10'), 3.58 (dd, J = 9.6, 7.0 Hz, 2H, H-9'', H-10''), 1.10 (t, J = 7.1 Hz, 6H, H-11, H-12).

^{13}C-NMR (126 MHz, DMSO-d_6): δ [ppm] = 152.77 (C-1), 135.17 (C-14), 129.09 (C-16, C-18), 128.67 (C-15, C-19), 128.39 (C-17), 94.74 (C-6), 63.39 (C-9, C-10), 51.32 (C-13), 15.18 (C-11, C-12).

ESI-MS (*m/z*): [M+H]$^+$ calcd for $C_{13}H_{19}N_4O_2^+$: 263.2 Da; found: 263.0 Da.
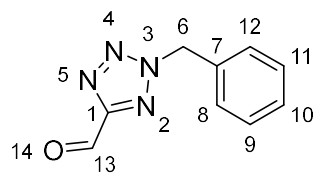
1-Benzyl-1*H*-tetrazole-5-carbaldehyde 34

1-benzyl-5-(diethoxymethyl)-1*H*-tetrazole **32** (200 mg) was dissolved in 4N HCl (1 mL) and the solution was heated at 50 °C for 2.5 h. After complete conversion, the pH was adjusted to 7 with saturated Na2CO3 solution. Extraction with ethyl acetate (3 × 3 mL) was then carried out. The combined organic phases were concentrated and lyophilized to give product **34** as a colorless oil.

Yield: 120 mg (85%)

^{1}H-NMR (500 MHz, DMSO-d_6): δ [ppm] = 10.12 (s, 1H, H-13), 7.44 – 7.39 (m, 5H, H-9, H-11, H-10, H-8, H-12), 6.08 (s, 2H, H-6).

^{13}C-NMR (126 MHz, DMSO-d_6): δ [ppm] = 182.96 (C-13), 162.75 (C-1), 134.00 (C-7), 129.51 (C-8, C-12), 129.44 (C-10), 129.27 (C-9, C-11), 57.24 (C-6).

ESI-MS (*m/z*): [M+H]$^+$ calcd for $C_9H_9N_4O^+$: 189.1 Da; found: 189.0 Da.

2-Benzyl-2*H*-tetrazole-5-carbaldehyde 35

2-benzyl-5-(diethoxymethyl)-2*H*-tetrazole **33** (270 mg) was dissolved in 4N HCl (2 mL) and the solution was heated at 70 °C for 3 h. After complete conversion of the starting material, the pH was adjusted to 7 with saturated Na2CO3 solution. Extraction with ethyl acetate (3 × 3 mL) was then carried out. The combined organic phases were concentrated and lyophilized to give product **35** as a white solid.
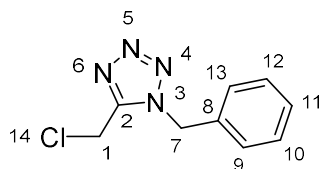
Yield: 160 mg (84%)

¹H-NMR (500 MHz, DMSO-*d₆*): δ [ppm] = 9.56 (s, 1H, H-13), 7.46 – 7.29 (m, 5H, H-8, H-12, H-9, H-11, H-10), 5.73 (s, 2H, H-6).

¹³C-NMR (126 MHz, DMSO-*d₆*): δ [ppm] = 186.23 (C-13), 144.63 (C-1), 135.43 (C-7), 129.46 (C-9, C-11), 129.03 (C-10), 128.73 (C-8, C-12), 51.34 (C-6).

ESI-MS (*m/z*): [M+H]⁺ calcd for $C_9H_9N_4O^+$: 189.1 Da; found: 189.0 Da.

Melting point: 59 °C

1-Benzyl-5-(chloromethyl)-1*H*-tetrazole 36

A solution of HN_3 in toluene was first prepared according to Method 3. To a stirred suspension of *N*-benzyl-2-chloroacetamide (183 mg, 1 mmol, 1 eq) in toluene (5 mL) was added phosphorus pentachloride (229 mg, 1.1 mmol, 1.1 eq) under cooling. After 1.5 h of

stirring at room temperature, HN_3 (3 mL) solution was added to the reaction mixture. The resulting mixture was heated to 80 °C and stirred overnight. After complete conversion of the starting material, toluene was removed under reduced pressure. To the residue was added water (10 mL) and extracted with ethyl acetate (3 × 10 mL). The combined organic phases were concentrated and lyophilized to give a pale yellow solid **36**.
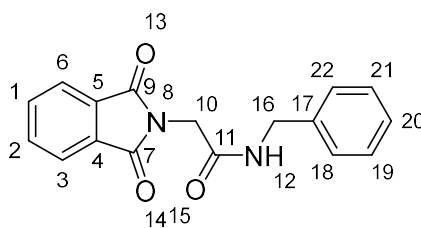
Yield: 200 mg (96%)

¹H-NMR (500 MHz, DMSO-d_6): δ [ppm] = 7.44 – 7.38 (m, 2H, H-12, H-10), 7.37 – 7.27 (m, 3H, H-11, H-13, H-9), 5.76 (s, 2H, H-7), 5.25 (s, 2H, H-1).

¹³C-NMR (126 MHz, DMSO-d_6): δ [ppm] = 152.94 (C-2), 134.68 (C-8), 129.38 (C-9, C-13), 129.05 (C-11), 128.84 (C-10, C-12), 50.88 (C-7), 31.68 (C-1).

ESI-MS (*m/z*): [M+H]⁺ calcd for $C_9H_{10}ClN_4^+$: 209.1 Da; found: 209.0 Da.

Melting point: 66 °C

N-Benzyl-2-(1,3-dioxoisoindolin-2-yl)acetamide 37

To a stirred solution of 2-(1,3-dioxoisoindolin-2-yl)acetic acid (410 mg, 2 mmol, 1 eq) in dichloromethane (7 mL) was added oxalyl dichloride (253 µL, 3 mmol, 1.5 eq) and DMF (2 drops) at room temperature. After 4 h, benzylamine (326 µL, 3 mmol, 1.5 eq) was added slowly into the reaction solution followed with addition of triethylamine (411 µL, 3 mmol, 1.5 eq). After 30 min stirring, the reaction solution was washed with 2N HCl (1 × 5 mL) and evaporated under reduced pressure. The residue was washed with water and hexane. A white solid **37** was obtained after drying.
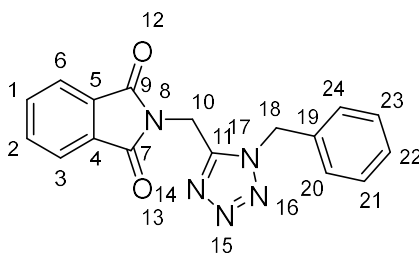
Yield: 567 mg (96%)

^{1}H-NMR (500 MHz, DMSO-d_6): δ [ppm] = 8.75 (t, J = 5.9 Hz, 1H, H-12), 7.95 – 7.90 (m, 2H, H-6, H-3), 7.90 – 7.85 (m, 2H, H-1, H-2), 7.37 – 7.29 (m, 2H, H-21, H-19), 7.29 – 7.21 (m, 3H, H-20, H-18, H-22), 4.30 (d, J = 5.9 Hz, 2H, H-16), 4.27 (s, 2H, H-10).

^{13}C-NMR (126 MHz, DMSO-d_6): δ [ppm] = 168.16 (C-7, C-9), 166.73 (C-11), 139.57 (C-17), 135.11 (C-1, C-2), 132.40 (C-4, C-5), 128.88 (C-19, C-21), 127.72 (C-18, C-22), 127.43 (C-20), 123.77 (C-3, C-6), 42.79 (C-10), 40.81 (C-16).

ESI-MS (*m/z*): [M+H]$^+$ calcd for $C_{17}H_{15}N_2O_3{}^+$: 295.1 Da; found: 295.0 Da.

Melting point: 217 °C

2-((1-Benzyl-1*H*-tetrazol-5-yl)methyl)isoindoline-1,3-dione 38

A solution of HN_3 in toluene was first prepared according to Method 3.

To a stirred suspension of *N*-benzyl-2-(1,3-dioxoisoindolin-2-yl)acetamide **37** (250 mg, 0.85 mmol, 1 eq) in toluene (5 mL) was added phosphorus pentachloride (200 mg, 0.96 mmol, 1.1 eq) under cooling. After 1.5 h of stirring at room temperature, HN_3 (3 mL) solution was added to the reaction mixture. The resulting mixture was heated to 80 °C and stirred overnight. After complete conversion of the starting material, toluene was removed under reduced pressure. To the residue was added water (10 mL) and extracted with ethyl acetate (3 × 10 mL). The combined organic phases were concentrated and lyophilized to give a colorless oil **38**.
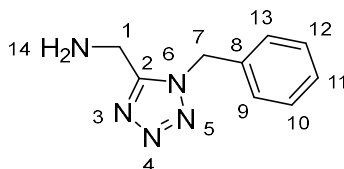
Yield: 213 mg (78%)

¹H-NMR (500 MHz, DMSO-d_6): δ [ppm] = 7.92 – 7.82 (m, 4H, H-6, H-3, H-1, H-2), 7.34 – 7.21 (m, 5H, H-23, H-21, H-22, H-20, H-24), 5.78 (s, 2H, H-18), 5.18 (s, 2H, H-10).

¹³C-NMR (126 MHz, DMSO-d_6): δ [ppm] = 167.54 (C-7, C-9), 152.01 (C-11), 135.36 (C-1, C-2), 134.65 (C-19), 131.87 (C-4, C-5), 129.40 (C-20, C-24), 128.81 (C-22), 128.00 (C-21, C-23), 124.00 (C-3, C-6), 50.70 (C-18), 31.47 (C-10).

ESI-MS (*m/z*): [M+H]⁺ calcd for $C_{17}H_{14}N_5O_2^+$: 320.1 Da; found: 320.3 Da.
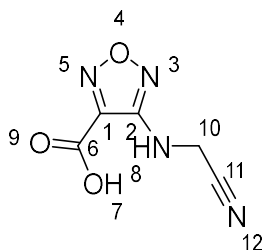
(1-Benzyl-1*H*-tetrazol-5-yl)methanamine 39

To a stirred solution of 2-((1-benzyl-1*H*-tetrazol-5-yl)methyl)isoindoline-1,3-dione **38** (210 mg, 0.66 mmol, 1 eq) in ethanol (10 mL) was added hydrazine monohydrate (131 µL, 2.6 mmol, 4 eq). The resulting solution was heated to reflux. After 1.5 h, the solution was concentrated under reduced pressure. To the residue was added water (20 mL) and the precipitate formed was removed by filtration. The filtrate was extracted with dichloromethane (3 × 15 mL) and the combined organic extracts were washed with brine (2 × 20 mL), concentrated and lyophilized to afford product **39** as a colorless oil.

Yield: 106 mg (85%)

¹H-NMR (500 MHz, DMSO-d_6): δ [ppm] = 7.57 – 7.11 (m, 7H, H-10, H-12, H-11, H-14, H-13, H-9), 5.72 (s, 2H, H-7), 4.01 (s, 2H, H-1).

¹³C-NMR (126 MHz, DMSO-d_6): δ [ppm] = 156.73 (C-2), 135.38 (C-8), 129.40 (C-9, C-13), 128.84 (C-11), 128.56 (C-10, C-12), 50.40 (C-7), 35.17 (C-1).

ESI-MS (*m/z*): [M+H]⁺ calcd for $C_9H_{12}N_5^+$: 190.1 Da; found: 190.3 Da.

4-((Cyanomethyl)amino)-furazan-3-carboxylic acid 40

To a stirred suspension of 4-amino-furazan-3-carboxylic acid **1** (387 mg, 3 mmol, 1 eq) and sodium cyanide (587 mg, 9 mmol, 3 eq) in DMSO (9 mL) at room temperature was added 36% formaldehyde solution (462 µL). After 5 h, water was added and the pH was adjusted to 2 with concentrated HCl. The mixture was extracted with ethyl acetate (6 × 30 mL). The combined organic phases were dried over Na_2SO_4, condensed under reduced pressure and purified by column chromatography (SiO_2, n-hexane/ethyl acetate, 40% → 80% ethyl acetate). After lyophilization, the product **40** was obtained as a white solid.
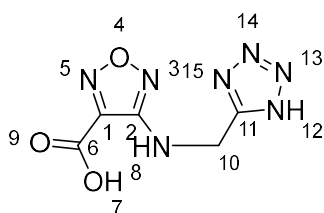
Yield: 340 mg (67%)

^{1}H-NMR (500 MHz, DMSO-d_6): δ [ppm] = 7.16 (t, J = 6.3 Hz, 1H, H-8), 4.28 (d, J = 6.3 Hz, 2H, H-10).

^{13}C-NMR (126 MHz, DMSO-d_6): δ [ppm] = 160.14 (C-6), 156.29 (C-2), 140.72 (C-1), 117.71 (C-11), 32.84 (C-10).

ESI-HRMS (*m/z*): [M-H]$^-$ calcd for $C_5H_3N_4O_3^-$: 167.0205 Da; found: 167.0215 Da.

Melting point: 81 °C

4-(((1*H*-Tetrazol-5-yl)methyl)amino)-furazan-3-carboxylic acid 41

To a stirred solution of 4-((cyanomethyl)amino)-furazan-3-carboxylic acid **40** (190 mg, 1.13 mmol, 1 eq) in water (5 mL) and isopropyl alcohol (2.5 mL) was added sodium azide (147 mg ,2.26 mmol, 2 eq) and zinc bromide (127 mg, 0.57 mmol, 0.5 eq). The reaction mixture was refluxed at 80 °C for 24 h. After cooling to room temperature, the solution was diluted with water (10 mL) acidified with concentrated HCl to pH = 2. The solution was extracted with ethyl acetate (3 × 20 mL). The combined organic phases were dried over Na_2SO_4. After removal of the solvent under reduced pressure, the product **41** was obtained as a white solid.
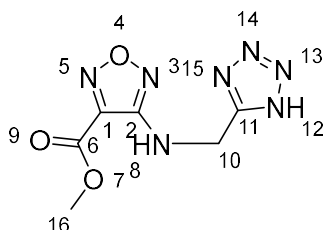
Yield: 201 mg (84%)

^{1}H-NMR (500 MHz, DMSO-d_6): δ [ppm] = 7.19 (t, J = 6.1 Hz, 1H, H-8), 4.76 (d, J = 6.2 Hz, 2H, H-10).

^{13}C-NMR (126 MHz, DMSO-d_6): δ [ppm] = 160.48 (C-11, C-6), 156.91 (C-2), 140.69 (C-1), 38.57 (C-10).

ESI-HRMS (*m/z*): [M+H]$^+$ calcd for $C_5H_6N_7O_3^+$: 212.0532 Da; found: 212.0525 Da.

Melting point: 176 °C

Methyl 4-(((1*H*-tetrazol-5-yl)methyl)amino)-furazan-3-carboxylate 42

4-(((1*H*-tetrazol-5-yl)methyl)amino)-furazan-3-carboxylic **41** (180 mg, 0.85 mmol, 1 eq) acid was dissolved in methanol (3 mL) with catalytic H_2SO_4. The reaction mixture was stirred and heated to reflux. After 24 h, the solution was cooled to room temperature and water (15 mL) was added. The resulting solution was extracted with ethyl acetate (3 × 20 mL). The combined organic phases was evaporated under reduced pressure. After lyophilization, the product **42** was obtained as a white solid.
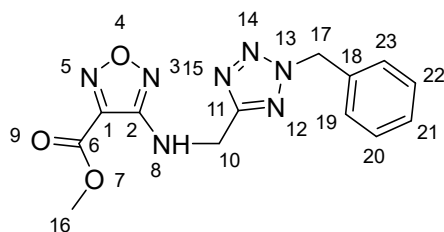
Yield: 175 mg (91%)

^{1}H-NMR (500 MHz, DMSO-d_6): δ [ppm] = 7.32 (t, J = 6.1 Hz, 1H, H-8), 4.77 (d, J = 6.1 Hz, 2H, H-10), 3.96 (s, 3H, H-16).

^{13}C-NMR (126 MHz, DMSO-d_6): δ [ppm] = 159.13 (C-6), 156.91 (C-11), 156.66 (C-2), 140.00 (C-1), 53.77 (C-16), 38.55 (C-10).

ESI-MS (*m/z*): [M+H]$^+$ calcd for $C_6H_8N_7O_3^+$: 226.1 Da; found: 226.0 Da.

Melting point: 48 °C

Methyl 4-(((2-benzyl-2*H*-tetrazol-5-yl)methyl)amino)-furazan-3-carboxylate 43

To a solution of methyl 4-(((1*H*-tetrazol-5-yl)methyl)amino)-furazan-3- carboxylate **42** (150 mg, 0.67 mmol, 1 eq) in acetonitrile (6 mL) was added benzyl bromide (93 µL, 0.80 mmol, 1.2 eq) and trimethylamine (93 µL, 0.67 mmol, 1 eq). The resulting solution was stirred at room temperature for 24 h. After completion of the reaction, the reaction mixture was evaporated under reduced pressure and the product 2,5-disubstituted tetrazole compound **43**

and its isomer 1,5-disubstituted tetrazole compound **44** were separated by column chromatography (SiO$_2$, n-hexane/ethyl acetate, 20% → 80% ethyl acetate). After lyophilization, the product was obtained as a white solid.

Yield: 50 mg (24%)

^{1}H-NMR (500 MHz, DMSO-d_6): δ [ppm] = 7.43 – 7.23 (m, 6H, H-8, H-20, H-22, H-19, H-23, H-21), 5.91 (s, 2H, H-17), 4.68 (d, J = 6.2 Hz, 2H, H-10), 3.94 (s, 3H, H-16).
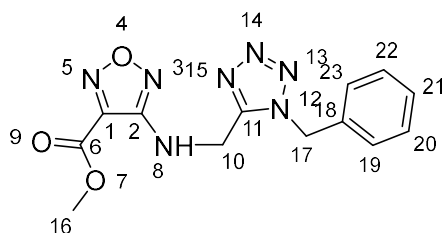
^{13}C-NMR (126 MHz, DMSO-d_6): δ [ppm] = 164.28 (C-11), 159.17 (C-6), 156.60 (C-2), 139.69 (C-18), 134.69 (C-19, C-23), 129.38 (C-20, C-22), 129.12 (C-21), 128.84 (C-1), 56.43 (C-16), 53.73 (C-17), 39.69 (C-10).

ESI-MS (*m/z*): [M+H]$^+$ calcd for C$_{13}$H$_{14}$N$_7$O$_3{}^+$: 316.1 Da; found: 316.0 Da.

Melting point: 91 °C

Methyl 4-(((1-benzyl-1*H*-tetrazol-5-yl)methyl)amino)-furazan-3-carboxylate 44

Methyl 4-(((1-benzyl-1*H*-tetrazol-5-yl)methyl)amino)-furazan-3-carboxylate **44** was obtained simultaneously with compound **43** a white solid.

Yield: 43 mg (21%)

^{1}H-NMR (500 MHz, DMSO-d_6): δ [ppm] = 7.42 – 7.06 (m, 6H, H-8, H-20, H-22, H-19, H-23, H-21), 5.75 (s, 2H, H-17), 4.80 (d, J = 6.2 Hz, 2H, H-10), 3.92 (s, 3H, H-16).
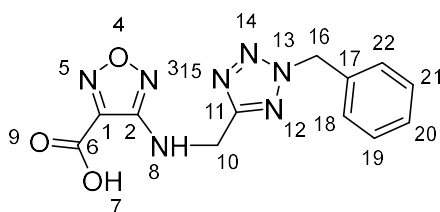
^{13}**C-NMR** (126 MHz, DMSO-d_6): δ [ppm] = 158.90 (C-6), 156.21 (C-2), 153.17 (C-11), 139.42 (C-18), 135.04 (C-20, C-22), 129.17 (C-19, C-23), 128.65 (C-21), 127.92 (C-1), 53.67 (C-16), 50.53 (C-17), 37.77 (C-10).

ESI-MS (*m/z*): [M+H]$^+$ calcd for C$_{13}$H$_{14}$N$_7$O$_3$$^+$: 316.1 Da; found: 316.0 Da.

Melting point: 102 °C

4-(((2-Benzyl-2*H*-tetrazol-5-yl)methyl)amino)-furazan-3-carboxylic acid 45

To a stirred solution of methyl 4-(((2-benzyl-2*H*-tetrazol-5-yl)methyl)amino)-1,2,5-oxadiazole-3-carboxylate **43** (200 mg, 0.63 mmol, 1 eq) in a mixture of methanol (1 ml) and water (1 ml) was added 1 N NaOH (1 mL). The mixture was stirred at room temperature for 1.5 h. Upon completion of reaction, the solvent was evaporated under reduced pressure. The residue was dissolved in water (20 mL), acidified with concentrated HCl to pH = 2 and a white precipitate was formed as product **45**.

Yield: 150 mg (79%)

^{1}**H-NMR** (500 MHz, DMSO-d_6): δ [ppm] = 7.57 – 7.15 (m, 5H, H-19, H-21, H-18, H-22, H-20), 7.09 (t, J = 6.2 Hz, 1H, H-8), 5.90 (s, 2H, H-16), 4.67 (d, J = 6.1 Hz, 2H, H-10).

^{13}**C-NMR** (126 MHz, DMSO-d_6): δ [ppm] = 164.34 (C-11), 160.52 (C-6), 156.86 (C-2), 140.35 (C-17), 134.70 (C-1), 129.38 (C-18, C-22), 129.11 (C-19, C-21), 128.83 (C-20), 56.42 (C-16), 39.69 (C-10).

ESI-HRMS (*m/z*): [M+H]$^+$ calcd for C$_{12}$H$_{12}$N$_7$O$_3$$^+$: 302.1007 Da; found: 302.1001 Da.

Melting point: 183 °C

4-(((1-Benzyl-1*H*-tetrazol-5-yl)methyl)amino)-furazan-3-carboxylic acid 46
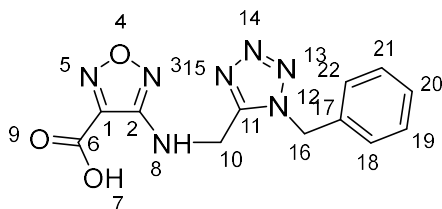
To a stirred solution of methyl 4-(((1-benzyl-1*H*-tetrazol-5-yl)methyl)amino)-1,2,5-oxadiazole-3-carboxylate **44** (200 mg, 0.63 mmol, 1 eq) in a mixture of methanol (1 ml) and water (1 ml) was added 1 N NaOH (1 mL). The mixture was stirred at room temperature for 1.5 h. Upon completion of reaction, the solvent was evaporated under reduced pressure. The residue was dissolved in water (20 mL), acidified with concentrated HCl to pH = 2 and a white precipitate was formed as product **46**.

Yield: 144 mg (76%)

^{1}H-NMR (500 MHz, DMSO-d_6): δ [ppm] = 7.59 – 6.83 (m, 6H, H-8, H-18, H-22, H-19, H-21, H-20), 5.75 (s, 2H, H-16), 4.79 (d, J = 5.9 Hz, 2H, H-10).

^{13}C-NMR (126 MHz, DMSO-d_6): δ [ppm] = 160.31 (C-6), 156.56 (C-2), 153.23 (C-11), 140.18 (C-17), 135.00 (C-1), 129.24 (C-19, C-21), 128.74 (C-18, C-22), 128.13 (C-20), 50.52 (C-16), 37.79 (C-10).

ESI-HRMS (*m/z*): [M+H]$^+$ calcd for C$_{12}$H$_{12}$N$_7$O$_3^+$: 302.1006 Da; found: 302.1001 Da.

Melting point: 214 °C

References

1. Azam, M.; Erdjument‑Bromage, H.; Kreider, B. L.; Xia, M.; Quelle, F.; Basu, R.; Saris, C.; Tempst, P.; Ihle, J. N.; Schindler, C., Interleukin‑3 signals through multiple isoforms of Stat5. *EMBO J* **1995,** *14* (7), 1402-11.

2. Ilaria, R. L.; Van Etten, R. A., P210 and P190BCR/ABL Induce the Tyrosine Phosphorylation and DNA Binding Activity of Multiple Specific STAT Family Members. *The Journal of biological chemistry* **1996,** *271* (49), 31704-10.

3. Ihle, J. N., STATs: Signal Transducers and Activators of Transcription. *Cell* **1996,** *84* (3), 331-34.

4. Hennighausen, L.; Robinson, G. W., Interpretation of cytokine signaling through the transcription factors STAT5A and STAT5B. *Genes Dev* **2008,** *22* (6), 711-21.

5. Akira, S., Functional Roles of STAT Family Proteins: Lessons from Knockout Mice. *Stem Cells* **1999,** *17* (3), 138-46.

6. Nosaka, T.; Kawashima, T.; Misawa, K.; Ikuta, K.; Mui, A. L.; Kitamura, T., STAT5 as a molecular regulator of proliferation, differentiation and apoptosis in hematopoietic cells. *EMBO J* **1999,** *18* (17), 4754-65.

7. Rani, A.; Murphy, J. J., STAT5 in Cancer and Immunity. *J Interferon Cytokine Res* **2016,** *36* (4), 226-37.

8. Birkenkamp, K. U.; Geugien, M.; Lemmink, H. H.; Kruijer, W.; Vellenga, E., Regulation of constitutive STAT5 phosphorylation in acute myeloid leukemia blasts. *Leukemia* **2001,** *15*, 1923-31.

9. Darnell, J. E., Jr., Transcription factors as targets for cancer therapy. *Nat Rev Cancer* **2002,** *2* (10), 740-9.

10. Levy, D. E.; Darnell, J. E., Jr., Stats: transcriptional control and biological impact. *Nat Rev Mol Cell Biol* **2002,** *3* (9), 651-62.

11. Ward, A. C., *STAT Inhibitors in Cancer*, Humana Press, **2016**.

References

12.   Tan, S. H.; Nevalainen, M. T., Signal transducer and activator of transcription 5A/B in prostate and breast cancers. *Endocr Relat Cancer* **2008,** *15* (2), 367-90.

13.   Schwaller, J.; Parganas, E.; Wang, D.; Cain, D.; Aster, J. C.; Williams, I. R.; Lee, C.; Gerthner, R.; Kitamura, T.; Frantsve, J.; Anastasiadou, E.; Loh, M. L.; Levy, D. E.; Ihle, J. N.; Gilliland, D. G., Stat5 Is Essential for the Myelo- and Lymphoproliferative Disease Induced by TEL/JAK2. *Mol Cell* **2000,** *6* (3), 693-704.

14.   Hoelbl, A.; Kovacic, B.; Kerenyi, M. A.; Simma, O.; Warsch, W.; Cui, Y.; Beug, H.; Hennighausen, L.; Moriggl, R.; Sexl, V., Clarifying the role of Stat5 in lymphoid development and Abelson-induced transformation. *Blood* **2006,** *107* (12), 4898-906.

15.   Grimley, P. M.; Dong, F.; Rui, H., Stat5a and Stat5b: fraternal twins of signal transduction and transcriptional   activation. *Growth Factor Rev* **1999,** *10* (2), 131-57.

16.   Waksman, G.; Shoelson, S. E.; Pant, N.; Cowburn, D.; Kuriyan, J., Binding of a high affinity phosphotyrosyl peptide to the Src SH2 domain: crystal structures of the complexed and peptide-free forms. *Cell* **1993,** *72* (5), 779-90.

17.   Liu, B. A.; Jablonowski, K.; Raina, M.; Arce, M.; Pawson, T.; Nash, P. D., The human and mouse complement of SH2 domain proteins-establishing the boundaries of phosphotyrosine signaling. *Mol Cell* **2006,** *22* (6), 851-68.

18.   Berger, A.; Sexl, V.; Valent, P.; Moriggl, R., Inhibition of STAT5: A therapeutic option in BCR-ABL1-driven leukemia. *Oncotarget* **2014,** *5* (20), 9564-76.

19.   Langenfeld, F.; Guarracino, Y.; Arock, M.; Trouve, A.; Tchertanov, L., How Intrinsic Molecular Dynamics Control Intramolecular Communication in Signal Transducers and Activators of Transcription Factor STAT5. *PLoS One* **2015,** *10* (12), e0145142.

20.   Neculai, D.; Neculai, A. M.; Verrier, S.; Straub, K.; Klumpp, K.; Pfitzner, E.; Becker, S., Structure of the unphosphorylated STAT5a dimer. *The Journal of biological chemistry* **2005,** *280* (49), 40782-7.

21.   Graber, M.; Janczyk, W.; Sperl, B.; Elumalai, N.; Kozany, C.; Hausch, F.; Holak, T. A.; Berg, T., Selective targeting of disease-relevant protein binding domains by O-phosphorylated natural product derivatives. *ACS Chem Biol* **2011,** *6* (10), 1008-14.

22.   Shao, S.; Yu, R.; Yu, Y.; Li, Y., Dual-inhibitors of STAT5 and STAT3: studies from molecular docking and molecular dynamics simulations. *J Mol Model* **2014,** *20* (8),

2399.

23.   Raj, U.;   Kumar, H.;   Gupta, S.;   Varadwaj, P. K., Exploring dual inhibitors for STAT1 and STAT5 receptors utilizing virtual screening and dynamics simulation validation. *J Biomol Struct Dyn* **2016,** *34* (10), 2115-29.

24.   Gianti, E.; Zauhar, R. J., An SH2 domain model of STAT5 in complex with phospho-peptides define "STAT5 Binding Signatures". *J Comput Aided Mol Des* **2015,** *29* (5), 451-70.

25.   Liao, Z.;   Gu, L.;   Vergalli, J.;   Mariani, S. A.;   De Dominici, M.;   Lokareddy, R. K.;   Dagvadorj, A.;   Purushottamachar, P.;   McCue, P. A.;   Trabulsi, E.;   Lallas, C. D.;   Gupta, S.;   Ellsworth, E.;   Blackmon, S.;   Ertel, A.;   Fortina, P.;   Leiby, B.;   Xia, G.;   Rui, H.;   Hoang, D. T.;   Gomella, L. G.;   Cingolani, G.;   Njar, V.;   Pattabiraman, N.;   Calabretta, B.;   Nevalainen, M. T., Structure-Based Screen Identifies a Potent Small Molecule Inhibitor of Stat5a/b with Therapeutic Potential for Prostate Cancer and Chronic Myeloid Leukemia. *Mol Cancer Ther* **2015,** *14* (8), 1777-93.

26.   de Araujo, E. D.;   Erdogan, F.;   Neubauer, H. A.;   Meneksedag-Erol, D.;   Manaswiyoungkul, P.;   Eram, M. S.;   Seo, H. S.;   Qadree, A. K.;   Israelian, J.;   Orlova, A.;   Suske, T.;   Pham, H. T. T.;   Boersma, A.;   Tangermann, S.;   Kenner, L.;   Rulicke, T.;   Dong, A.;   Ravichandran, M.;   Brown, P. J.;   Audette, G. F.;   Rauscher, S.;   Dhe-Paganon, S.;   Moriggl, R.; Gunning, P. T., Structural and functional consequences of the STAT5B(N642H) driver mutation. *Nat Commun* **2019,** *10* (1), 2517.

27.   Moucadel, V.;   Constantinescu, S. N., Differential STAT5 Signaling by Ligand-dependent and Constitutively Active Cytokine Receptors. *Journal of Biological Chemistry* **2005,** *280* (14), 13364-13373.

28.   Haetscher, N.;   Feuermann, Y.;   Wingert, S.;   Rehage, M.;   Thalheimer, F. B.;   Weiser, C.;   Bohnenberger, H.;   Jung, K.;   Schroeder, T.;   Serve, H.;   Oellerich, T.;   Hennighausen, L.;   Rieger, M. A., STAT5-regulated microRNA-193b controls haematopoietic stem and progenitor cell expansion by modulating cytokine receptor signalling. *Nature Communications* **2015,** *6* (1).

29.   Hung, L.-Y.;   Tseng, J. T.;   Lee, Y.-C.;   Xia, W.;   Wang, Y.-N.;   Wu, M.-L.;   Chuang, Y.-H.;   Lai, C.-H.; Chang, W.-C., Nuclear epidermal growth factor receptor (EGFR) interacts with signal transducer and activator of transcription 5 (STAT5) in activating Aurora-A gene expression. *Nucleic Acids Research* **2008,** *36* (13), 4337-4351.

30.   Uyttendaele, I.; Lemmens, I.; Verhee, A.; De Smet, A.-S.; Vandekerckhove, J.; Lavens, D.; Peelman, F.; Tavernier, J., Mammalian Protein-Protein Interaction Trap (MAPPIT) Analysis of STAT5, CIS, and SOCS2 Interactions with the Growth Hormone Receptor. *Molecular Endocrinology* **2007,** *21* (11), 2821-2831.

31.   Paukku, K.; Silvennoinen, O., STATs as critical mediators of signal transduction and transcription: lessons learned from STAT5. *Cytokine Growth Factor Rev* **2004,** *15* (6), 435-55.

32.   Brooks, A. J.; Dai, W.; O'Mara, M. L.; Abankwa, D.; Chhabra, Y.; Pelekanos, R. A.; Gardon, O.; Tunny, K. A.; Blucher, K. M.; Morton, C. J.; Parker, M. W.; Sierecki, E.; Gambin, Y.; Gomez, G. A.; Alexandrov, K.; Wilson, I. A.; Doxastakis, M.; Mark, A. E.; Waters, M. J., Mechanism of activation of protein kinase JAK2 by the growth hormone receptor. *Science* **2014,** *344* (6185), 1249783.

33.   Wallweber, H. J.; Tam, C.; Franke, Y.; Starovasnik, M. A.; Lupardus, P. J., Structural basis of recognition of interferon-alpha receptor by tyrosine kinase 2. *Nat Struct Mol Biol* **2014,** *21* (5), 443-8.

34.   Kisseleva, T.; Bhattacharya, S.; Braunstein, J.; Schindler, C. W., Signaling through the JAK/STAT pathway, recent advances and future challenges. *Gene* **2002,** *285* (1-2), 1-24.

35.   Fahrenkamp, D.; Li, J.; Ernst, S.; Schmitz-Van de Leur, H.; Chatain, N.; Kuster, A.; Koschmieder, S.; Luscher, B.; Rossetti, G.; Muller-Newen, G., Intramolecular hydrophobic interactions are critical mediators of STAT5 dimerization. *Sci Rep* **2016,** *6*, 35454.

36.   Muller, J.; Sperl, B.; Reindl, W.; Kiessling, A.; Berg, T., Discovery of chromone-based inhibitors of the transcription factor STAT5. *Chembiochem* **2008,** *9* (5), 723-7.

37.   Gouilleux-Gruart, V.; Gouilleux, F.; Desaint, C.; Claisse, J. C.; Capiod, J. F.; Delobel, J.; Weber-Nordt, R.; Dusanter-Fourt, I.; Dreyfus, F.; Groner, B.; Prin, L., STAT-related transcription factors are constitutively activated in peripheral blood cells from acute leukemia patients. *Blood* **1996,** *87* (5), 1692-7.

38.   Ferbeyre, G.; Moriggl, R., The role of Stat5 transcription factors as tumor suppressors or oncogenes. *Biochim Biophys Acta* **2011,** *1815* (1), 104-14.

39.   Harir, N.; Pecquet, C.; Kerenyi, M.; Sonneck, K.; Kovacic, B.; Nyga, R.; Brevet, M.; Dhennin, I.; Gouilleux-Gruart, V.; Beug, H.; Valent, P.; Lassoued, K.; Moriggl, R.; Gouilleux, F., Constitutive activation of Stat5 promotes its

cytoplasmic localization and association with PI3-kinase in myeloid leukemias. *Blood* **2006,** *109* (4), 1678-1686.

40.   Meshinchi, S.; Appelbaum, F. R., Structural and functional alterations of FLT3 in acute myeloid leukemia. *Clin Cancer Res* **2009,** *15* (13), 4263-9.

41.   Cao, T.; Jiang, N.; Liao, H.; Shuai, X.; Su, J.; Zheng, Q., The FLT3-ITD mutation and the expression of its downstream signaling intermediates STAT5 and Pim-1 are positively correlated with CXCR4 expression in patients with acute myeloid leukemia. *Sci Rep* **2019,** *9* (1), 12209.

42.   Okada, K.; Nogami, A.; Ishida, S.; Akiyama, H.; Chen, C.; Umezawa, Y.; Miura, O., FLT3-ITD induces expression of Pim kinases through STAT5 to confer resistance to the PI3K/Akt pathway inhibitors on leukemic cells by enhancing the mTORC1/Mcl-1 pathway. *Oncotarget* **2017,** *9* (10), 8870-86.

43.   Cilloni, D.; Saglio, G., Molecular pathways: BCR-ABL. *Clin Cancer Res* **2012,** *18* (4), 930-7.

44.   Quintas-Cardama, A.; Kantarjian, H.; Cortes, J., Flying under the radar: the new wave of BCR-ABL inhibitors. *Nature reviews. Drug discovery* **2007,** *6* (10), 834-48.

45.   Basham, B.; Sathe, M.; Grein, J.; McClanahan, T.; D'Andrea, A.; Lees, E.; Rascle, A., In vivo identification of novel STAT5 target genes. *Nucleic Acids Res* **2008,** *36* (11), 3802-18.

46.   Kanai, T.; Seki, S.; Jenks, J. A.; Kohli, A.; Kawli, T.; Martin, D. P.; Snyder, M.; Bacchetta, R.; Nadeau, K. C., Identification of STAT5A and STAT5B target genes in human T cells. *PLoS One* **2014,** *9* (1), e86790.

47.   Guo, Z.; Wang, A.; Zhang, W.; Levit, M.; Gao, Q.; Barberis, C.; Tabart, M.; Zhang, J.; Hoffmann, D.; Wiederschain, D.; Rocnik, J.; Sun, F.; Murtie, J.; Lengauer, C.; Gross, S.; Zhang, B.; Cheng, H.; Patel, V.; Schio, L.; Adrian, F.; Dorsch, M.; Garcia-Echeverria, C.; Huang, S. M., PIM inhibitors target CD25-positive AML cells through concomitant suppression of STAT5 activation and degradation of MYC oncogene. *Blood* **2014,** *124* (11), 1777-89.

48.   Wittig, I.; Groner, B., Signal transducer and activator of transcription 5 (STAT5), a crucial regulator of immune and cancer cells. *Curr Drug Targets Immune Endocr Metabol Disord* **2005,** *5* (4), 449-63.

49.   Huang, M.; Dorsey, J. F.; Epling-Burnette, P. K.; Nimmanapalli, R.; Landowski, T. H.; Mora, L. B.; Niu, G.; Sinibaldi, D.; Bai, F.; Kraker, A.;

Yu, H.; Moscinski, L.; Wei, S.; Djeu, J.; Dalton, W. S.; Bhalla, K.; Loughran, T. P.; Wu, J.; Jove, R., Inhibition of Bcr-Abl kinase activity by PD180970 blocks constitutive activation of Stat5 and growth of CML cells. *Oncogene* **2002,** *21* (57), 8804-16.

50.   Fathi, A. T.; Grant, S.; Karp, J. E., Exploiting cellular pathways to develop new treatment strategies for AML. *Cancer Treat Rev* **2010,** *36* (2), 142-50.

51.   Sato, T.; Yang, X.; Knapper, S.; White, P.; Smith, B. D.; Galkin, S.; Small, D.; Burnett, A.; Levis, M., FLT3 ligand impedes the efficacy of FLT3 inhibitors in vitro and in vivo. *Blood* **2011,** *117* (12), 3286-93.

52.   Orlova, A.; Neubauer, H. A.; Moriggl, R., The stromal microenvironment provides an escape route from FLT3 inhibitors through the GAS6-AXL-STAT5 axis. *Haematologica* **2019,** *104* (10), 1907-1909.

53.   Pardanani, A.; Lasho, T.; Smith, G.; Burns, C. J.; Fantino, E.; Tefferi, A., CYT387, a selective JAK1/JAK2 inhibitor: in vitro assessment of kinase selectivity and preclinical studies using cell lines and primary cells from polycythemia vera patients. *Leukemia* **2009,** *23* (8), 1441-5.

54.   Gu, L.; Liao, Z.; Hoang, D. T.; Dagvadorj, A.; Gupta, S.; Blackmon, S.; Ellsworth, E.; Talati, P.; Leiby, B.; Zinda, M.; Lallas, C. D.; Trabulsi, E. J.; McCue, P.; Gomella, L.; Huszar, D.; Nevalainen, M. T., Pharmacologic inhibition of Jak2-Stat5 signaling By Jak2 inhibitor AZD1480 potently suppresses growth of both primary and castrate-resistant prostate cancer. *Clin Cancer Res* **2013,** *19* (20), 5658-74.

55.   Ghiaur, G.; Levis, M., Mechanisms of Resistance to FLT3 Inhibitors and the Role of the Bone Marrow Microenvironment. *Hematol Oncol Clin North Am* **2017,** *31* (4), 681-692.

56.   Ghiaur, G.; Levis, M., Mechanisms of resistance to FLT3 inhibitors and the role of the bone marrow microenvironment. *Hematol Oncol Clin North Am* **2018,** *31* (4), 681-92.

57.   Wu, L.; Zepp, J. A.; Qian, W.; Martin, B. N.; Ouyang, W.; Yin, W.; Bunting, K. D.; Aronica, M.; Erzurum, S.; Li, X., A novel IL-25 signaling pathway through STAT5. *J Immunol* **2015,** *194* (9), 4528-34.

58.   Horatscheck, A.; Wagner, S.; Ortwein, J.; Kim, B. G.; Lisurek, M.; Beligny, S.; Schutz, A.; Rademann, J., Benzoylphosphonate-based photoactive phosphopeptide mimetics for modulation of protein tyrosine phosphatases and highly specific labeling of SH2 domains. *Angew Chem Int Ed Engl* **2012,** *51* (37), 9441-7.

59.   Schust, J.;   Sperl, B.;   Hollis, A.;   Mayer, T. U.; Berg, T., Stattic: a small-molecule inhibitor of STAT3 activation and dimerization. *Chem Biol* **2006,** *13* (11), 1235-42.

60.   Page, B. D.;   Khoury, H.;   Laister, R. C.;   Fletcher, S.;   Vellozo, M.;   Manzoli, A.;   Yue, P.;   Turkson, J.;   Minden, M. D.; Gunning, P. T., Small molecule STAT5-SH2 domain inhibitors exhibit potent antileukemia activity. *Journal of medicinal chemistry* **2012,** *55* (3), 1047-55.

61.   Romagnoli, R.;   Baraldi, P. G.;   Prencipe, F.;   Lopez-Cara, C.;   Rondanin, R.;   Simoni, D.;   Hamel, E.;   Grimaudo, S.;   Pipitone, R. M.;   Meli, M.; Tolomeo, M., Novel iodoacetamido benzoheterocyclic derivatives with potent antileukemic activity are inhibitors of STAT5 phosphorylation. *European journal of medicinal chemistry* **2016,** *108*, 39-52.

62.   Juen, L.;   Brachet-Botineau, M.;   Parmenon, C.;   Bourgeais, J.;   Herault, O.;   Gouilleux, F.;   Viaud-Massuard, M. C.; Prie, G., New Inhibitor Targeting Signal Transducer and Activator of Transcription 5 (STAT5) Signaling in Myeloid Leukemias. *Journal of medicinal chemistry* **2017,** *60* (14), 6119-6136.

63.   Cumaraswamy, A. A.; Gunning, P. T., Progress towards direct inhibitors of Stat5 protein. *Horm Mol Biol Clin Investig* **2012,** *10* (2), 281-6.

64.   Miklossy, G.;   Hilliard, T. S.; Turkson, J., Therapeutic modulators of STAT signalling for human diseases. *Nature reviews. Drug discovery* **2013,** *12* (8), 611-29.

65.   Wong, E. L.;   Nawrotzky, E.;   Arkona, C.;   Kim, B. G.;   Beligny, S.;   Wang, X.;   Wagner, S.;   Lisurek, M.;   Carstanjen, D.; Rademann, J., The transcription factor STAT5 catalyzes Mannich ligation reactions yielding inhibitors of leukemic cell proliferation. *Nat Commun* **2019,** *10* (1), 66.

66.   Hopkins, A. L.;   Keseru, G. M.;   Leeson, P. D.;   Rees, D. C.; Reynolds, C. H., The role of ligand efficiency metrics in drug discovery. *Nature reviews. Drug discovery* **2014,** *13* (2), 105-21.

67.   Pham, H. T. T.;   Maurer, B.;   Prchal-Murphy, M.;   Grausenburger, R.;   Grundschober, E.;   Javaheri, T.;   Nivarthi, H.;   Boersma, A.;   Kolbe, T.;   Elabd, M.;   Halbritter, F.;   Pencik, J.;   Kazemi, Z.;   Grebien, F.;   Hengstschlager, M.;   Kenner, L.;   Kubicek, S.;   Farlik, M.;   Bock, C.;   Valent, P.;   Muller, M.;   Rulicke, T.;   Sexl, V.; Moriggl, R., STAT5BN642H is a driver mutation for T cell neoplasia. *J Clin Invest* **2018,** *128* (1), 387-401.

68.   Ma, X.;   Wen, L.;   Wu, L.;   Wang, Q.;   Yao, H.;   Wang, Q.;   Ma, L.; Chen, S., Rare occurrence of a STAT5B N642H mutation in adult T-cell acute lymphoblastic

leukemia. *Cancer Genet* **2015,** *208* (1-2), 52-3.

69.   Bandapalli, O. R.;   Schuessele, S.; Kunz, J. B., The activating STAT5B N642H mutation is a common abnormality in pediatric T-cell acute lymphoblastic leukemia and confers a higher risk of relapse. *Haematologica* **2014,** *99* (10), 188-92.

70.   Mondal, M.; Hirsch, A. K., Dynamic combinatorial chemistry: a tool to facilitate the identification of inhibitors for protein targets. *Chem Soc Rev* **2015,** *44* (8), 2455-88.

71.   Storici, P.;   De Biase, D.;   Bossa, F.;   Bruno, S.;   Mozzarelli, A.;   Peneff, C.; Silverman, R. B.; Schirmer, T., Structures of gamma-aminobutyric acid (GABA) aminotransferase, a pyridoxal 5'-phosphate, and [2Fe-2S] cluster-containing enzyme, complexed with gamma-ethynyl-GABA and with the antiepilepsy drug vigabatrin. *The Journal of biological chemistry* **2004,** *279* (1), 363-73.

72.   Borštnar, R.;   Repič, M.;   Kržan, M.;   Mavri, J.; Vianello, R., Irreversible Inhibition of Monoamine Oxidase B by the Antiparkinsonian Medicines Rasagiline and Selegiline: A Computational Study. *European Journal of Organic Chemistry* **2011,** *2011* (32), 6419-6433.

73.   Jaegle, M.;   Wong, E. L.;   Tauber, C.;   Nawrotzky, E.;   Arkona, C.; Rademann, J., Protein-Templated Fragment Ligations-From Molecular Recognition to Drug Discovery. *Angew Chem Int Ed Engl* **2017,** *56* (26), 7358-7378.

74.   Burda, E.; Rademann, J., Catalytic activation of pre-substrates via dynamic fragment assembly on protein templates. *Nat Commun* **2014,** *5*, 5170.

75.   Black, S. P.;   Sanders, J. K.; Stefankiewicz, A. R., Disulfide exchange: exposing supramolecular reactivity through dynamic covalent chemistry. *Chem Soc Rev* **2014,** *43* (6), 1861-72.

76.   Atcher, J.; Alfonso, I., The effect of DMSO in the aqueous thiol–disulphide dynamic covalent chemistry of model pseudopeptides. *RSC Advances* **2013,** *3* (48).

77.   Gladysz, R.;   Vrijdag, J.;   Van Rompaey, D.;   Lambeir, A. M.;   Augustyns, K.; De Winter, H.; Van der Veken, P., Efforts towards an On-Target Version of the Groebke-Blackburn-Bienayme (GBB) Reaction for Discovery of Druglike Urokinase (uPA) Inhibitors. *Chemistry* **2019,** *25* (53), 12380-12393.

78.   Jaegle, M.;   Steinmetzer, T.; Rademann, J., Protein-Templated Formation of an Inhibitor of the Blood Coagulation Factor Xa through a Background-Free Amidation Reaction. *Angewandte Chemie International Edition* **2017,** *56* (13), 3718-3722.

References

79. Lagunas-Rangel, F. A.; Chávez-Valencia, V., FLT3–ITD and its current role in acute myeloid leukaemia. *Medical Oncology* **2017,** *34* (6).

80. Liu, S.; Walker, S. R.; Nelson, E. A.; Cerulli, R.; Xiang, M.; Toniolo, P. A.; Qi, J.; Stone, R. M.; Wadleigh, M.; Bradner, J. E.; Frank, D. A., Targeting STAT5 in Hematologic Malignancies through Inhibition of the Bromodomain and Extra-Terminal (BET) Bromodomain Protein BRD2. *Molecular Cancer Therapeutics* **2014,** *13* (5), 1194-1205.

81. Arndt, H.-D., Small Molecule Modulators of Transcription. *Angewandte Chemie International Edition* **2006,** *45* (28), 4552-4560.

82. Welsch, K.; Holstein, J.; Laurence, A.; Ghoreschi, K., Targeting JAK/STAT signalling in inflammatory skin diseases with small molecule inhibitors. *European Journal of Immunology* **2017,** *47* (7), 1096-1107.

83. Quintás-Cardama, A.; Vaddi, K.; Liu, P.; Manshouri, T.; Li, J.; Scherle, P. A.; Caulder, E.; Wen, X.; Li, Y.; Waeltz, P.; Rupar, M.; Burn, T.; Lo, Y.; Kelley, J.; Covington, M.; Shepard, S.; Rodgers, J. D.; Haley, P.; Kantarjian, H.; Fridman, J. S.; Verstovsek, S., Preclinical characterization of the selective JAK1/2 inhibitor INCB018424: therapeutic implications for the treatment of myeloproliferative neoplasms. *Blood* **2010,** *115* (15), 3109-3117.

84. Elumalai, N.; Berg, A.; Rubner, S.; Blechschmidt, L.; Song, C.; Natarajan, K.; Matysik, J.; Berg, T., Rational development of Stafib-2: a selective, nanomolar inhibitor of the transcription factor STAT5b. *Sci Rep* **2017,** *7* (1), 819.

85. Cumaraswamy, A. A.; Lewis, A. M.; Geletu, M.; Todic, A.; Diaz, D. B.; Cheng, X. R.; Brown, C. E.; Laister, R. C.; Muench, D.; Kerman, K.; Grimes, H. L.; Minden, M. D.; Gunning, P. T., Nanomolar-Potency Small Molecule Inhibitor of STAT5 Protein. *ACS medicinal chemistry letters* **2014,** *5* (11), 1202-1206.

86. Duncia, J. V.; Pierce, M. E.; Santella, J. B., Three synthetic routes to a sterically hindered tetrazole. A new one-step mild conversion of an amide into a tetrazole. *J Org Chem* **1991,** *56* (7), 2395-400.

87. Sisido, K.; Nabika, K.; Isida, T.; Kozima, S., Formation of organotin-nitrogen bonds III. N-trialkyltin-5-substituted tetrazoles. *J Organomet Chem* **1971,** *33* (3), 337-46.

88. Zhang, C.; Shen, Z.; Tian, L.; Chen, L., Synthesis of deuterium-labeled olmesartan and candesartan. *Journal of Labelled Compounds and Radiopharmaceuticals* **2012,** *55* (11), 401-405.

89. Prieto, A.; HallandKarl, N.; Jørgensen, A., Novel Imidazolidine-Tetrazole Organocatalyst for Asymmetric Conjugate Addition of Nitroalkanes. *Org Lett* **2005,** *7* (18), 3897-900.

90. Cardoso, A. L.; Sousa, C.; Henriques, M. S.; Paixao, J. A.; Pinho e Melo, T. M., Synthesis of New 2-Halo-2-(1H-tetrazol-5-yl)-2H-azirines via a Non-Classical Wittig Reaction. *Molecules* **2015,** *20* (12), 22351-63.

91. Touti, F.; Maurin, P.; Hasserodt, J., A Tetrakis(tetrazolyl) Analogue of EDTA. *European Journal of Organic Chemistry* **2009,** *2009* (10), 1495-1498.

92. Wessjohann, L. A.; Wild, H.; Ferreira, L. A.; Schrekker, H. S., Synthesis of α-alkenyl-β-hydroxy adducts by α-addition of unprotected 4-bromocrotonic acid and amides with aldehydes and ketones by chromium(II)-mediated reactions. *Applied Organometallic Chemistry* **2016,** *30* (8), 674-679.

93. Devasagayaraj, A.; Stüdemann, T.; Knochel, P., A New Nickel‐Catalyzed Cross‐Coupling Reaction between sp3 Carbon Centers. *Angew Chem Int Ed Engl* **1996,** *34* (23-24), 2723-25.

94. Sinenko, V. O.; Slivchuk, S. R.; Mityukhin, O. P.; Brovarets, V. S., Synthesis of New 1,3-Thiazolecarbaldehydes. *Russian Journal of General Chemistry* **2018,** *87* (12), 2766-2775.

95. Houssin, R.; Pommery, J.; Salaün, M.; Deweer, S.; Goossens, J.; Chavatte, P.; Hénichart, J., Design, Synthesis, and Pharmacological Evaluation of New Farnesyl Protein Transferase Inhibitors. *Journal of medicinal chemistry* **2002,** *45* (2), 533-6.

96. Kouznetsov, V. V.; Galvis, C. E. P., Strecker reaction and α-amino nitriles: Recent advances in their chemistry, synthesis, and biological properties. *Tetrahedron* **2018,** *74* (8), 773-810.

97. Sakai, N.; Takahashi, N.; Inoda, D.; Ikeda, R.; Konakahara, T., Copper-catalyzed three- five- or seven-component coupling reactions: the selective synthesis of cyanomethylamines, N,N-bis(cyanomethyl)amines and N,N'-bis(cyanomethyl) methylenediamines based on a Strecker-type synthesis. *Molecules* **2013,** *18* (10), 12488-99.

98. Sakai, N.; Uchida, N.; Konakahara, T., Facile and Selective Synthesis of Propargylic Amines and 1,6-Diynes: One-Pot Three-Component Coupling Reactions of Alkynylsilanes, Aldehydes and Amines by a Cooperative Catalytic System Comprised of CuCl and Cu(OTf)2. *Synlett* **2008,** *2008* (10), 1515-1519.

References

99. Demko, Z. P.; Sharpless, K. B., Preparation of 5-Substituted 1H-Tetrazoles from Nitriles in Water. *J Org Chem* **2001,** *66* (24), 7945-50.

100. Demko, Z. P.; Sharpless, K. B., An Expedient Route to the Tetrazole Analogues of α-Amino Acids. *Org Lett* **2002,** *4* (15), 2525-27.

101. El Remaily, M. A. E. A. A. A.; Mohamed, S. K., Eco-friendly synthesis of guanidinyltetrazole compounds and 5-substituted 1H-tetrazoles in water under microwave irradiation. *Tetrahedron* **2014,** *70* (2), 270-275.

102. Shie, J.; Fang, J., Microwave-Assisted One-Pot Tandem Reactions for Direct Conversion of Primary Alcohols and Aldehydes to Triazines and Tetrazoles in Aqueous Media. *J Org Chem* **2007,** *72* (8), 3141-44.

103. Ostrovskii, V. A.; Koren, A. O., Alkylation and Related Electrophilic Reactions at Endocyclic Nitrogen Atoms in the Chemistry of Tetrazoles. *Heterocycles* **2000,** *53* (6), 1421-48.

104. Koldobskii, G. I.; Kharbash, R. B., 2-Substituted and 2,5-Disubstituted Tetrazoles. *Russian Journal of Organic Chemistry* **2003,** *39* (4), 453-70.

105. Ortar, G.; Cascio, M. G.; Moriello, A. S.; Camalli, M.; Morera, E.; Nalli, M.; Di Marzo, V., Carbamoyl tetrazoles as inhibitors of endocannabinoid inactivation: a critical revisitation. *European journal of medicinal chemistry* **2008,** *43* (1), 62-72.

106. Sadlej-Sosnowska, N., Application of Natural Bond Orbital Analysis to Delocalization and Aromaticity in C-Substituted Tetrazoles. *J Org Chem* **2001,** *66* (26), 8737-43.

107. Muller, J.; Schust, J.; Berg, T., A high-throughput assay for signal transducer and activator of transcription 5b based on fluorescence polarization. *Anal Biochem* **2008,** *375* (2), 249-54.

108. Owicki, J. C., Fluorescence polarization and anisotropy in high throughput screening: perspectives and primer. *J Biomol Screen* **2000,** *5* (5), 297-306.

109. Schust, J.; Berg, T., A high-throughput fluorescence polarization assay for signal transducer and activator of transcription 3. *Anal Biochem* **2004,** *330* (1), 114-8.

110. Burlingham, B. T.; Widlanski, T., S., An Intuitive Look at the Relationship of Ki and IC50: A More General Use for the Dixon Plot. *J Chem Educ* **2003,** *80* (2), 214-18.

111. Cheng, Y.; Prusoft, W. H., Relationship between the inhibition constant (K1) and the concentration of inhibitor which causes 50 per cent inhibition (I50) of an enzymatic

reaction. *Biochem Pharmacol* **1973,** *22* (23), 3099-108.

112.   Burlingham, B. T.; Widlanski, T., S., An Intuitive Look at the Relationship of Ki and IC50: A More General Use for the Dixon Plot. *J Chem Edu* **2003,** *80* (2), 218-8.

113.   Nikolovska-Coleska, Z.;   Wang, R.;   Fang, X.;   Pan, H.;   Tomita, Y.;   Li, P.;   Roller, P. P.;   Krajewski, K.;   Saito, N. G.;   Stuckey, J. A.; Wang, S., Development and optimization of a binding assay for the XIAP BIR3 domain using fluorescence polarization. *Analytical Biochemistry* **2004,** *332* (2), 261-273.

114.   Sheremetev, A. B.;   Aleksandrova, N. S.;   Dmitriev, D. E.;   Averkiev, B. B.;   Antipin, M. Y., Synthesis and x-ray study of novel azofurazan - annulated macrocyclic lactams. *J Heterocyclic Chem* **2005,** *42* (4), 519-25.

115.   Finogenov, A. O.;   Epishina, M. A.;   Kulikov, A. S.;   Makhova, N. N.;   Anan'ev, I. V.;   Tartakovsky, V. A., Synthesis and nitration of N,N´-bis(3-R-furoxan-4-yl methylenediamines. *Russian Chemical Bulletin* **2010,** *59* (11), 2108-13.

116.   Finnegan, W. G.;   Henry, R. A.; Lofquist, R., An Improved Synthesis of 5-Substituted Tetrazoles. *J Am Chem Soc* **1958,** *80* (15), 3908-11.

117.   Alterman, M.; Hallberg, A., Fast Microwave-Assisted Preparation of Aryl and Vinyl Nitriles and the Corresponding Tetrazoles from Organo-halides. *J Org Chem* **2000,** *65* (23), 7984-9.

118.   Coca, A.;   Feinn, L.; Dudley, J., Microwave Synthesis of 5-Substituted 1H-Tetrazoles Catalyzed by Bismuth Chloride in Water. *Synthetic Communications* **2015,** *45* (8), 1023-1030.

119.   Joshi, S. M.;   Mane, R. B.;   Pulagam, K. R.;   Gomez-Vallejo, V.;   Llop, J.; Rode, C., The microwave-assisted synthesis of 5-substituted 1H-tetrazoles via [3+2] cycloaddition over a heterogeneous Cu-based catalyst: application to the preparation of 13N-labelled tetrazoles. *New Journal of Chemistry* **2017,** *41* (16), 8084-8091.

120.   Konermann, L., Addressing a Common Misconception: Ammonium Acetate as Neutral pH "Buffer" for Native Electrospray Mass Spectrometry. *J Am Soc Mass Spectrom* **2017,** *28* (9), 1827-1835.

121.   McMahon, R. M.;   Scanlon, M. J.; Martin, J. L., Interrogating Fragments Using a Protein Thermal Shift Assay. *Australian Journal of Chemistry* **2013,** *66* (12).

122.   Martinez Molina, D.; Nordlund, P., The Cellular Thermal Shift Assay: A Novel Biophysical Assay for In Situ Drug Target Engagement and Mechanistic Biomarker

Studies. *Annu Rev Pharmacol Toxicol* **2016,** *56*, 141-61.

123.   Martinez Molina, D.;   Jafari, R.;   Ignatushchenko, M.;   Seki, T.;   Larsson, E. A.;   Dan, C.;   Sreekumar, L.;   Cao, Y.; P., N., Monitoring drug target engagement in cells and tissues using the cellular thermal shift assay. *Science* **2013,** *341* (6141), 84-7.

124.   Jung, M.;   Krishna, S. N.;   Luan, C.-H.;   Mishra, R. K.;   Xu, L.;   Scheidt, K. A.;   Anderson, W. F.; Bergan, R. C., A Fluorescence-Based Thermal Shift Assay Identifies Inhibitors of Mitogen Activated Protein Kinase Kinase 4. *PLoS ONE* **2013,** *8* (12).

125.   Stirewalt, D. L.; Radich, J. P., The role of FLT3 in haematopoietic malignancies. *Nature Reviews Cancer* **2003,** *3* (9), 650-665.

126.   Choudhary, C.;   Brandts, C.;   Schwable, J.;   Tickenbrock, L.;   Sargin, B.;   Ueker, A.;   Bohmer, F. D.;   Berdel, W. E.;   Muller-Tidow, C.; Serve, H., Activation mechanisms of STAT5 by oncogenic Flt3-ITD. *Blood* **2007,** *110* (1), 370-4.

127.   Weisberg, E.;   Sattler, M.;   Ray, A.;   Griffin, J. D., Drug resistance in mutant FLT3-positive AML. *Oncogene* **2010,** *29* (37), 5120-34.

NMR Spectra
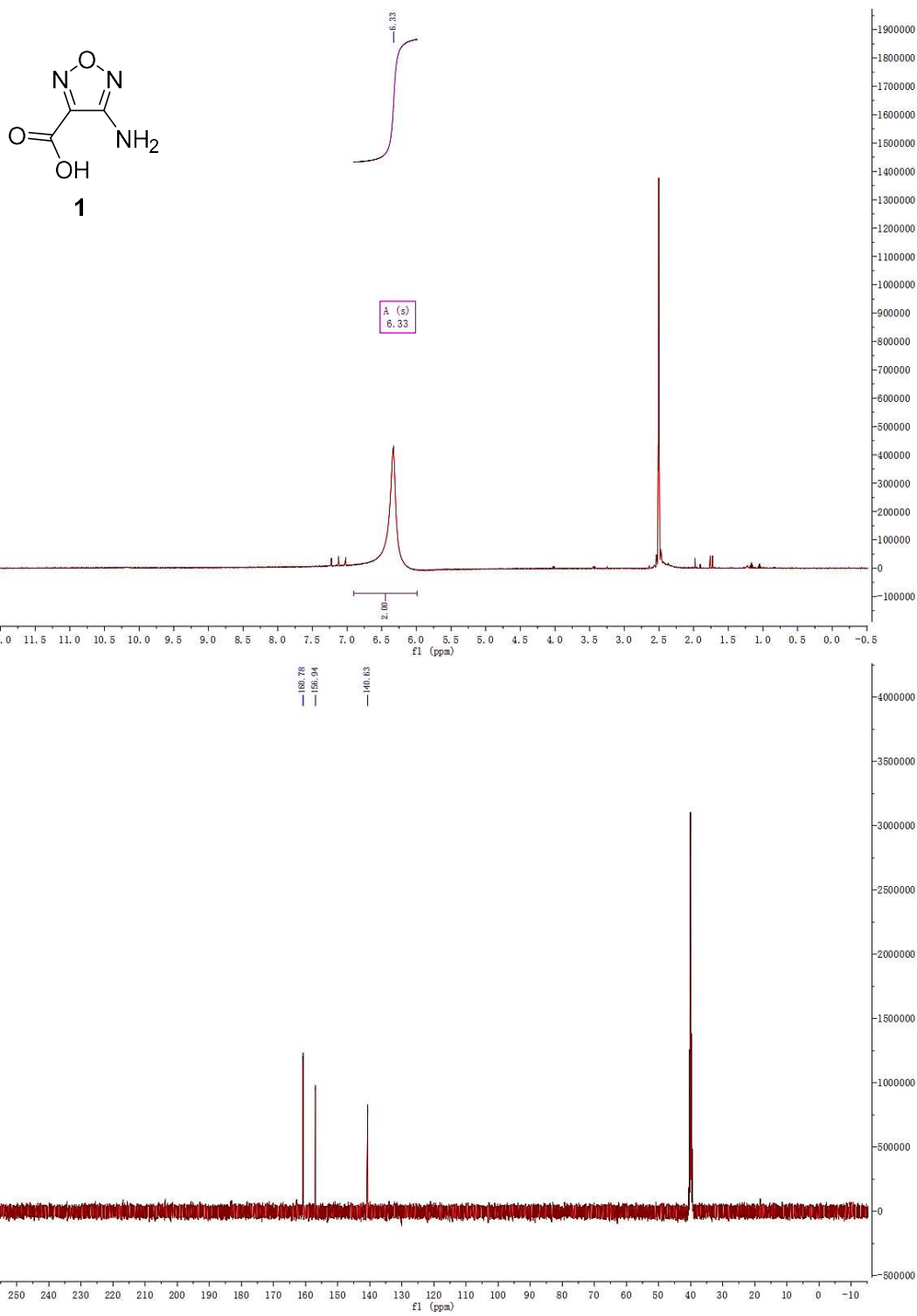
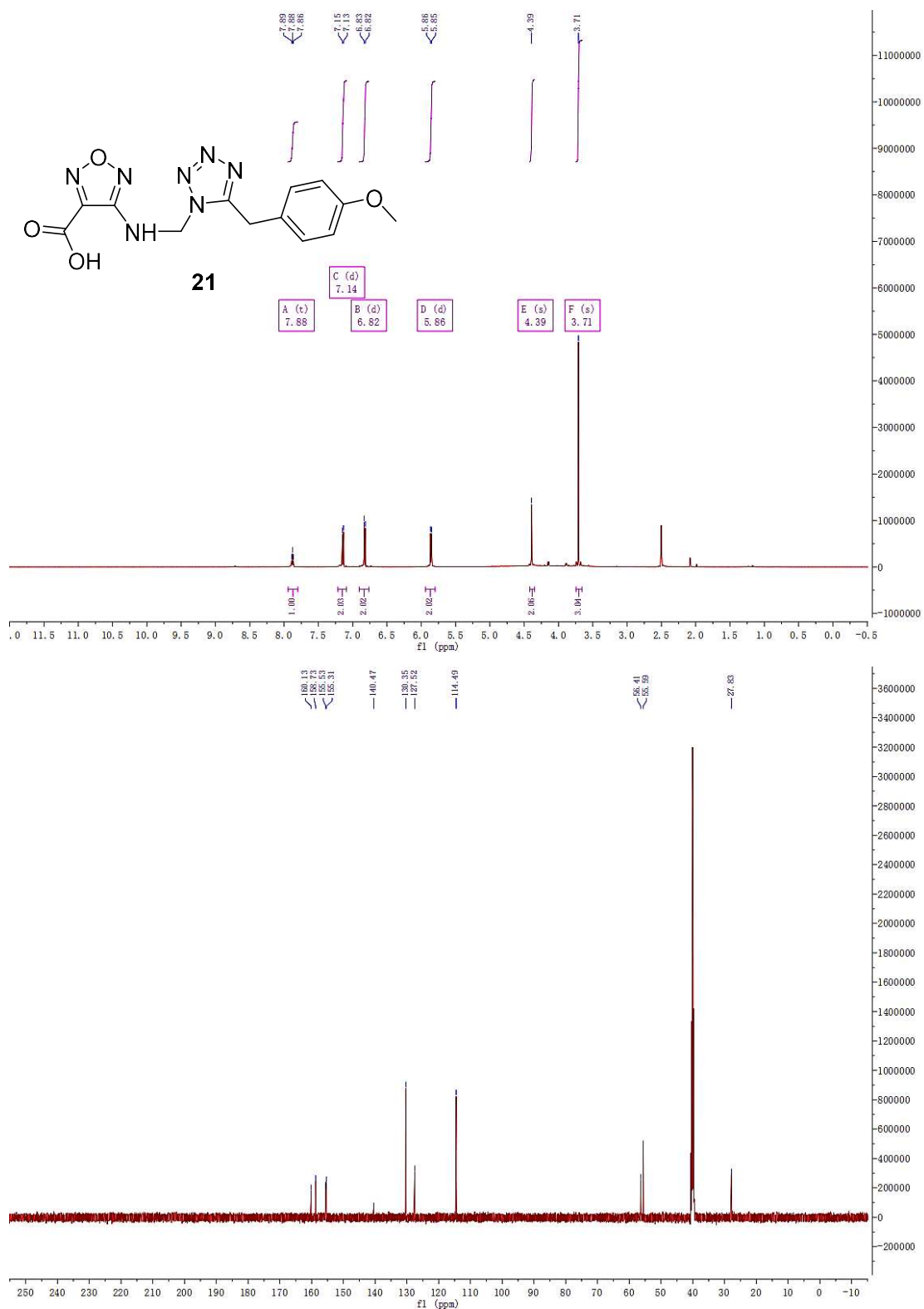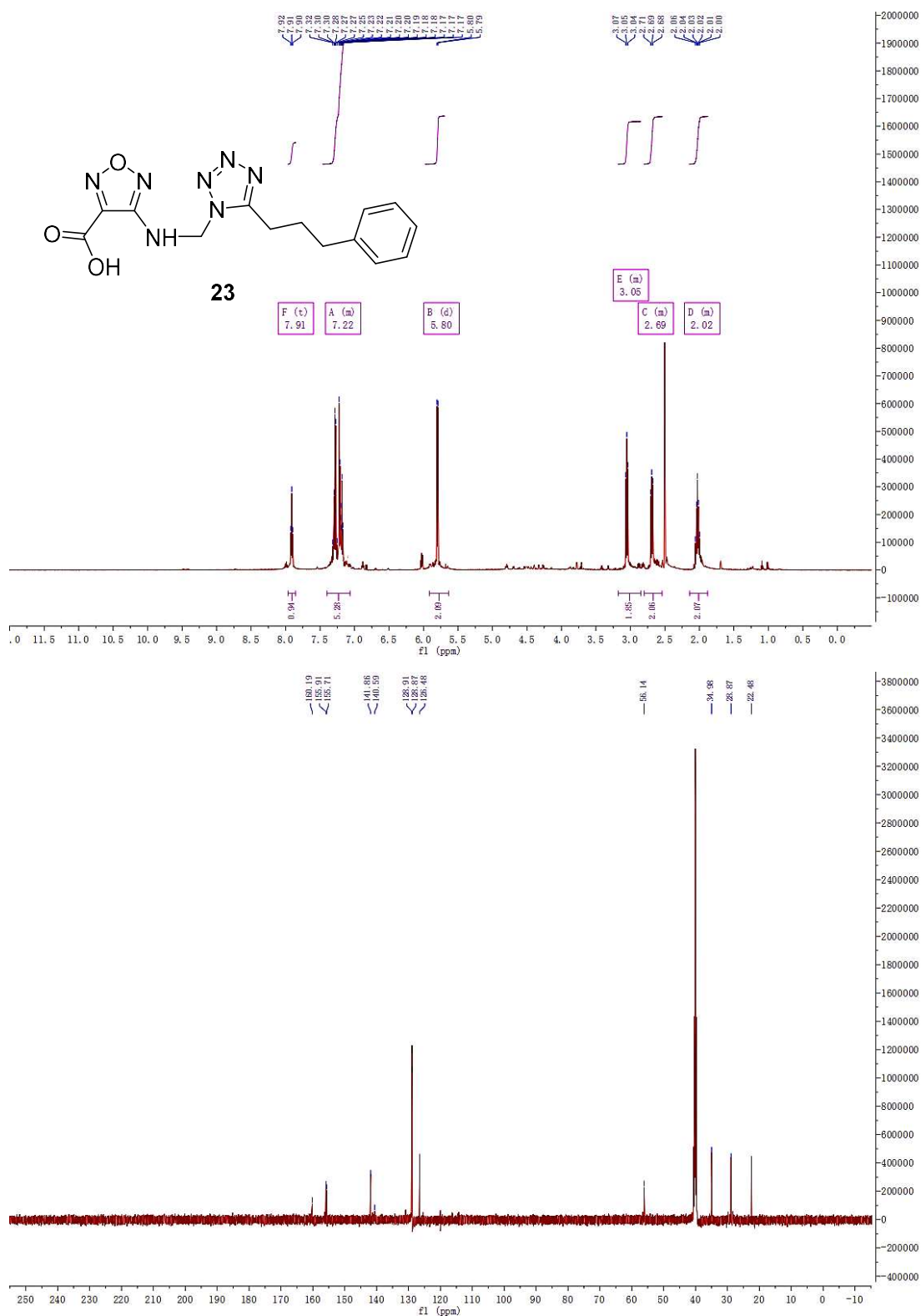¹H-NMR spectrum (500 MHz, DMSO-*d₆*) and ¹³C-NMR spectrum (126 MHz, DMSO-*d₆*) of **1**
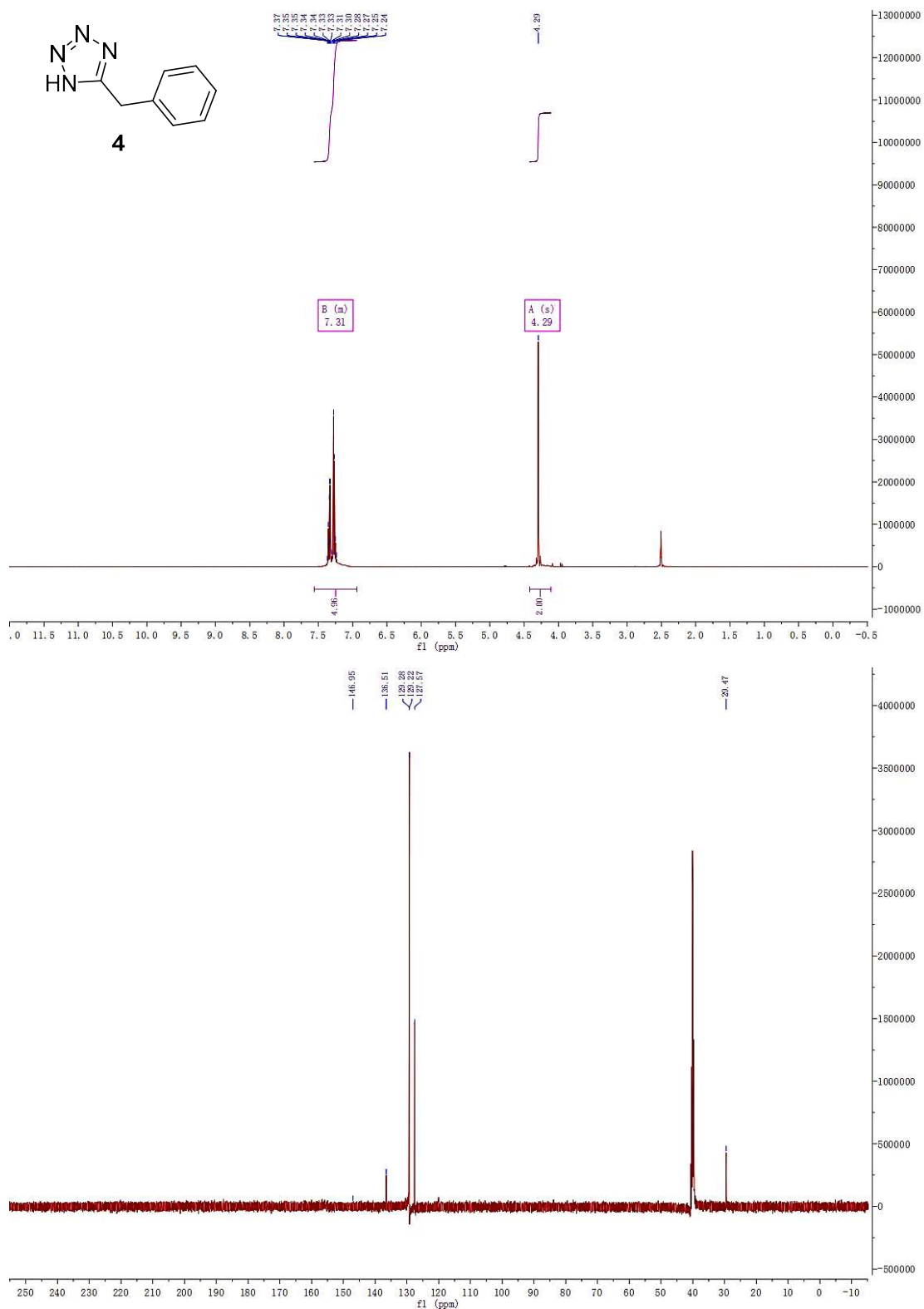
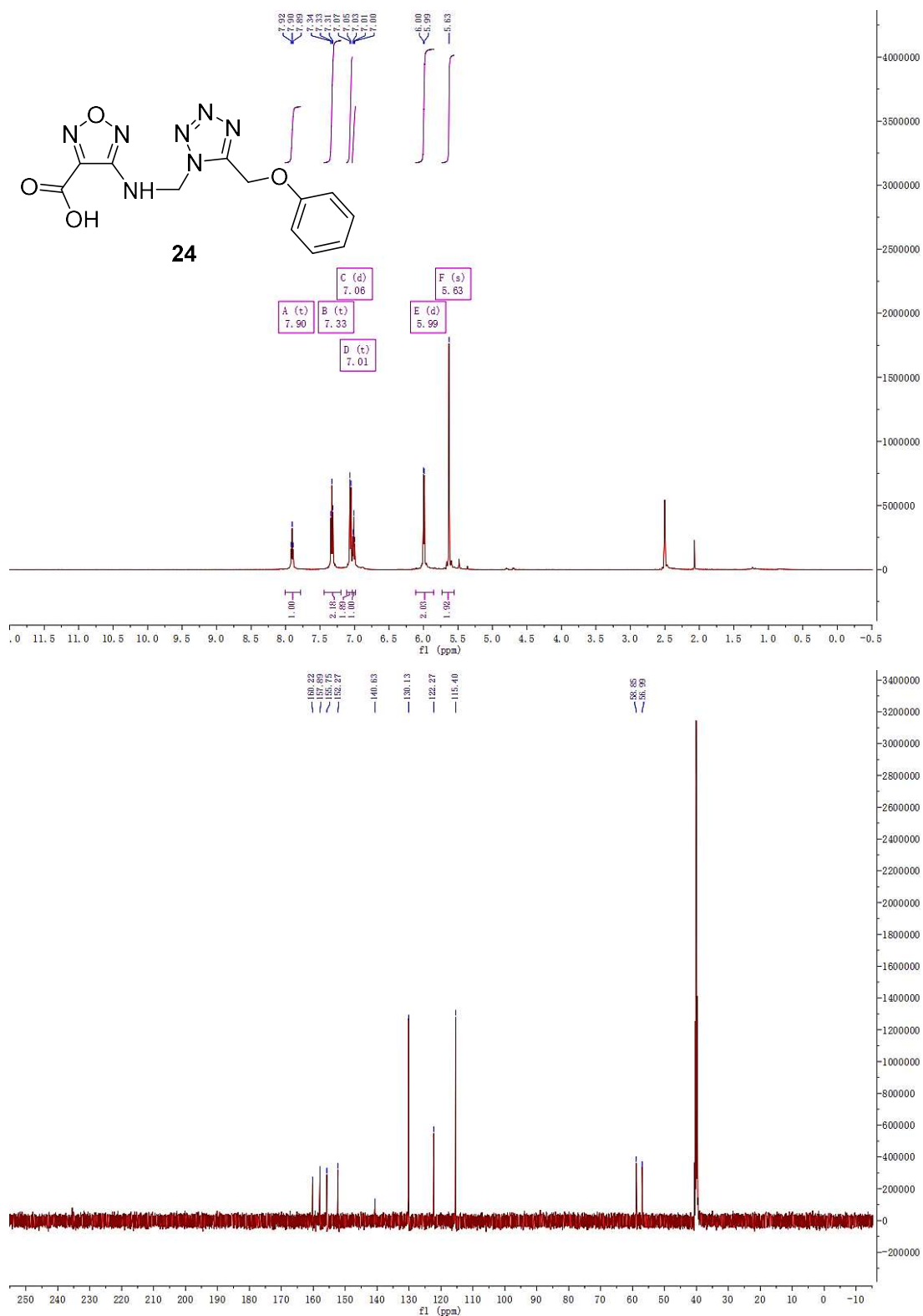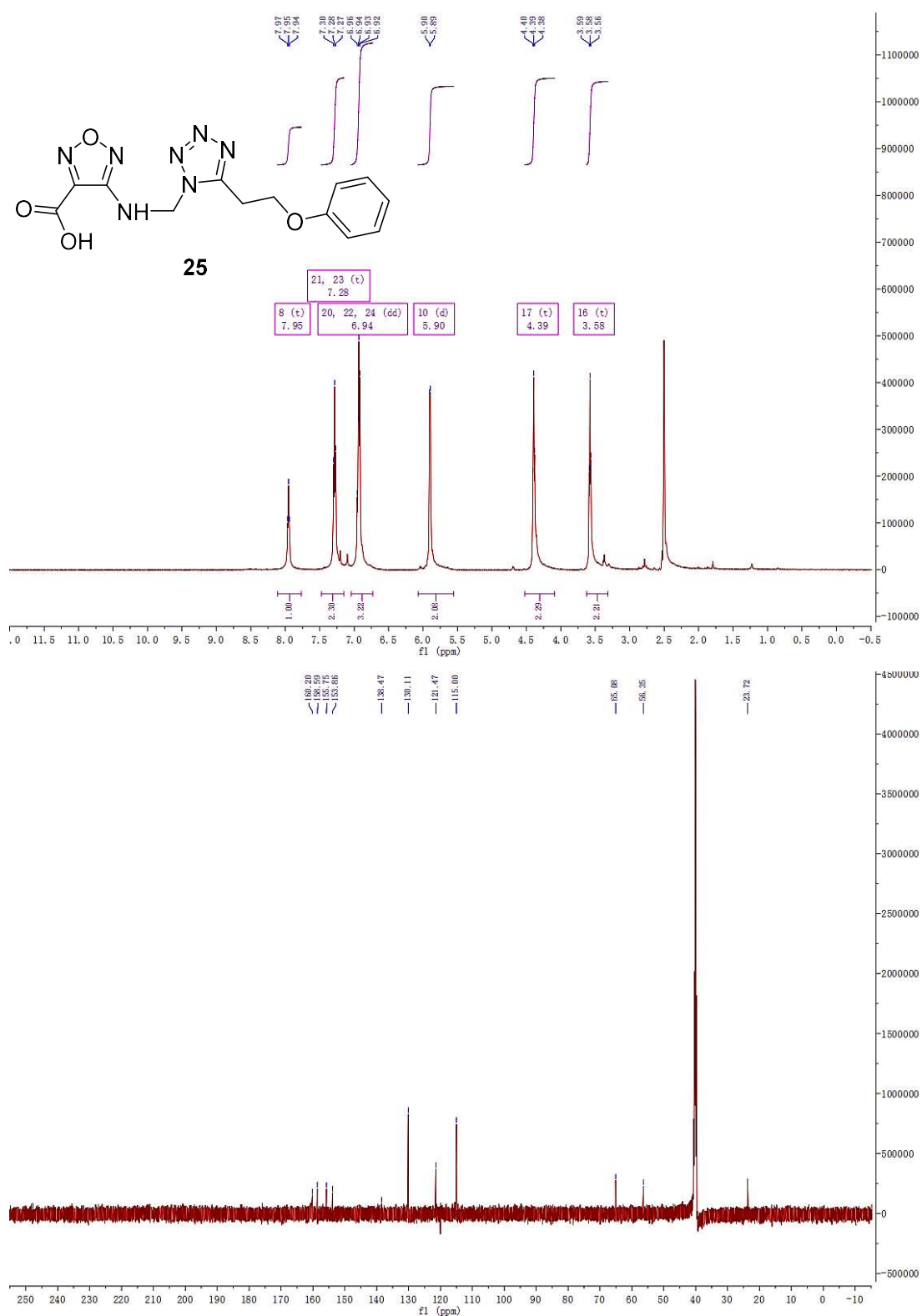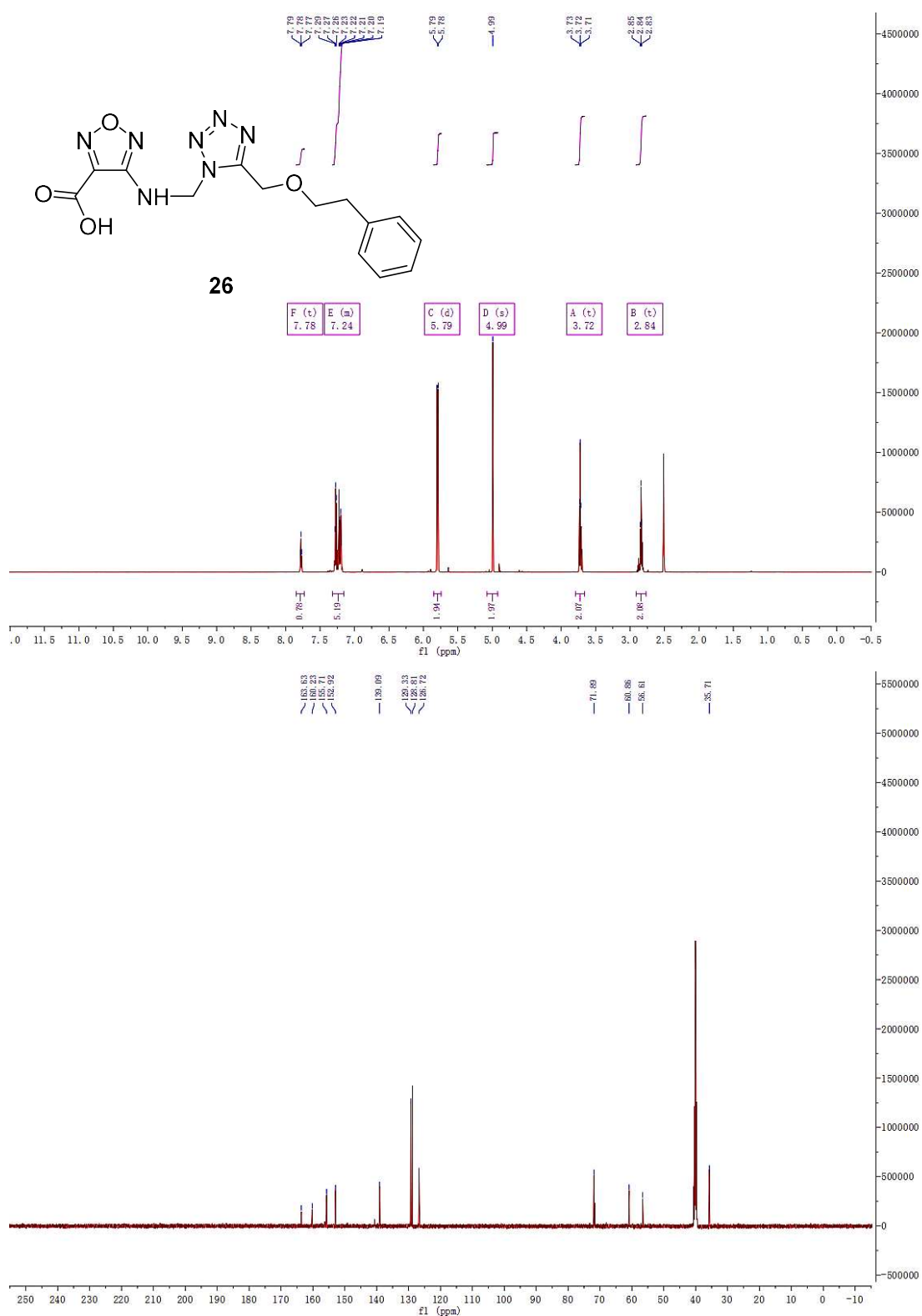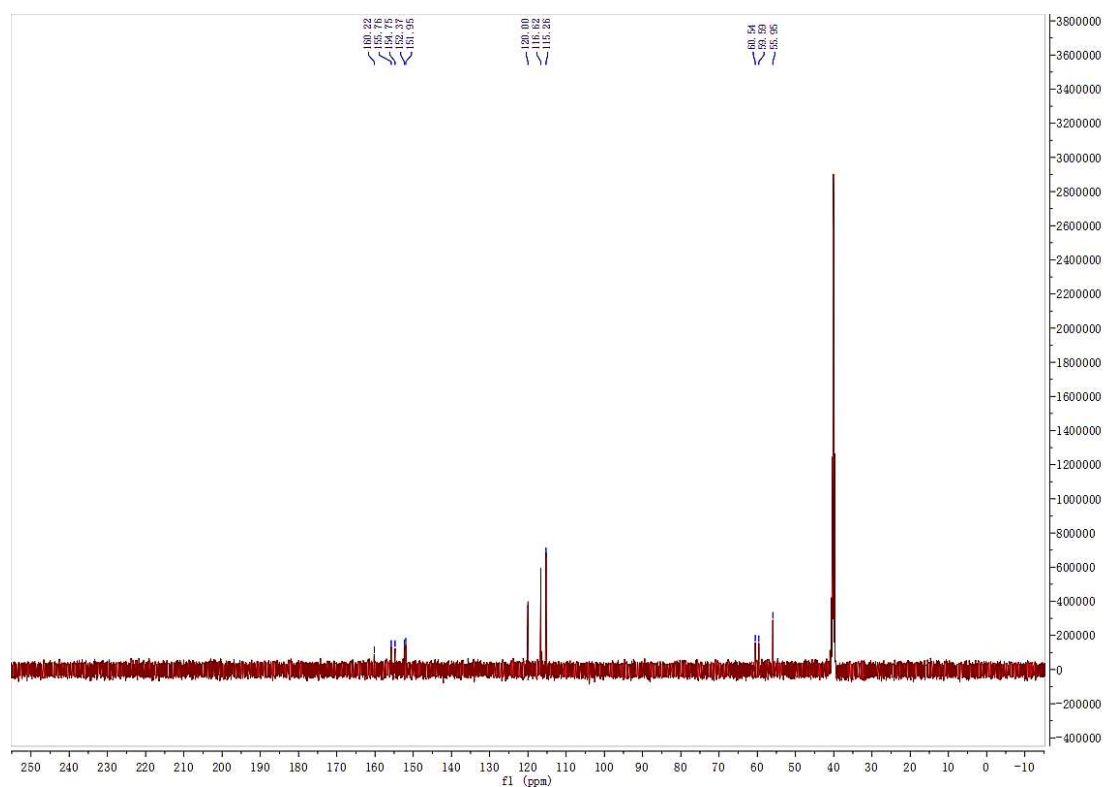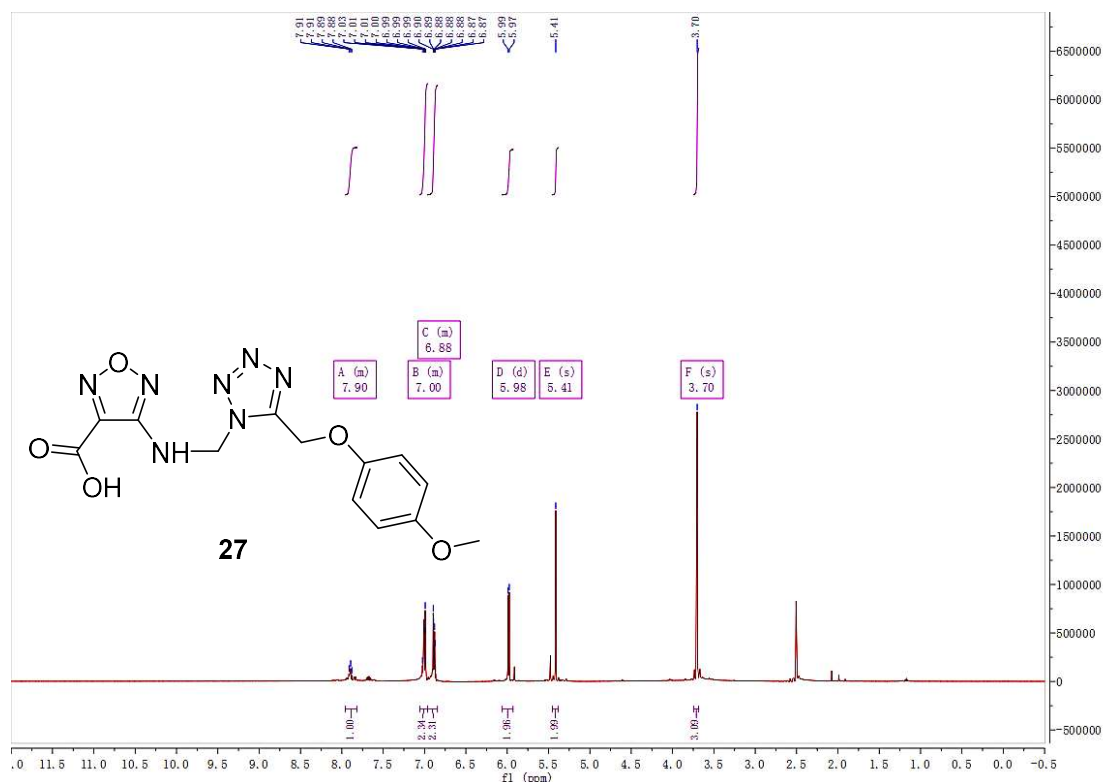¹H-NMR spectrum (500 MHz, DMSO-*d₆*) and ¹³C-NMR spectrum (126 MHz, DMSO-*d₆*) of **4**
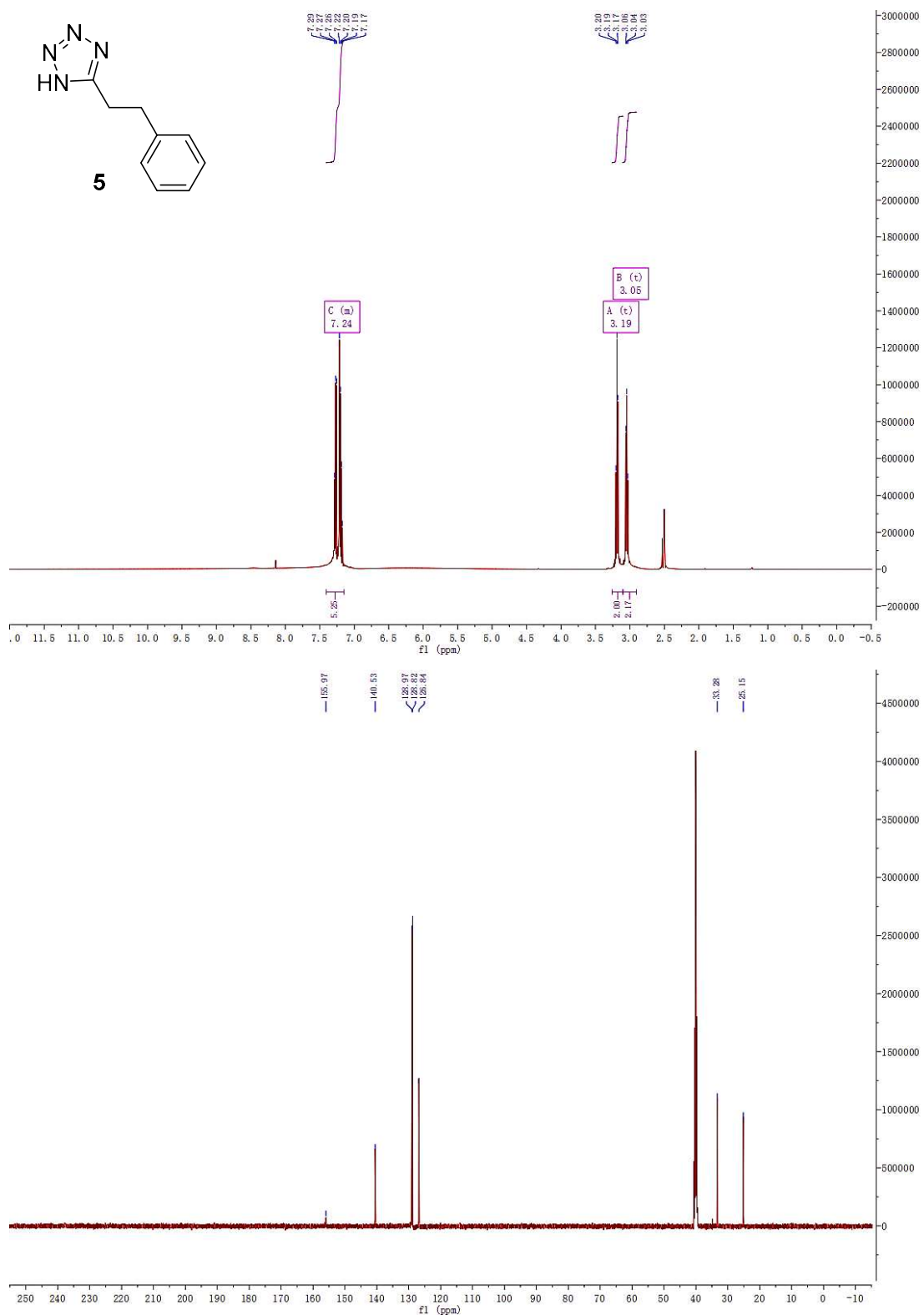
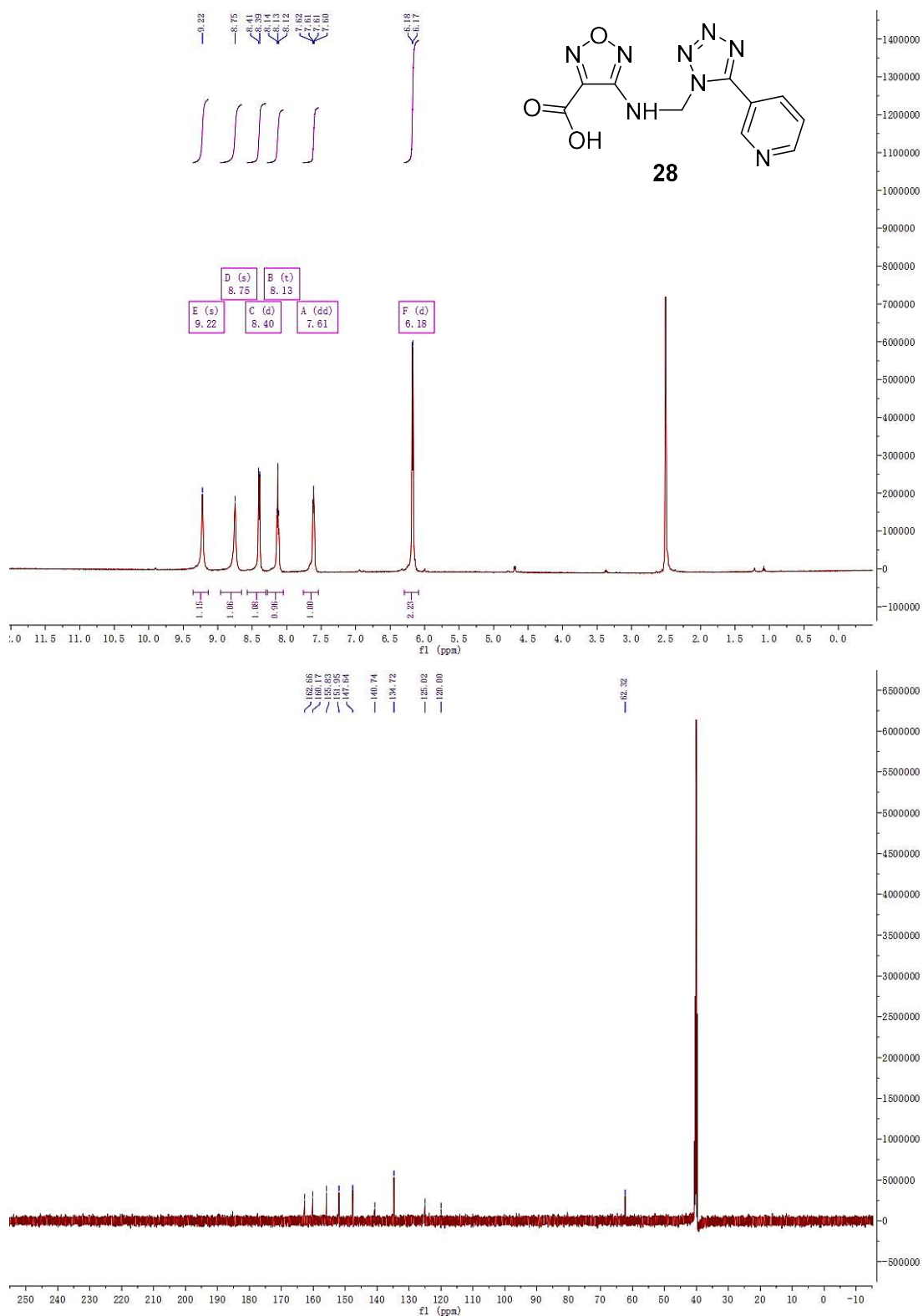^{1}H-NMR spectrum (500 MHz, DMSO-*d₆*) and ^{13}C-NMR spectrum (126 MHz, DMSO-*d₆*) of **5**
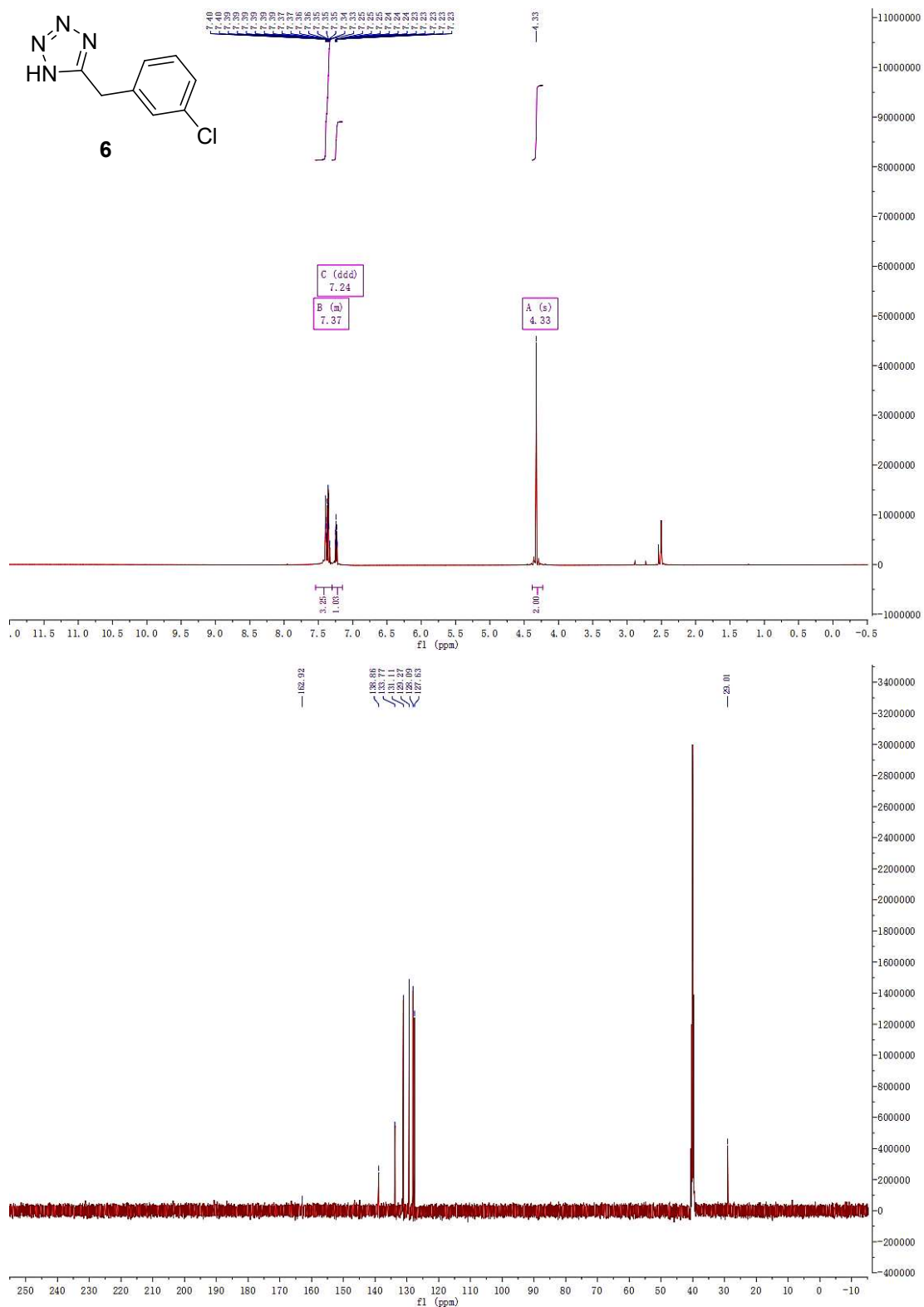
^{1}H-NMR spectrum (500 MHz, DMSO-d_6) and ^{13}C-NMR spectrum (126 MHz, DMSO-d_6) of **6**
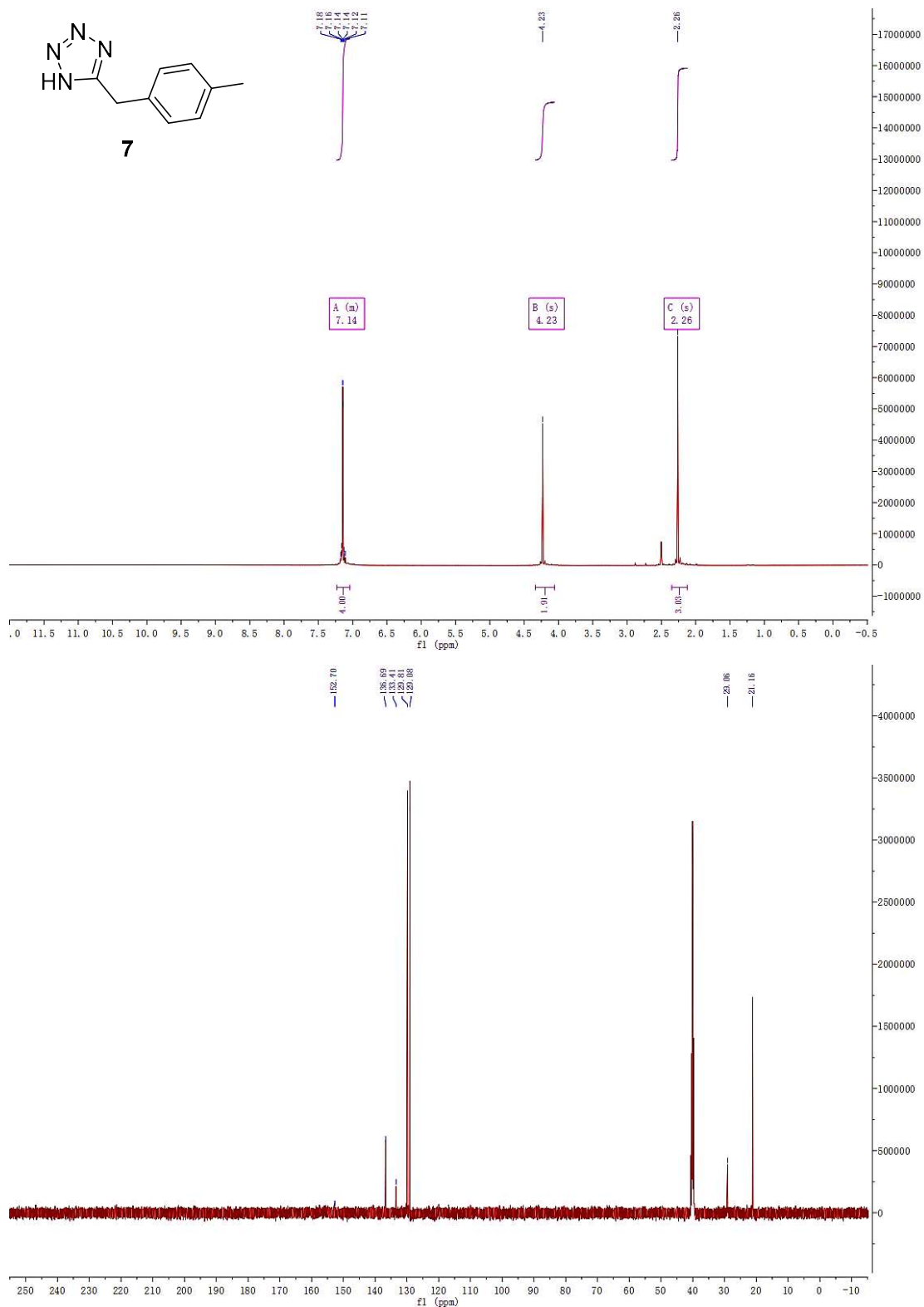
^{1}H-NMR spectrum (500 MHz, DMSO-*d$_6$*) and ^{13}C-NMR spectrum (126 MHz, DMSO-*d$_6$*) of **7**
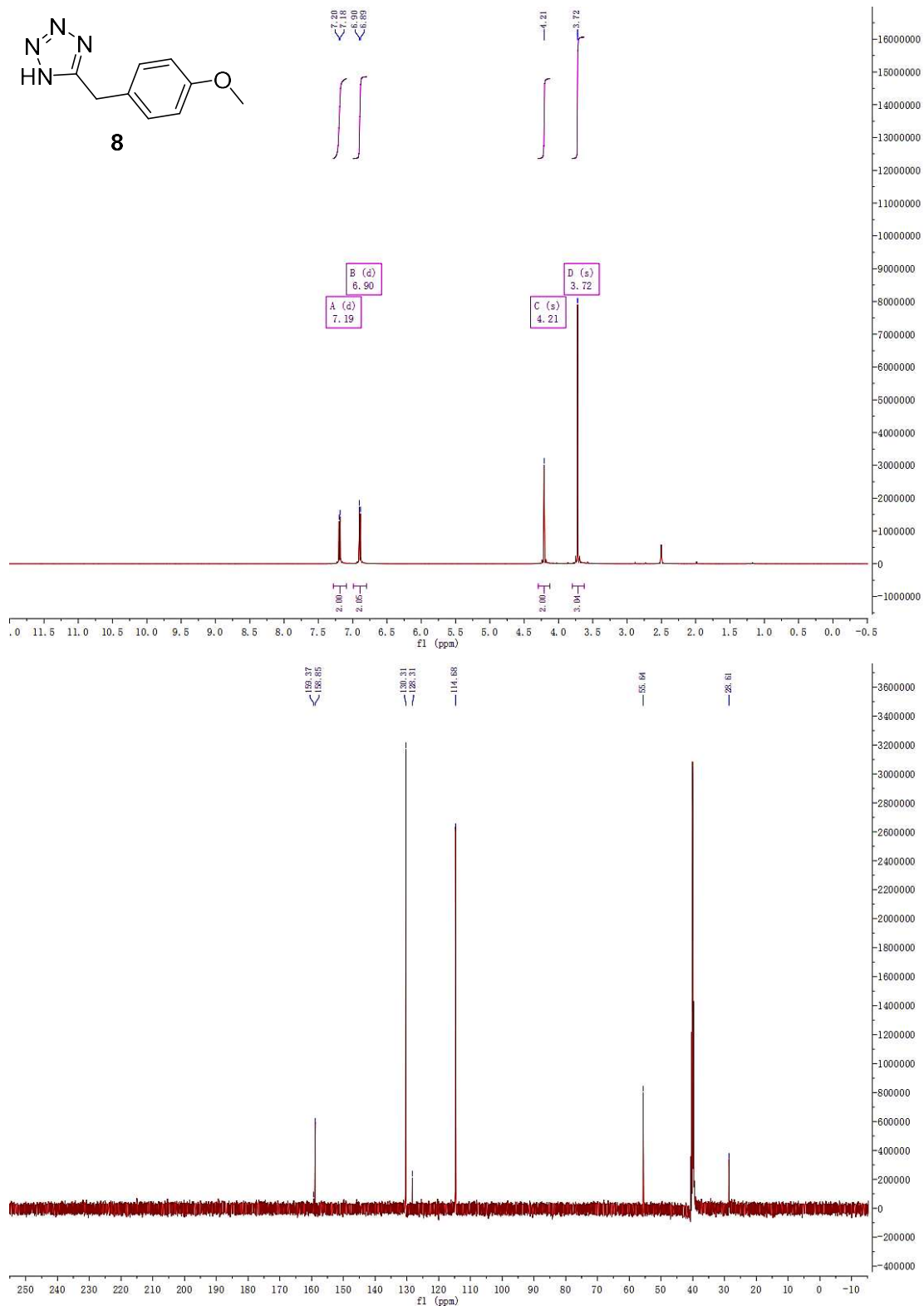
^{1}H-NMR spectrum (500 MHz, DMSO-d_6) and ^{13}C-NMR spectrum (126 MHz, DMSO-d_6) of **8**
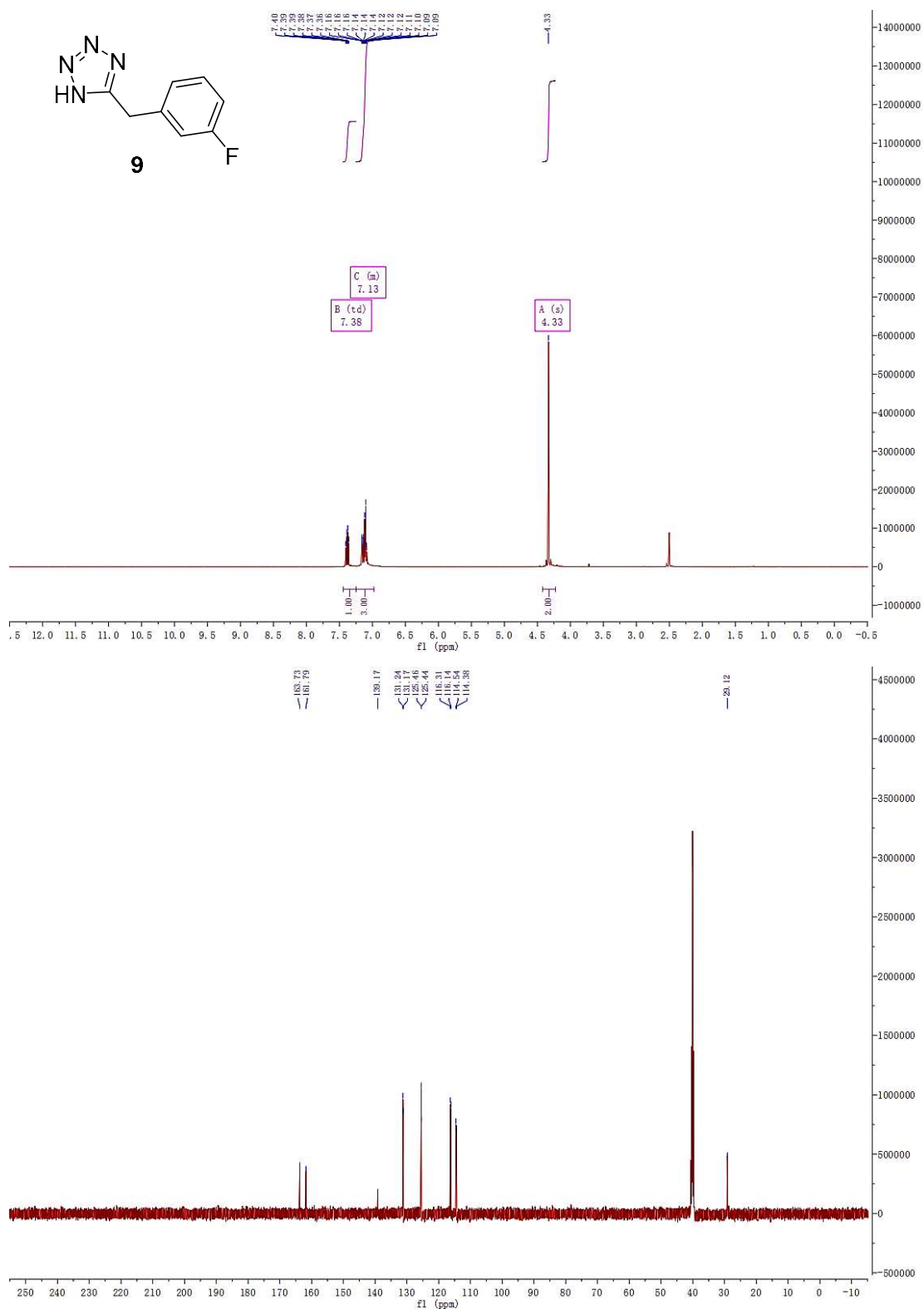
^{1}H-NMR spectrum (500 MHz, DMSO-d_6) and ^{13}C-NMR spectrum (126 MHz, DMSO-d_6) of **9**
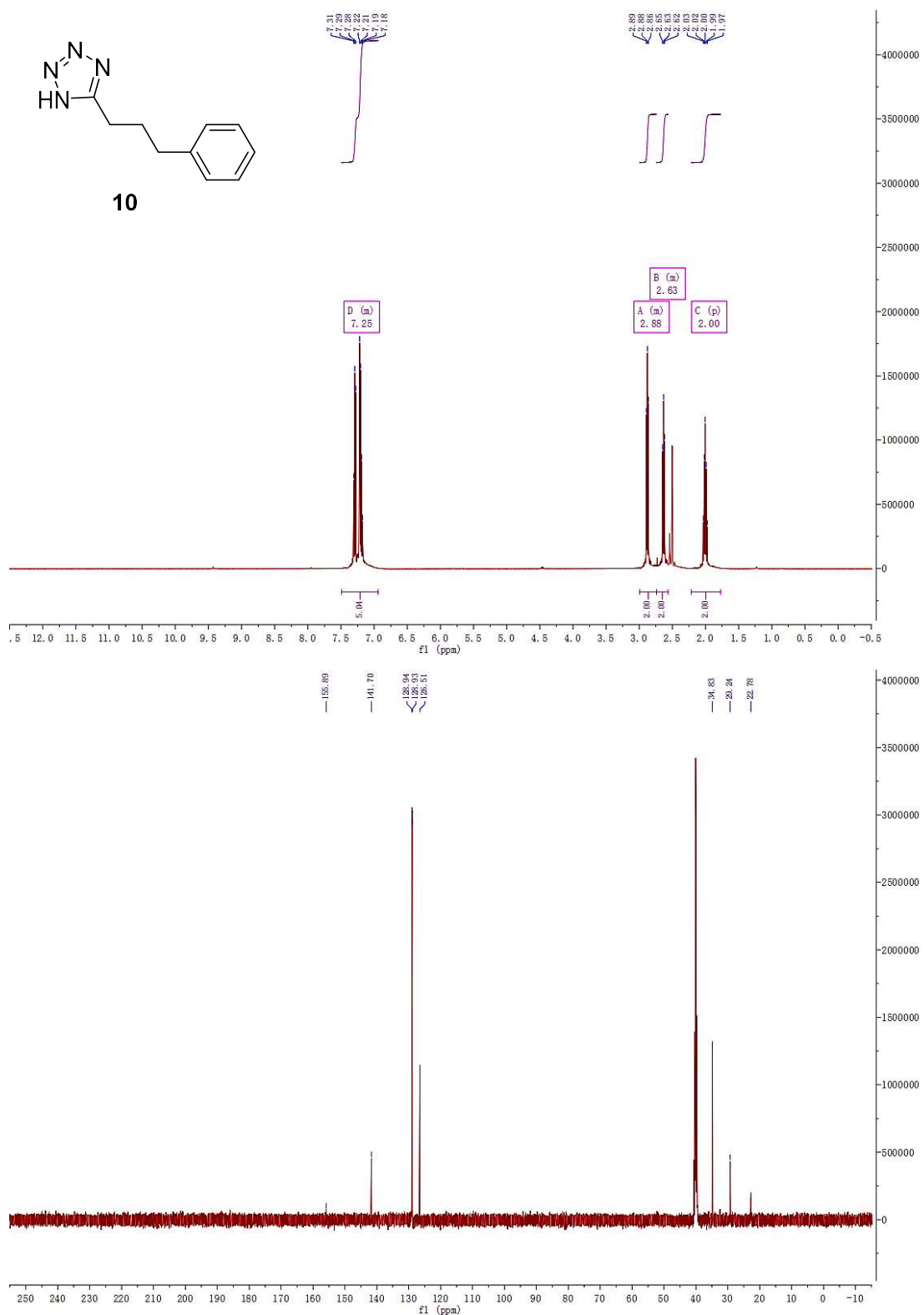
^{1}H-NMR spectrum (500 MHz, DMSO-d_6) and ^{13}C-NMR spectrum (126 MHz, DMSO-d_6) of **10**
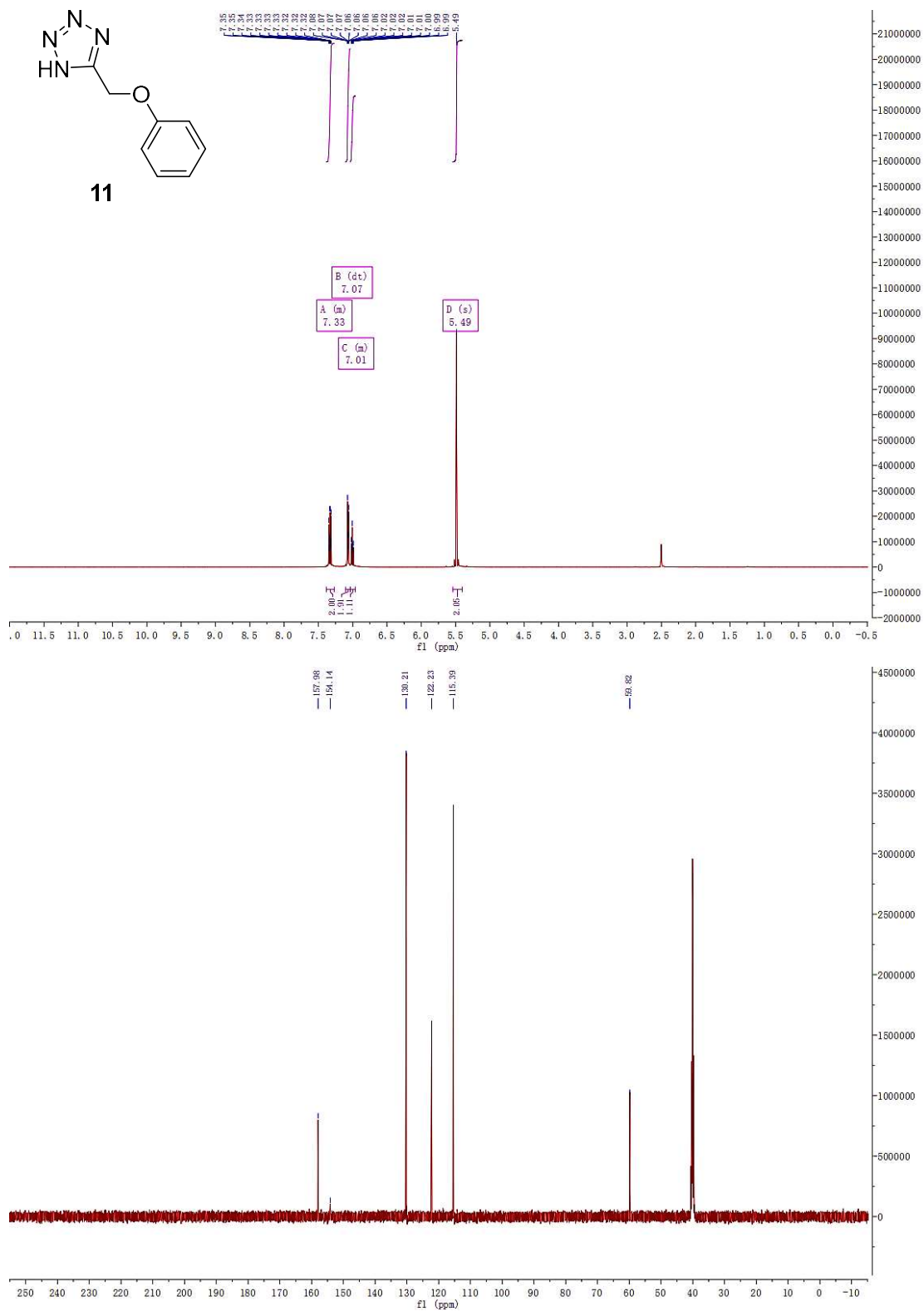
^{1}H-NMR spectrum (500 MHz, DMSO-d_6) and ^{13}C-NMR spectrum (126 MHz, DMSO-d_6) of **11**
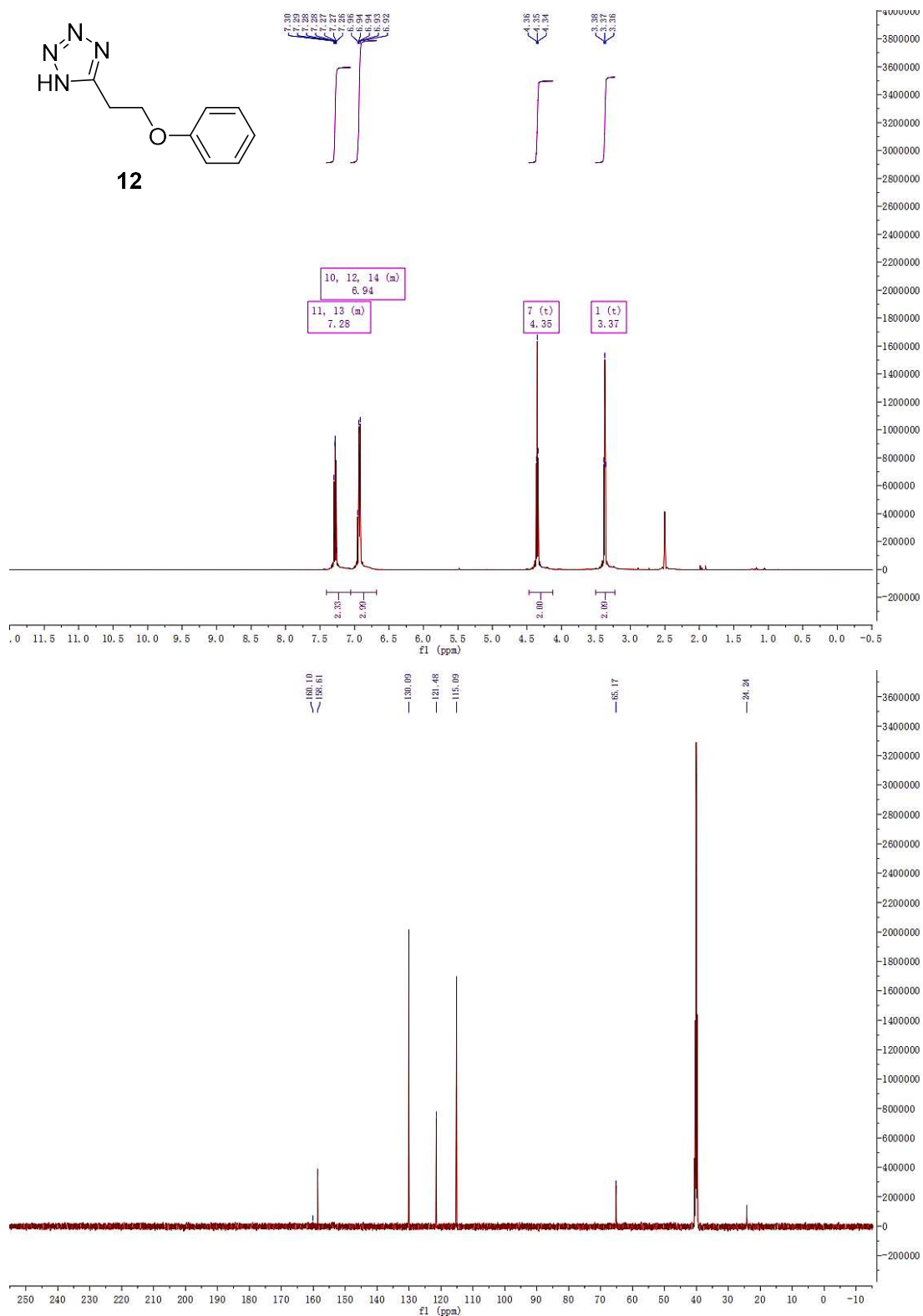
^{1}H-NMR spectrum (500 MHz, DMSO-d_6) and ^{13}C-NMR spectrum (126 MHz, DMSO-d_6) of **12**
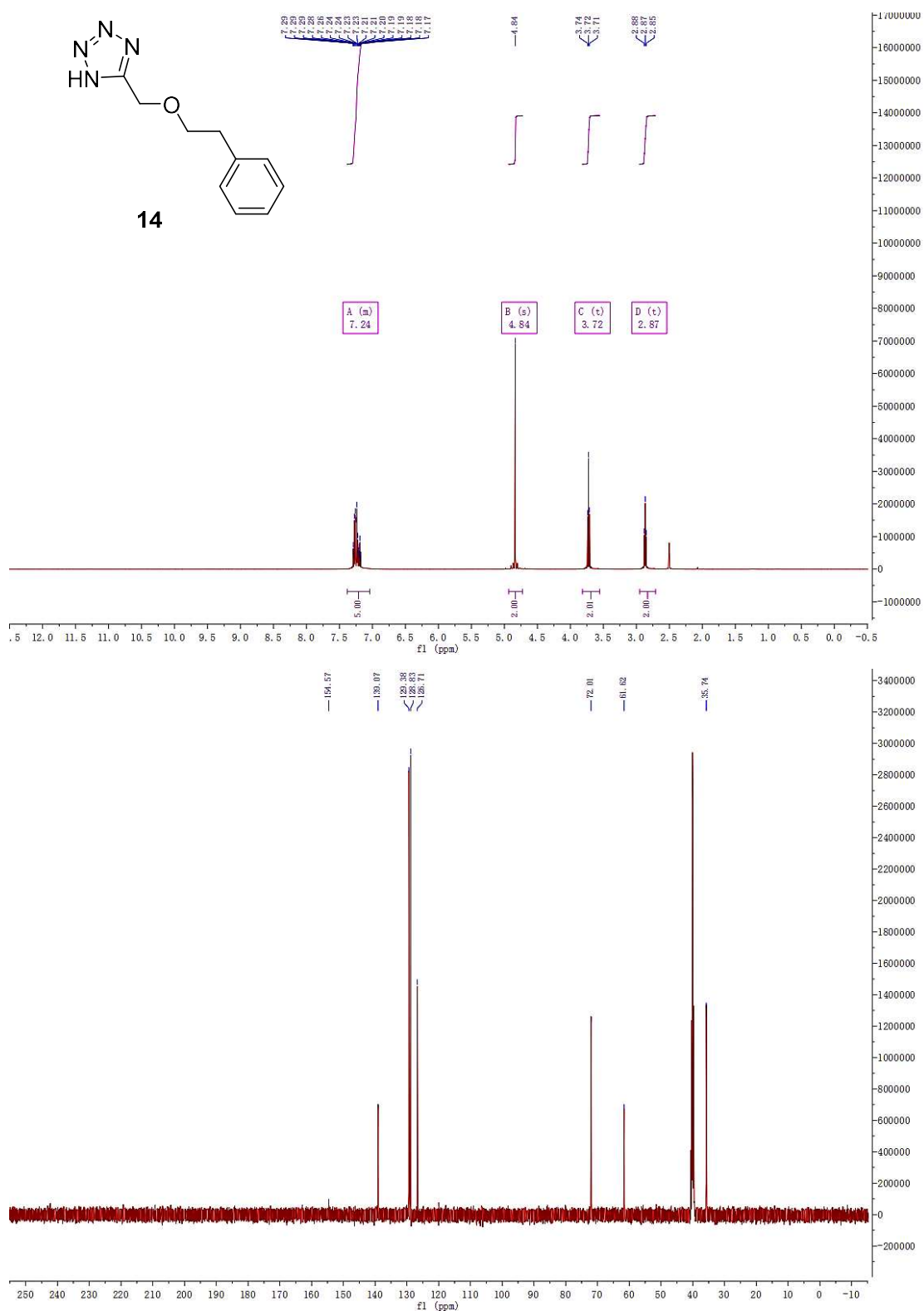
^{1}H-NMR spectrum (500 MHz, DMSO-d_6) and ^{13}C-NMR spectrum (126 MHz, DMSO-d_6) of **14**
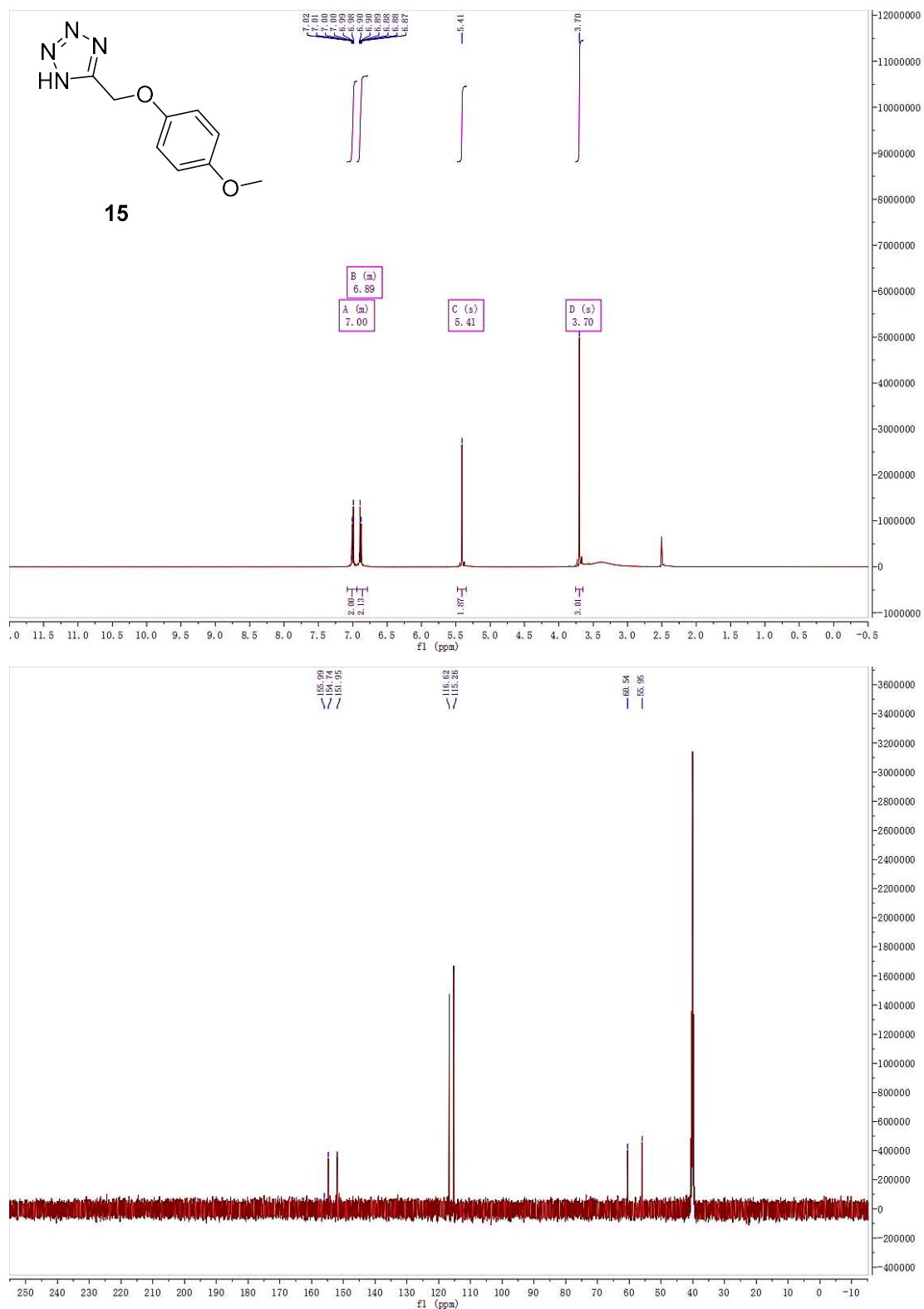
^{1}H-NMR spectrum (500 MHz, DMSO-d_6) and ^{13}C-NMR spectrum (126 MHz, DMSO-d_6) of **15**

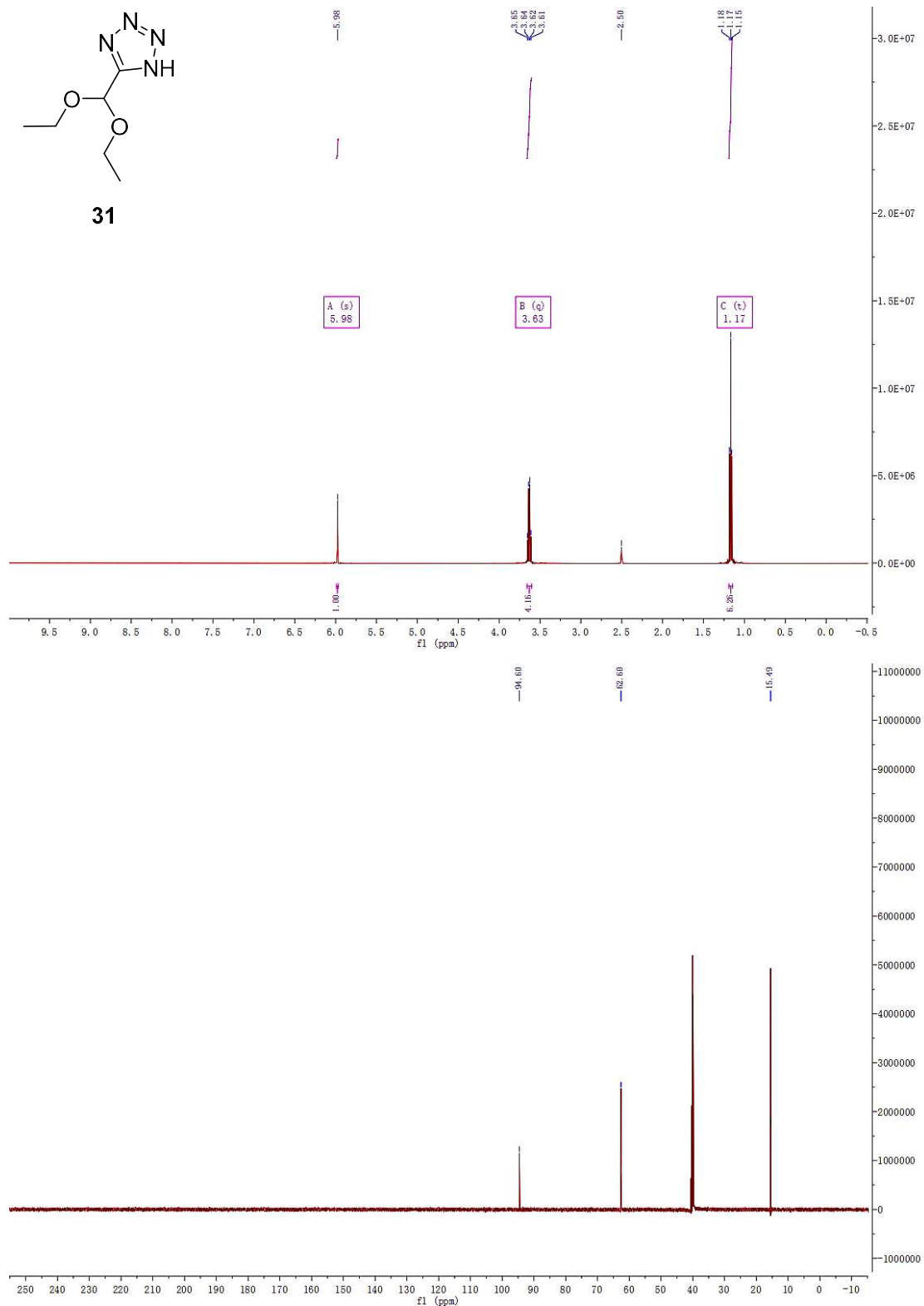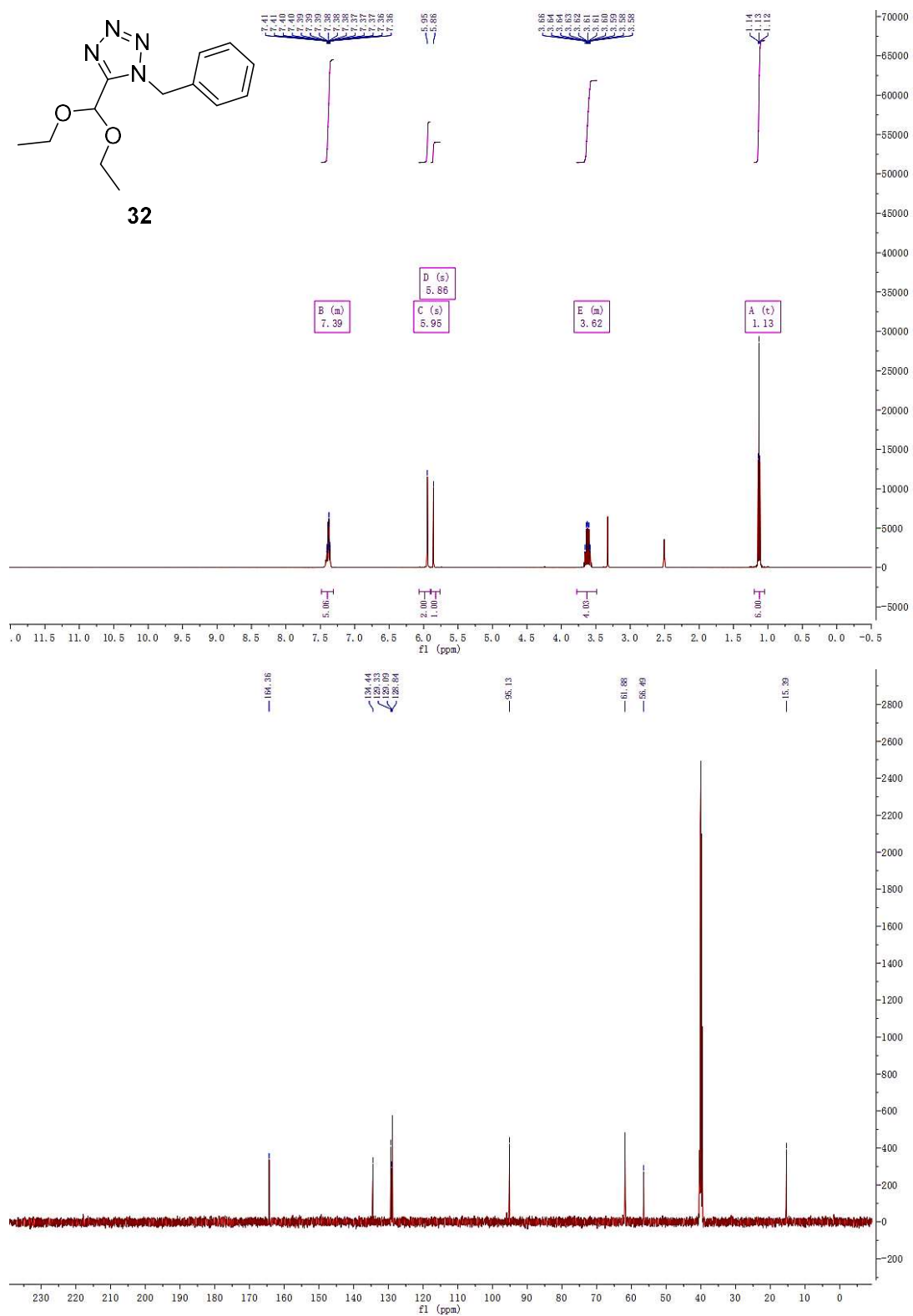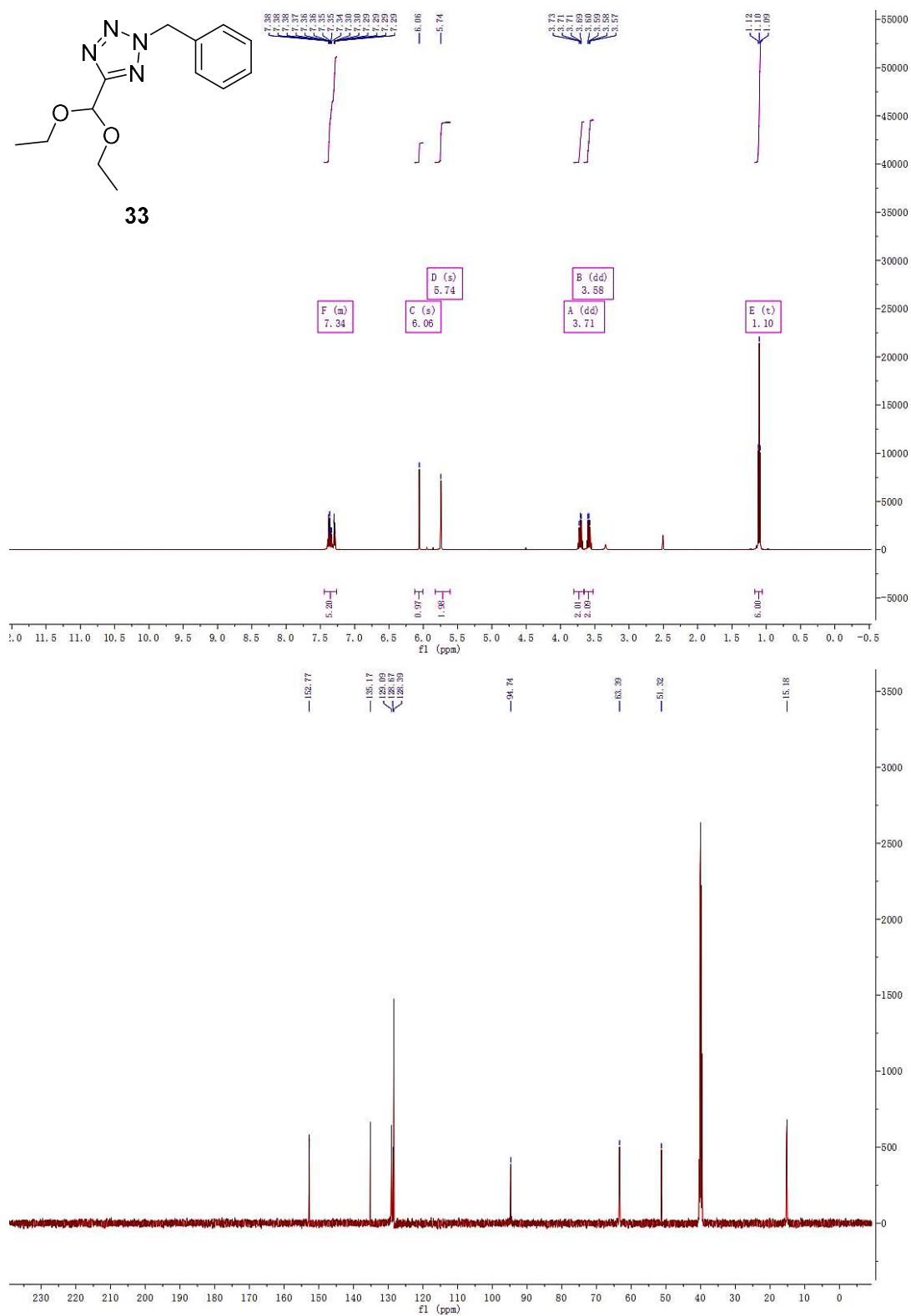¹H-NMR spectrum (500 MHz, DMSO-d_6) and ¹³C-NMR spectrum (126 MHz, DMSO-d_6) of **16**
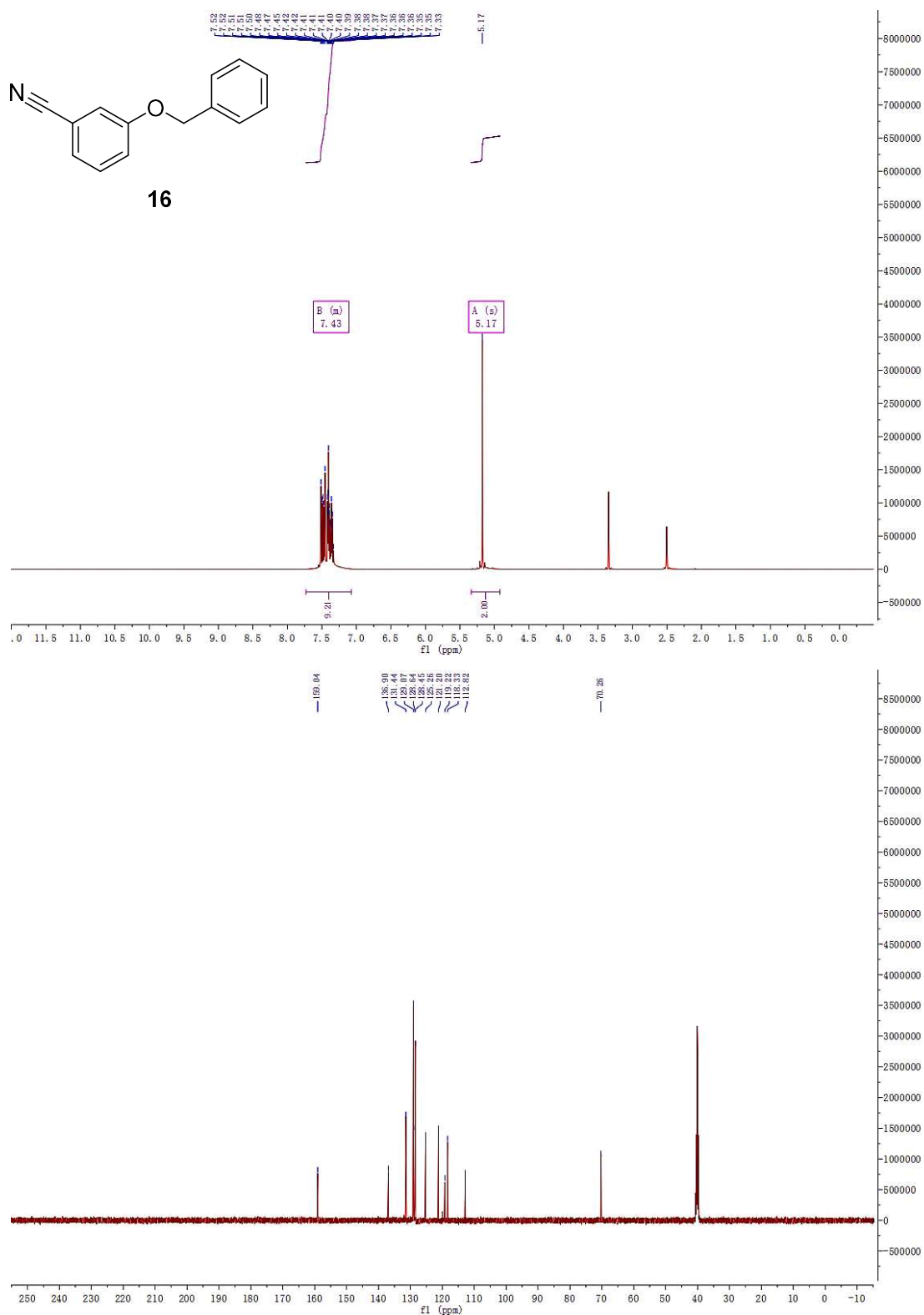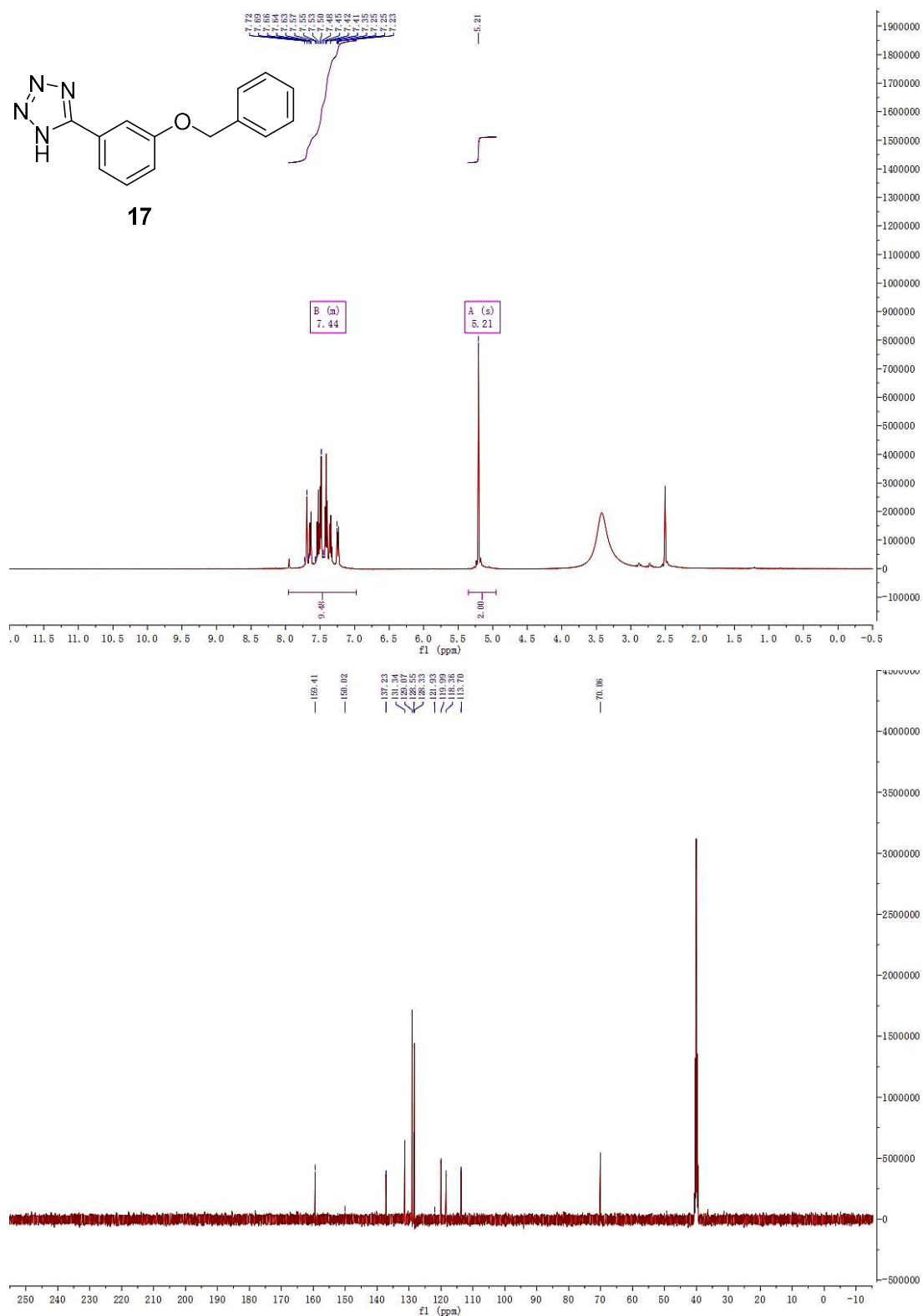
^{1}H-NMR spectrum (500 MHz, DMSO-d_6) and ^{13}C-NMR spectrum (126 MHz, DMSO-d_6) of **17**
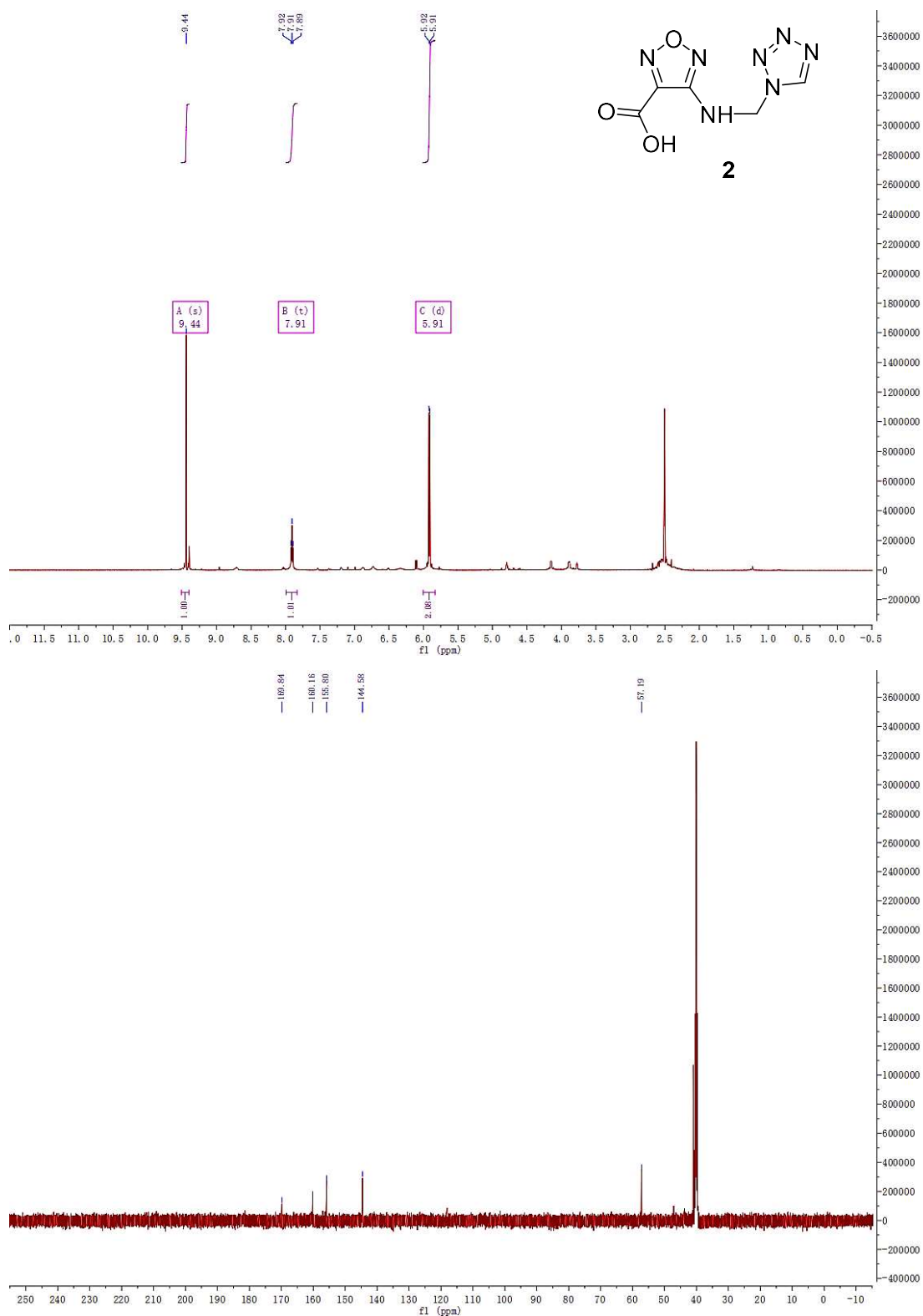
^{1}H-NMR spectrum (500 MHz, DMSO-d_6) and ^{13}C-NMR spectrum (126 MHz, DMSO-d_6) of **2**
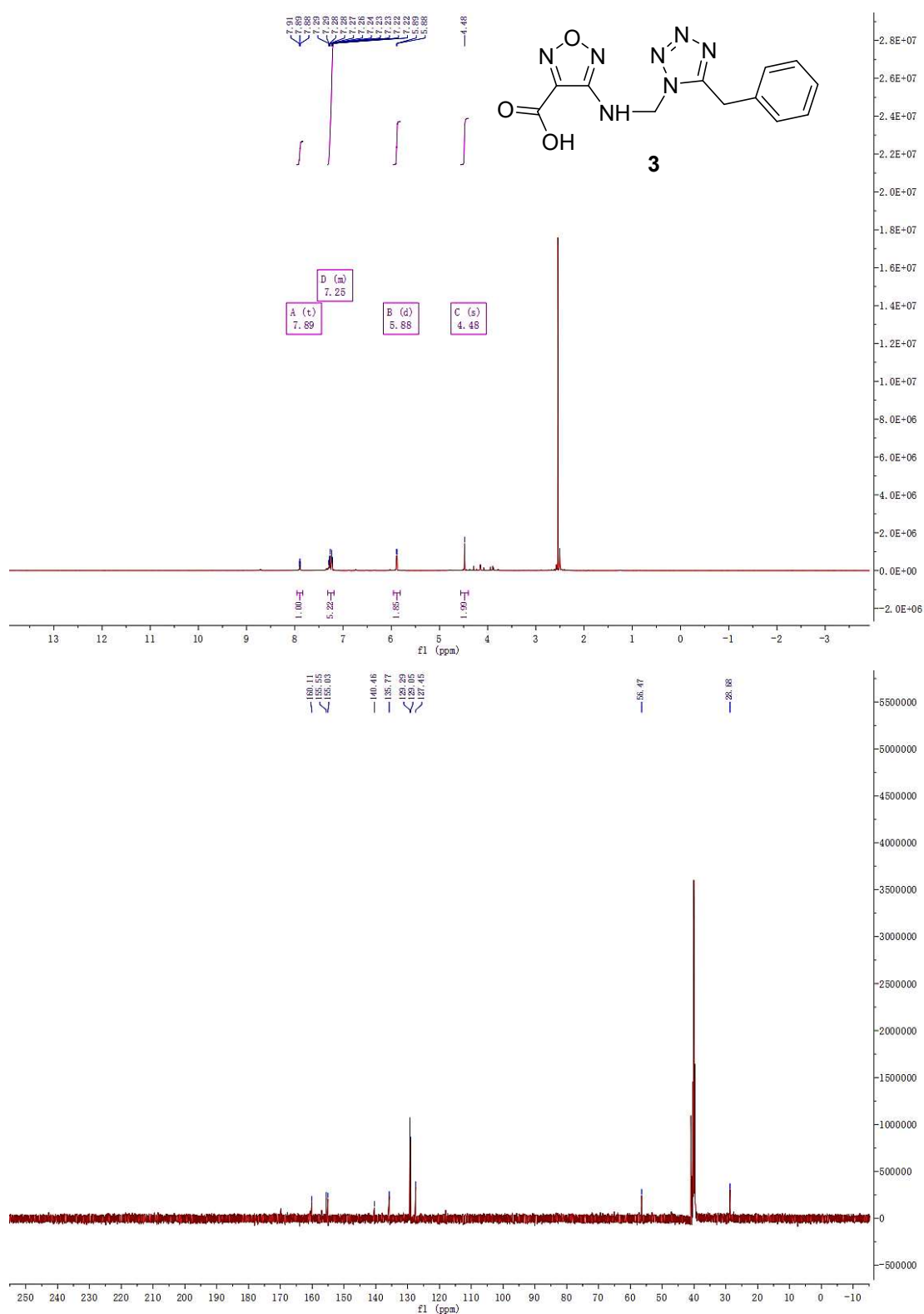
^{1}H-NMR spectrum (500 MHz, DMSO-d_6) and ^{13}C-NMR spectrum (126 MHz, DMSO-d_6) of **3**
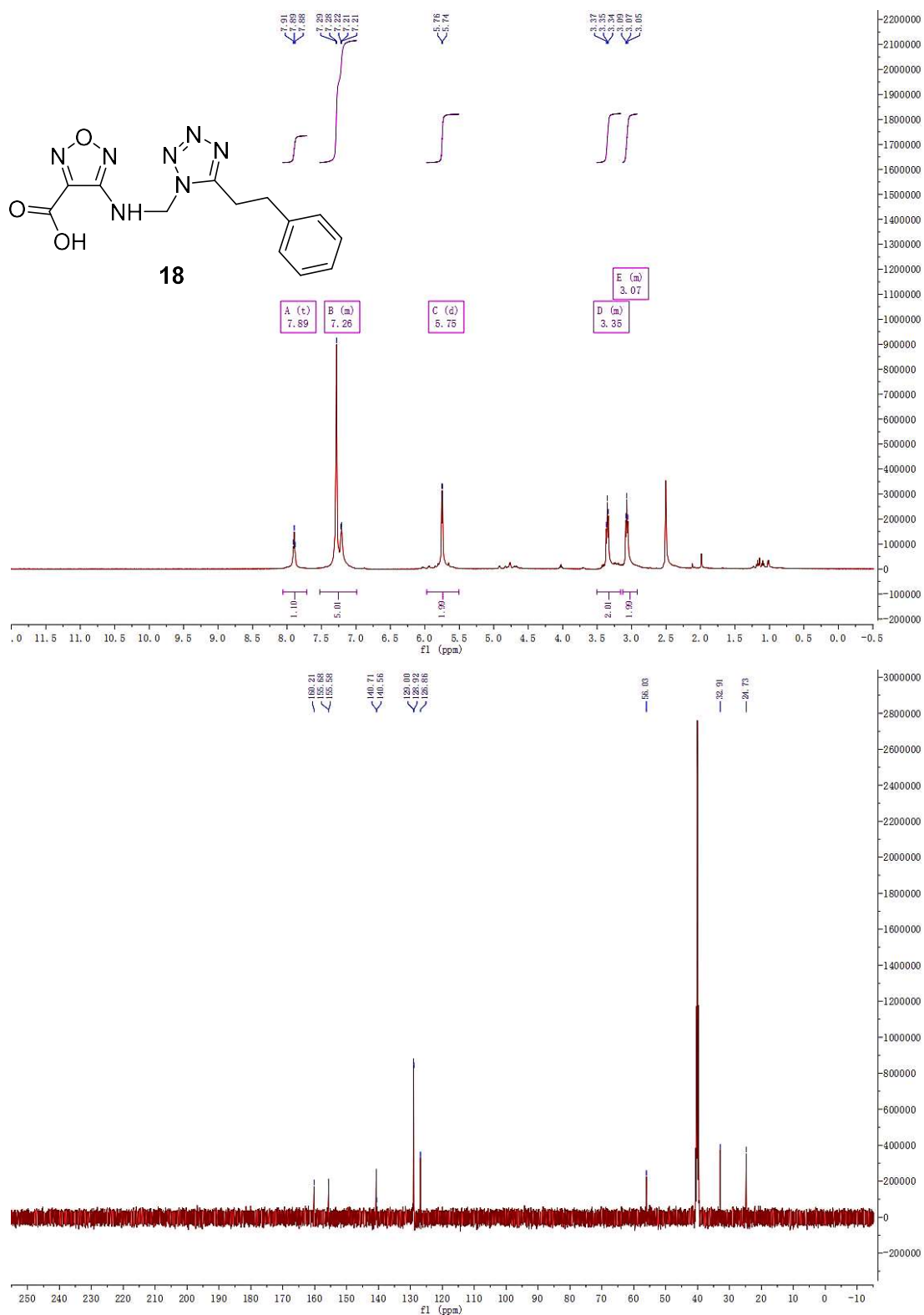
^{1}H-NMR spectrum (500 MHz, DMSO-d_6) and ^{13}C-NMR spectrum (126 MHz, DMSO-d_6) of **18**
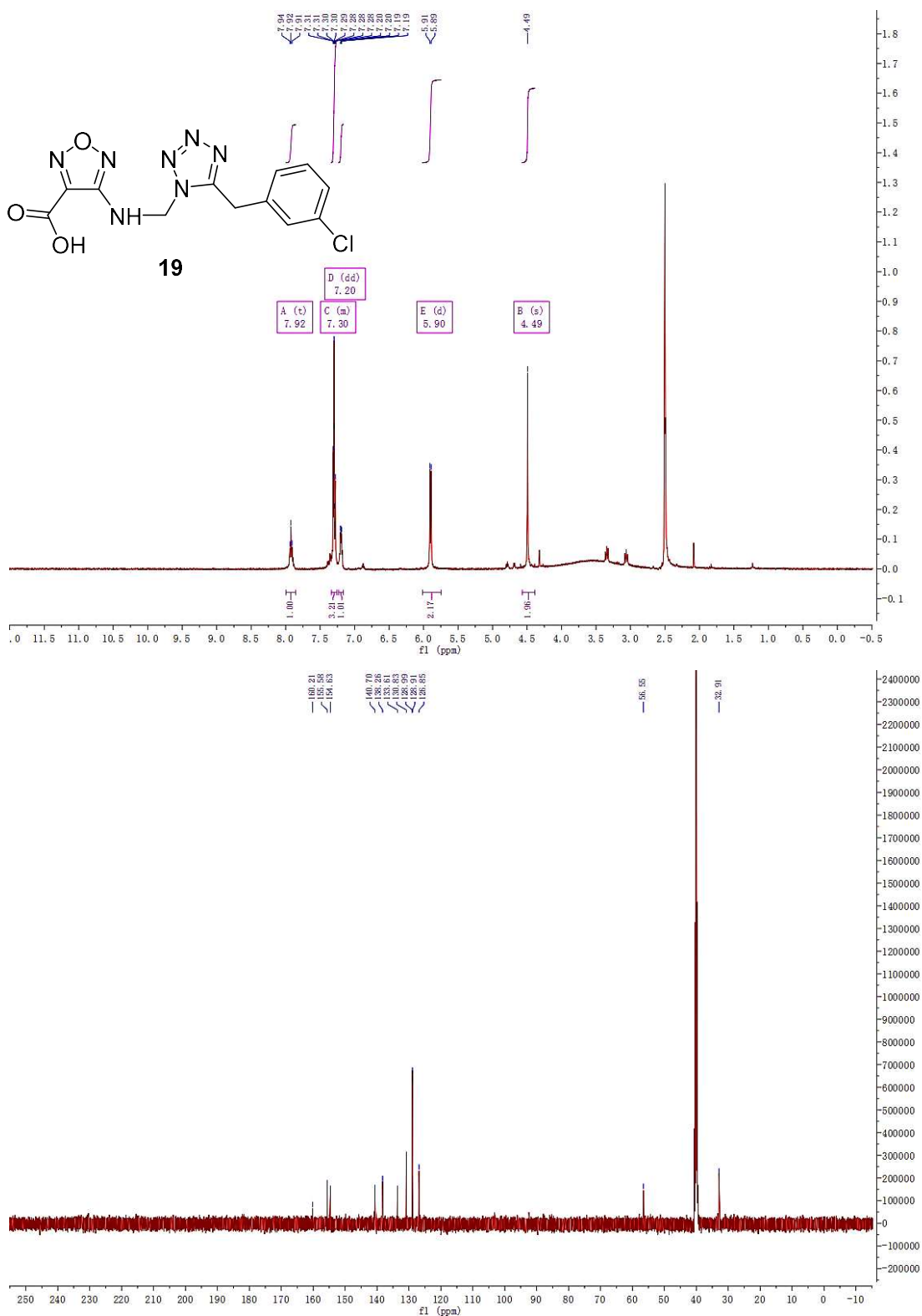
^{1}H-NMR spectrum (500 MHz, DMSO-d_6) and ^{13}C-NMR spectrum (126 MHz, DMSO-d_6) of **19**
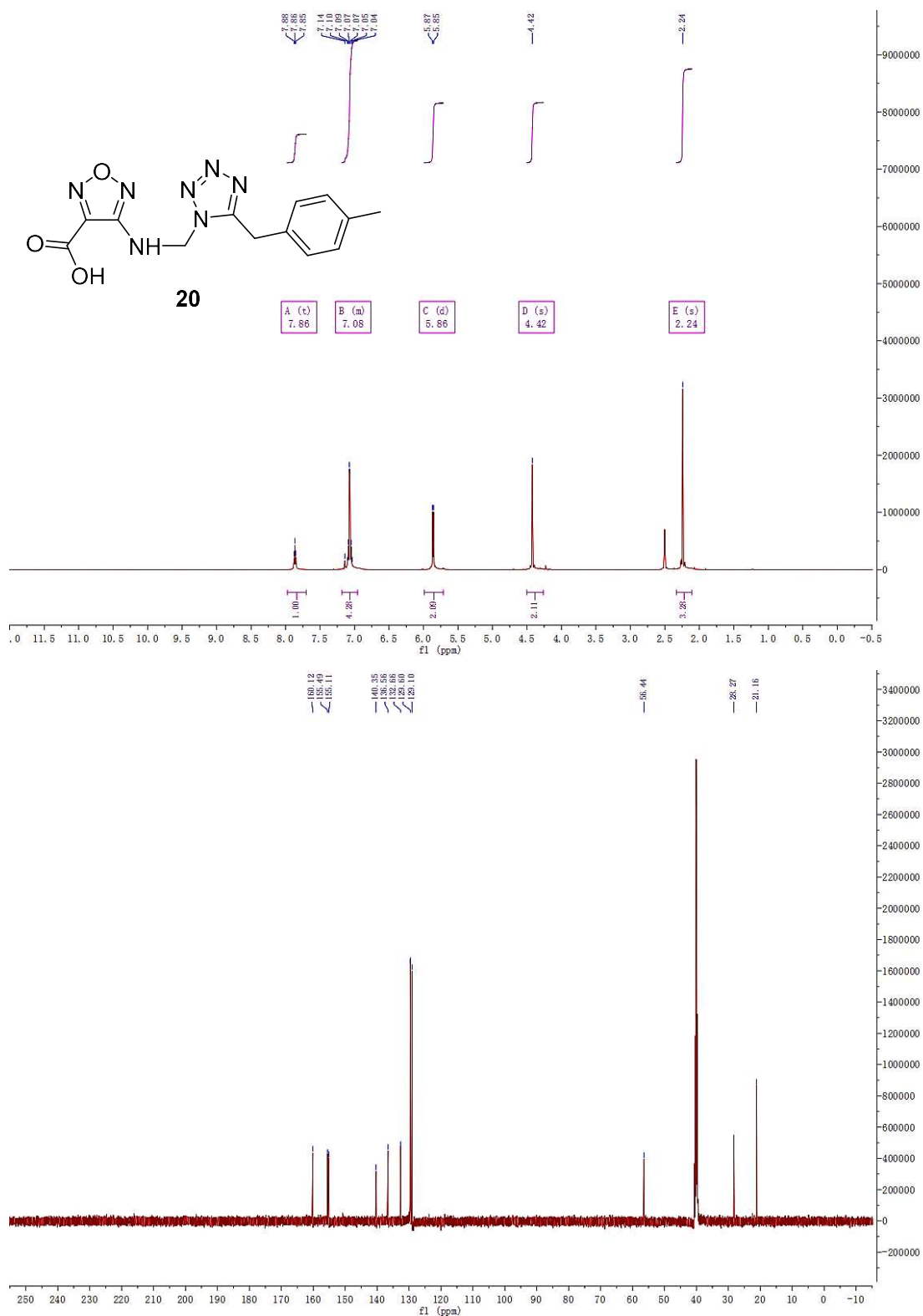
^{1}H-NMR spectrum (500 MHz, DMSO-d_6) and ^{13}C-NMR spectrum (126 MHz, DMSO-d_6) of **20**

^{1}H-NMR spectrum (500 MHz, DMSO-d_6) and ^{13}C-NMR spectrum (126 MHz, DMSO-d_6) of **21**

^{1}H-NMR spectrum (500 MHz, DMSO-d_6) and ^{13}C-NMR spectrum (126 MHz, DMSO-d_6) of **22**

23

^{1}H-NMR spectrum (500 MHz, DMSO-d_6) and ^{13}C-NMR spectrum (126 MHz, DMSO-d_6) of **23**

^{1}H-NMR spectrum (500 MHz, DMSO-d_6) and ^{13}C-NMR spectrum (126 MHz, DMSO-d_6) of **24**

25

^{1}H-NMR spectrum (500 MHz, DMSO-d_6) and ^{13}C-NMR spectrum (126 MHz, DMSO-d_6) of **25**

^{1}H-NMR spectrum (500 MHz, DMSO-d_6) and ^{13}C-NMR spectrum (126 MHz, DMSO-d_6) of **26**

^{1}H-NMR spectrum (500 MHz, DMSO-d_6) and ^{13}C-NMR spectrum (126 MHz, DMSO-d_6) of **27**

^{1}H-NMR spectrum (500 MHz, DMSO-d_6) and ^{13}C-NMR spectrum (126 MHz, DMSO-d_6) of **28**
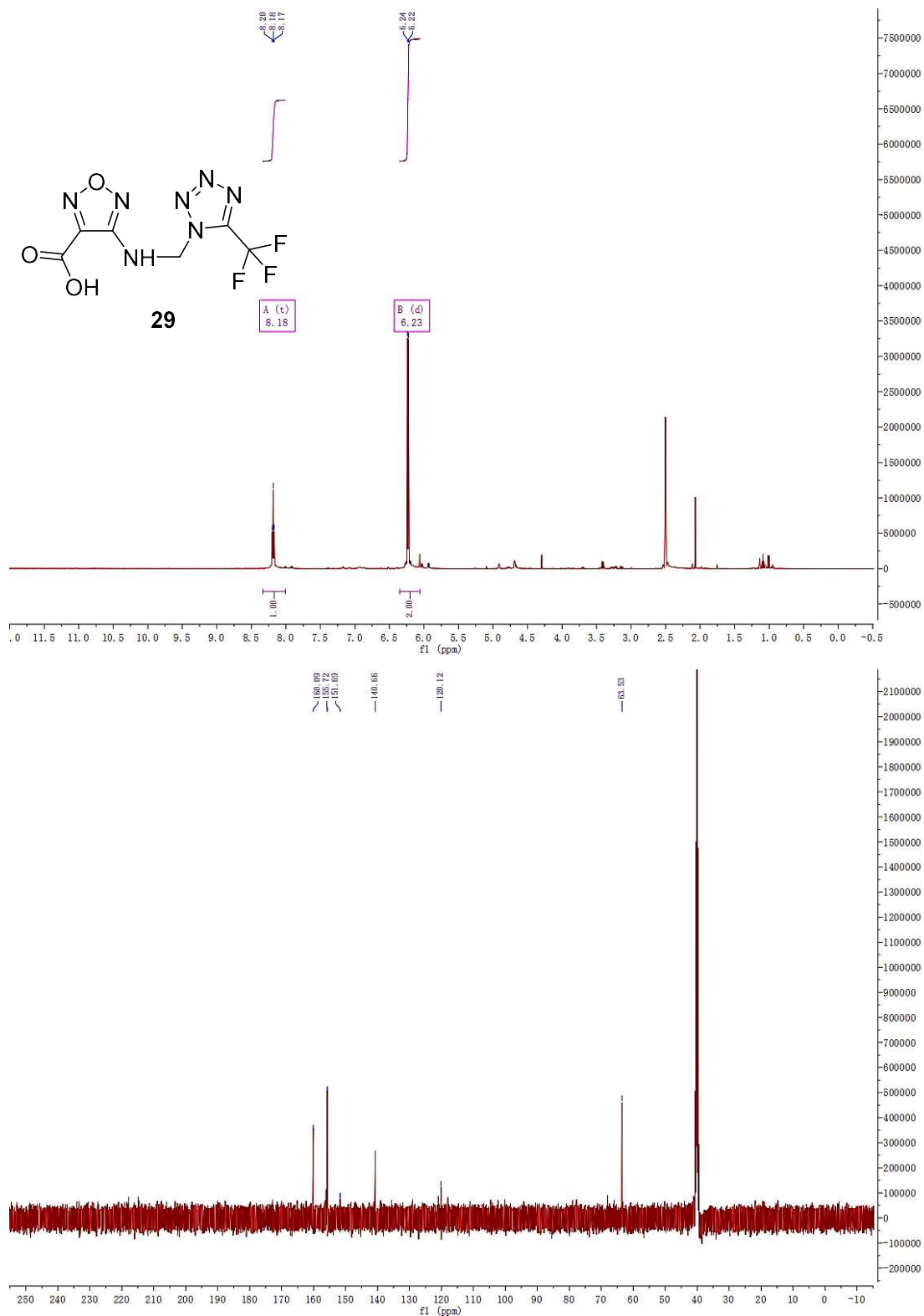
^{1}H-NMR spectrum (500 MHz, DMSO-d_6) and ^{13}C-NMR spectrum (126 MHz, DMSO-d_6) of **29**

^{1}H-NMR spectrum (500 MHz, DMSO-d_6) and ^{13}C-NMR spectrum (126 MHz, DMSO-d_6) of **30**

^{1}H-NMR spectrum (500 MHz, DMSO-d_6) and ^{13}C-NMR spectrum (126 MHz, DMSO-d_6) of **31**

^{1}H-NMR spectrum (500 MHz, DMSO-d_6) and ^{13}C-NMR spectrum (126 MHz, DMSO-d_6) of **32**

^{1}H-NMR spectrum (500 MHz, DMSO-d_6) and ^{13}C-NMR spectrum (126 MHz, DMSO-d_6) of **33**
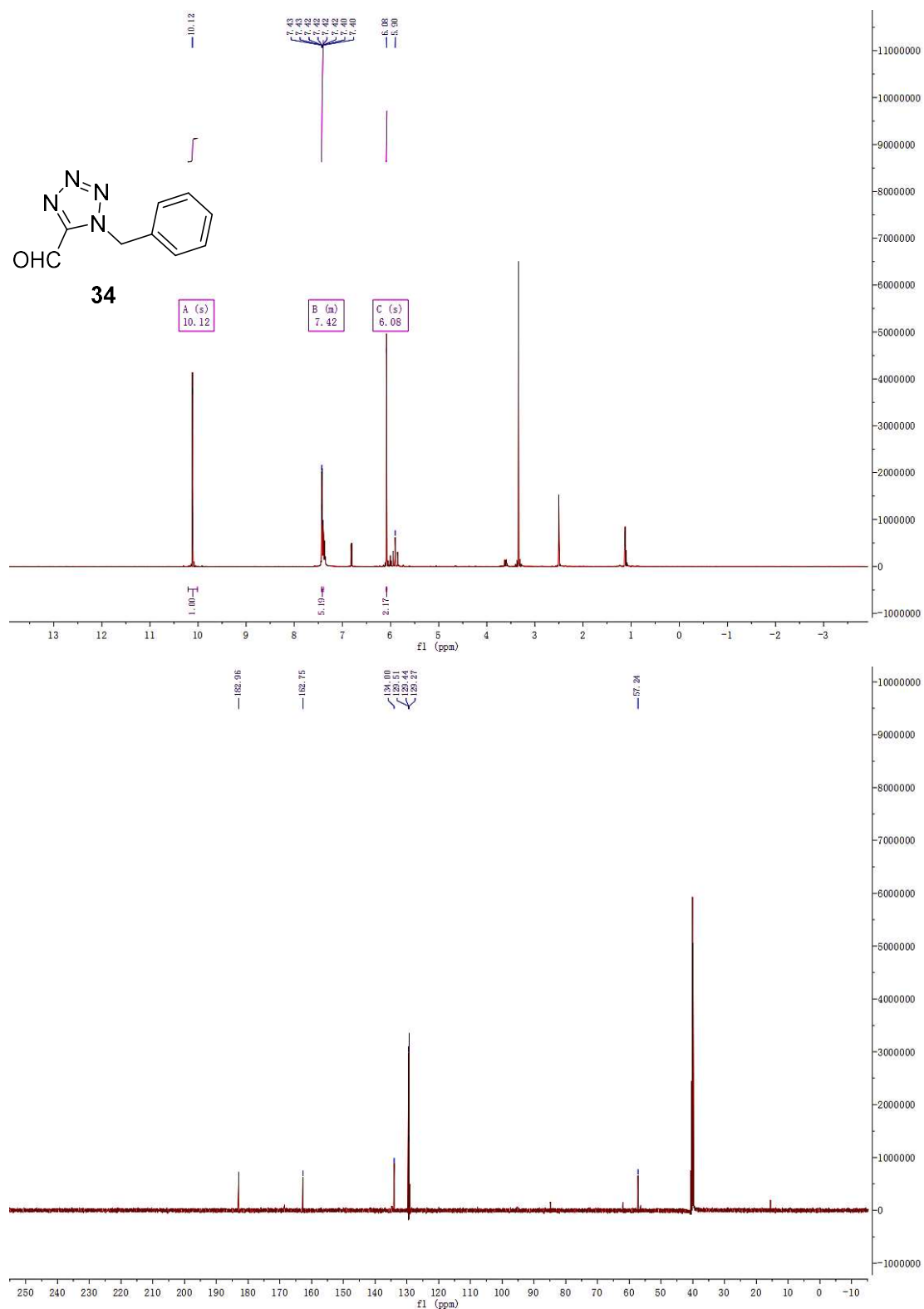
^{1}H-NMR spectrum (500 MHz, DMSO-d_6) and ^{13}C-NMR spectrum (126 MHz, DMSO-d_6) of **34**
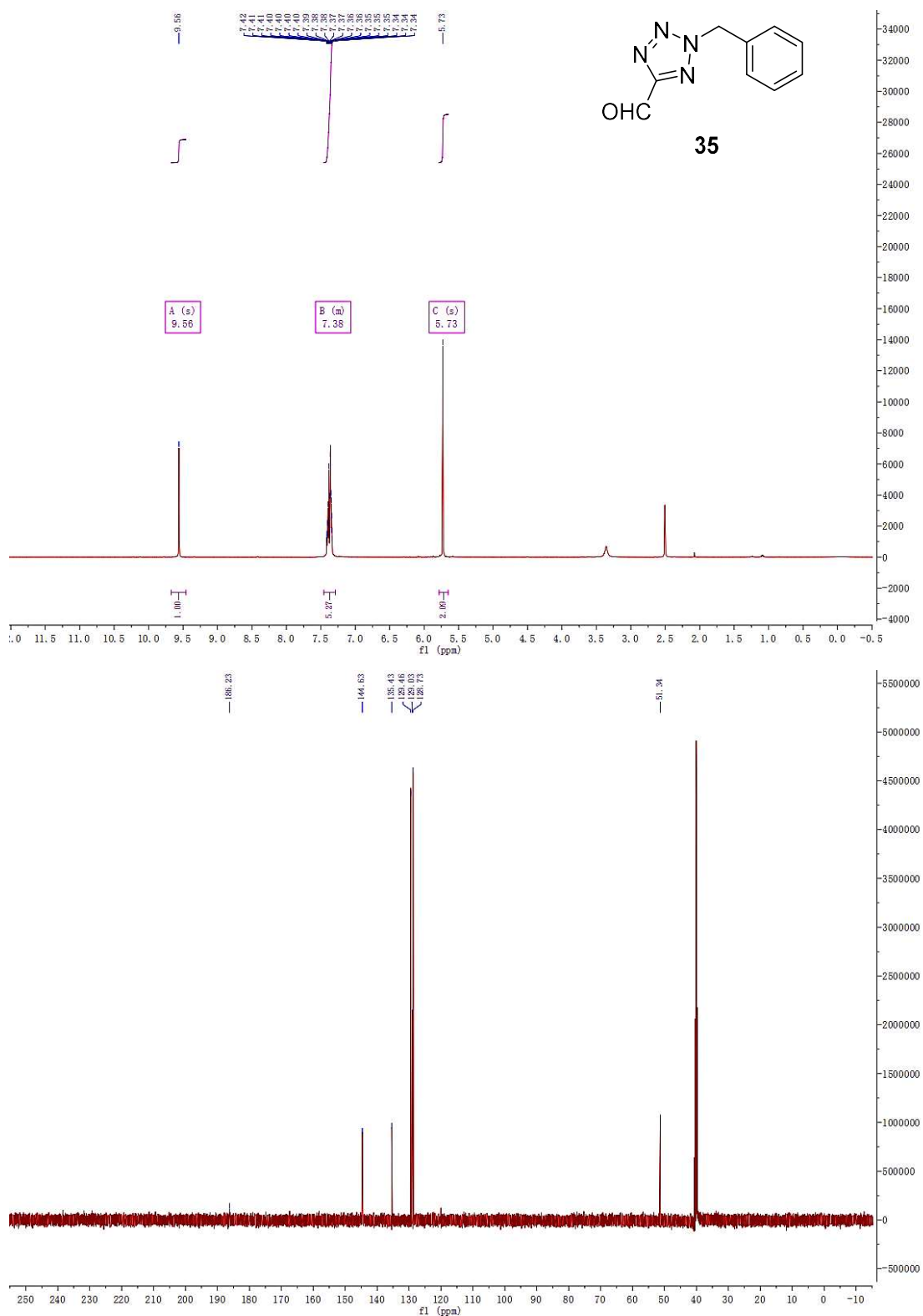
^{1}H-NMR spectrum (500 MHz, DMSO-d_6) and ^{13}C-NMR spectrum (126 MHz, DMSO-d_6) of **35**

^{1}H-NMR spectrum (500 MHz, DMSO-d_6) and ^{13}C-NMR spectrum (126 MHz, DMSO-d_6) of **36**
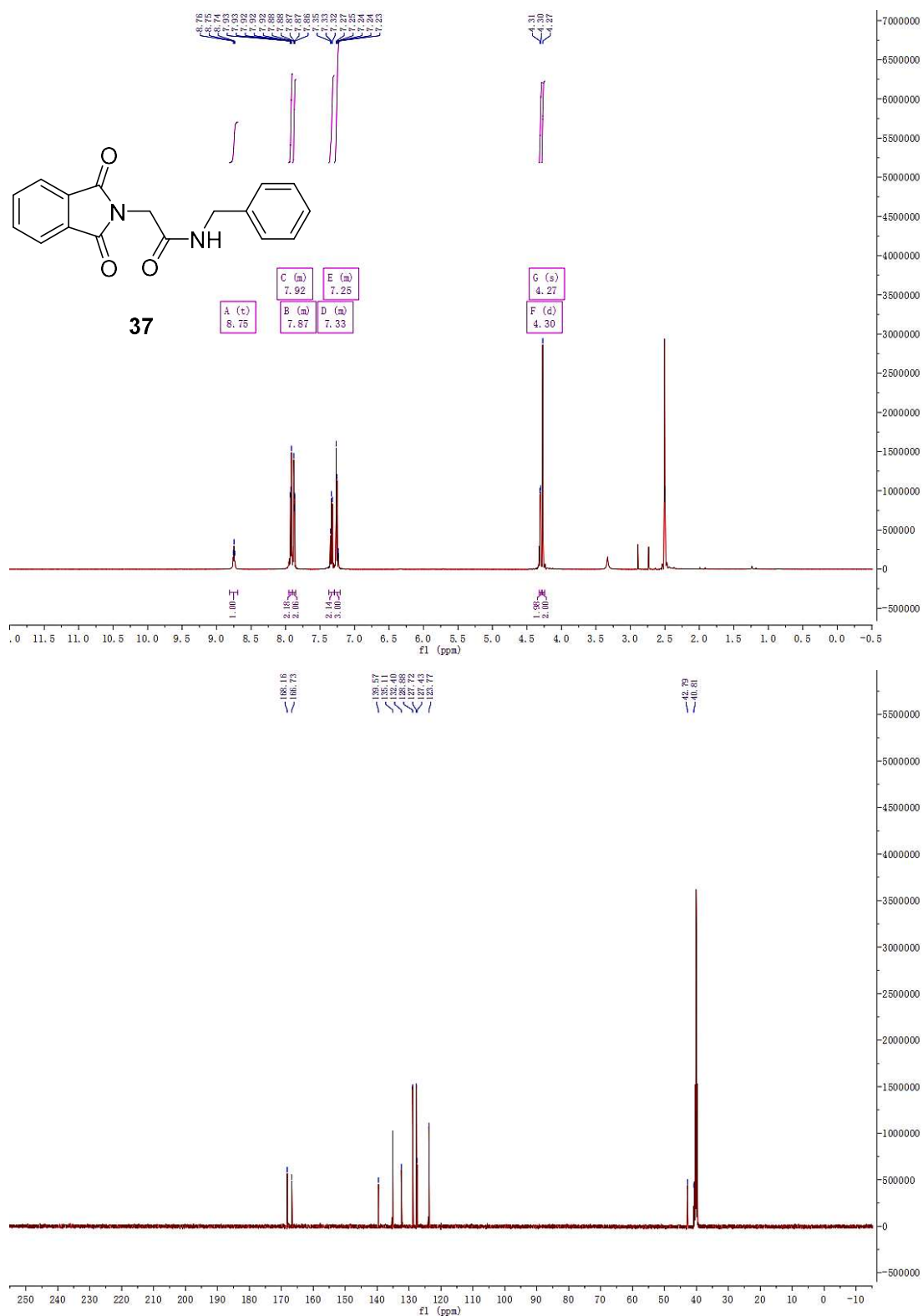
^{1}H-NMR spectrum (500 MHz, DMSO-*d$_6$*) and ^{13}C-NMR spectrum (126 MHz, DMSO-*d$_6$*) of **37**
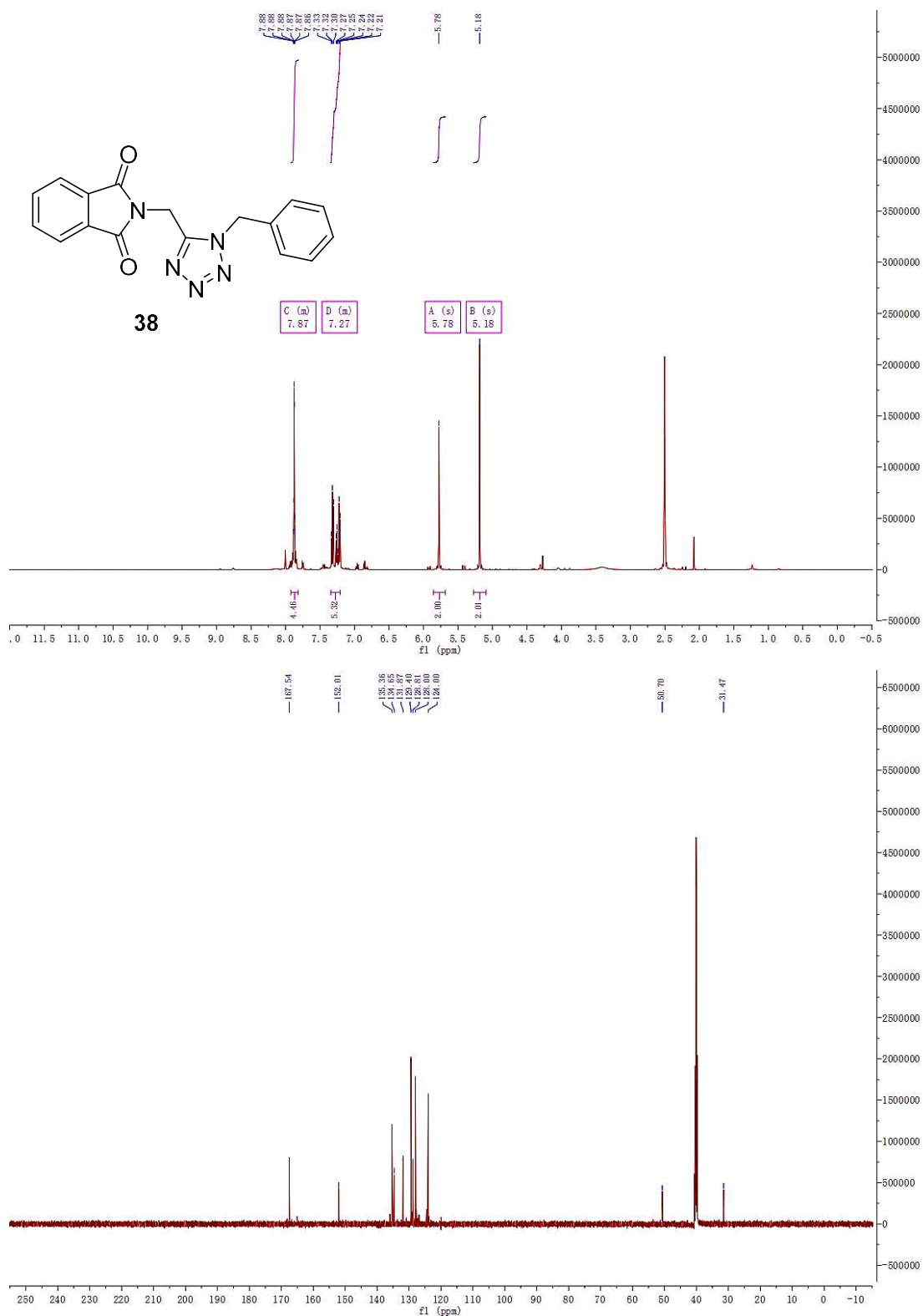
^{1}H-NMR spectrum (500 MHz, DMSO-d_6) and ^{13}C-NMR spectrum (126 MHz, DMSO-d_6) of **38**
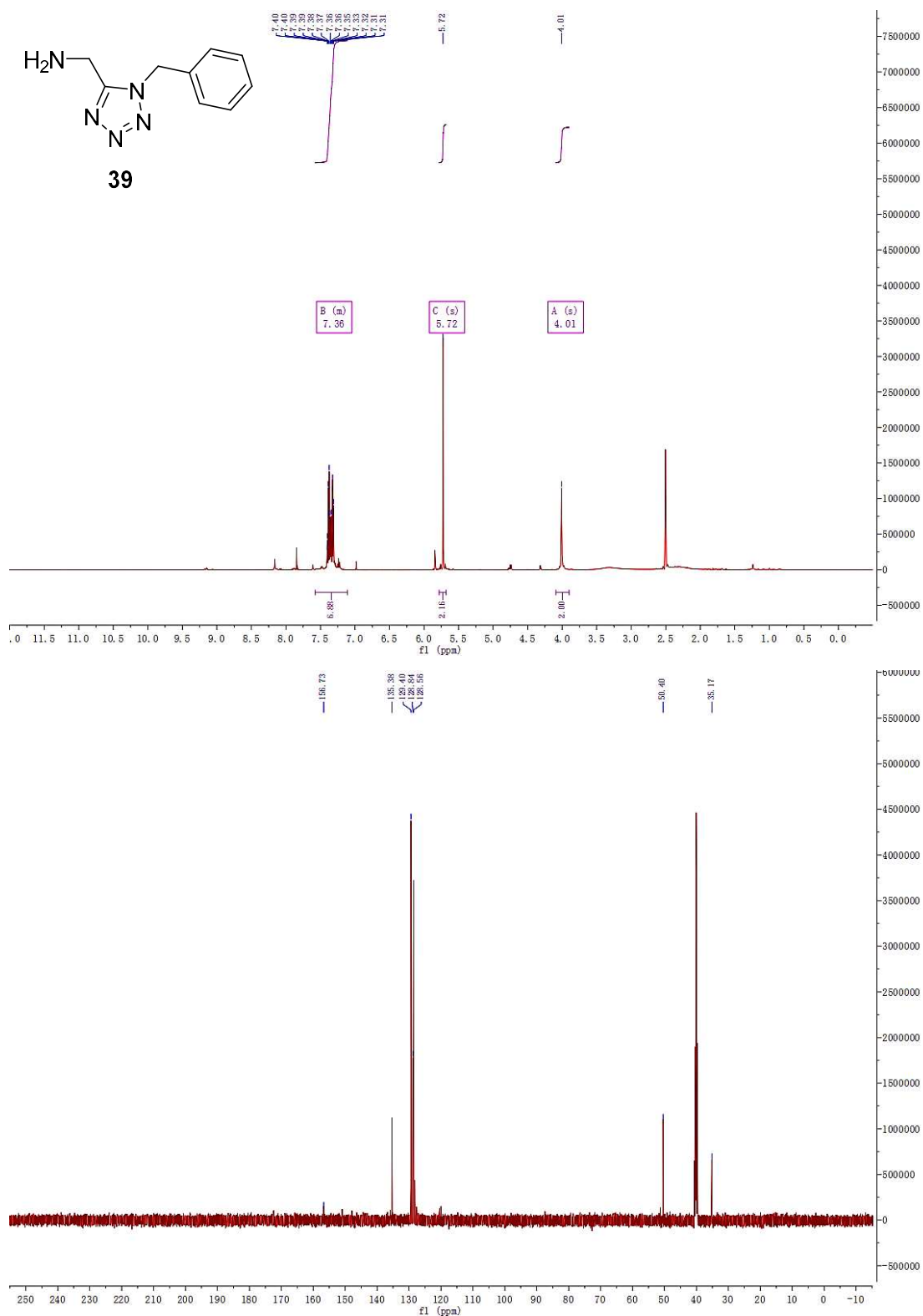
^{1}H-NMR spectrum (500 MHz, DMSO-d_6) and ^{13}C-NMR spectrum (126 MHz, DMSO-d_6) of **39**
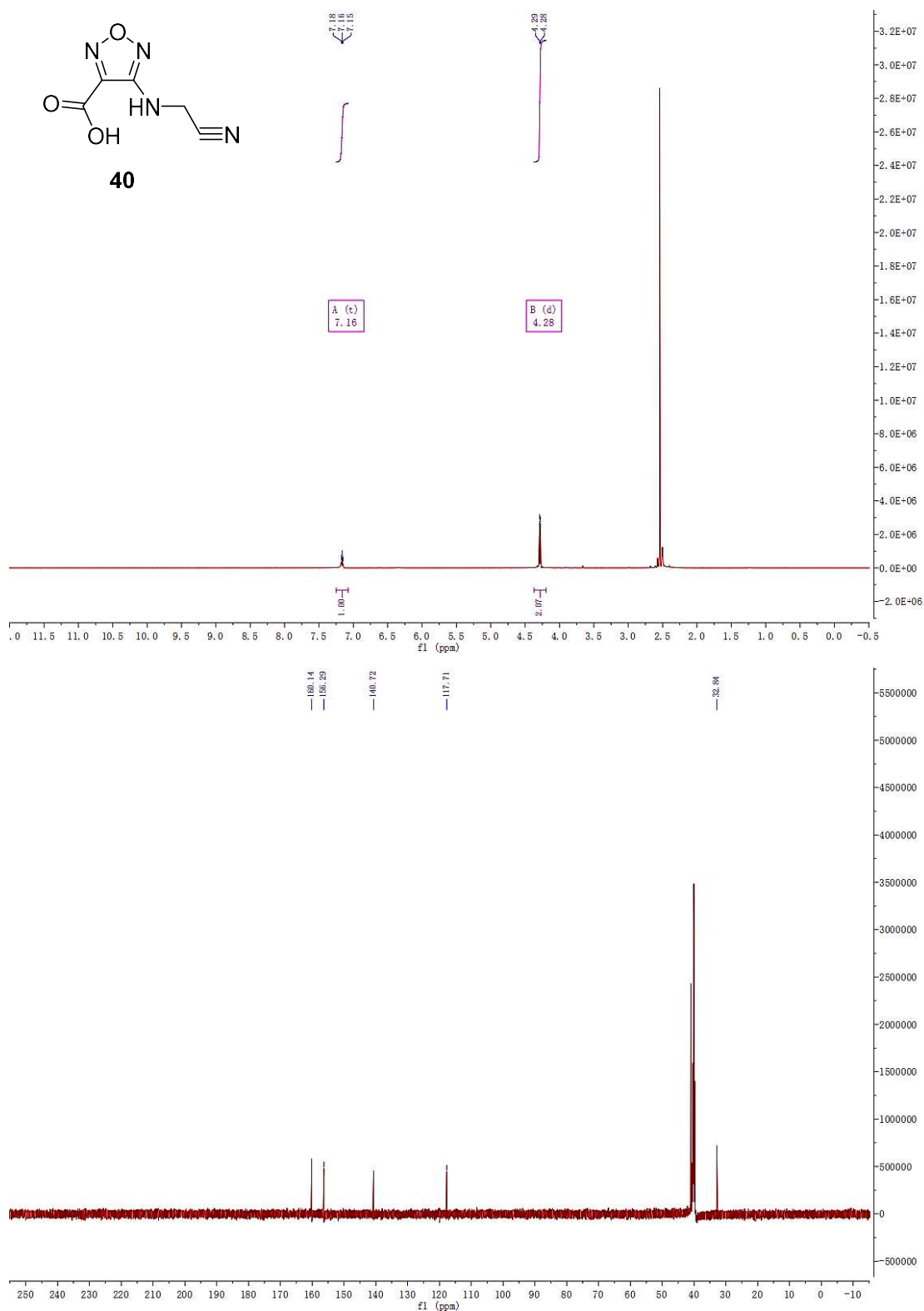
^{1}H-NMR spectrum (500 MHz, DMSO-d_6) and ^{13}C-NMR spectrum (126 MHz, DMSO-d_6) of **40**
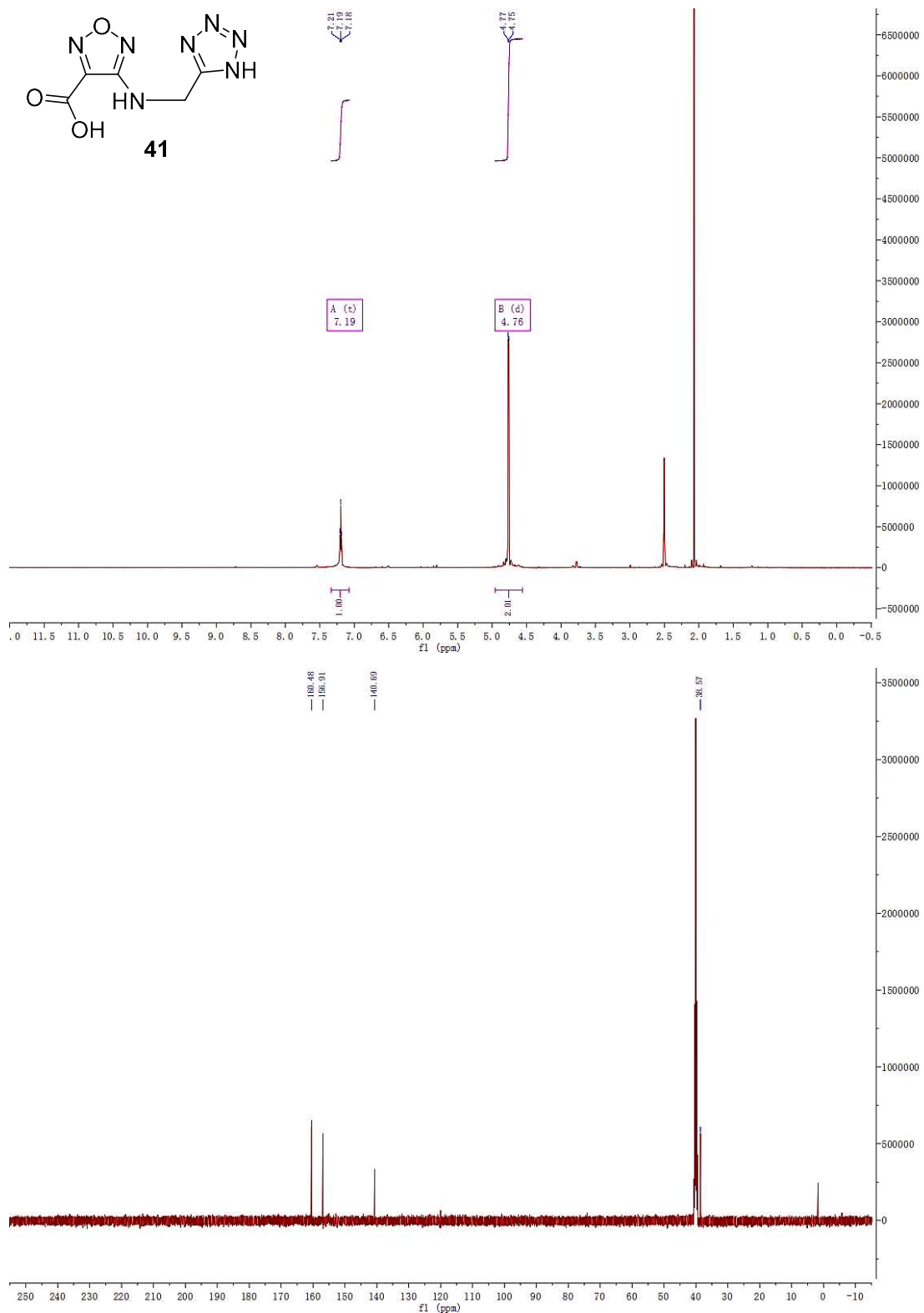
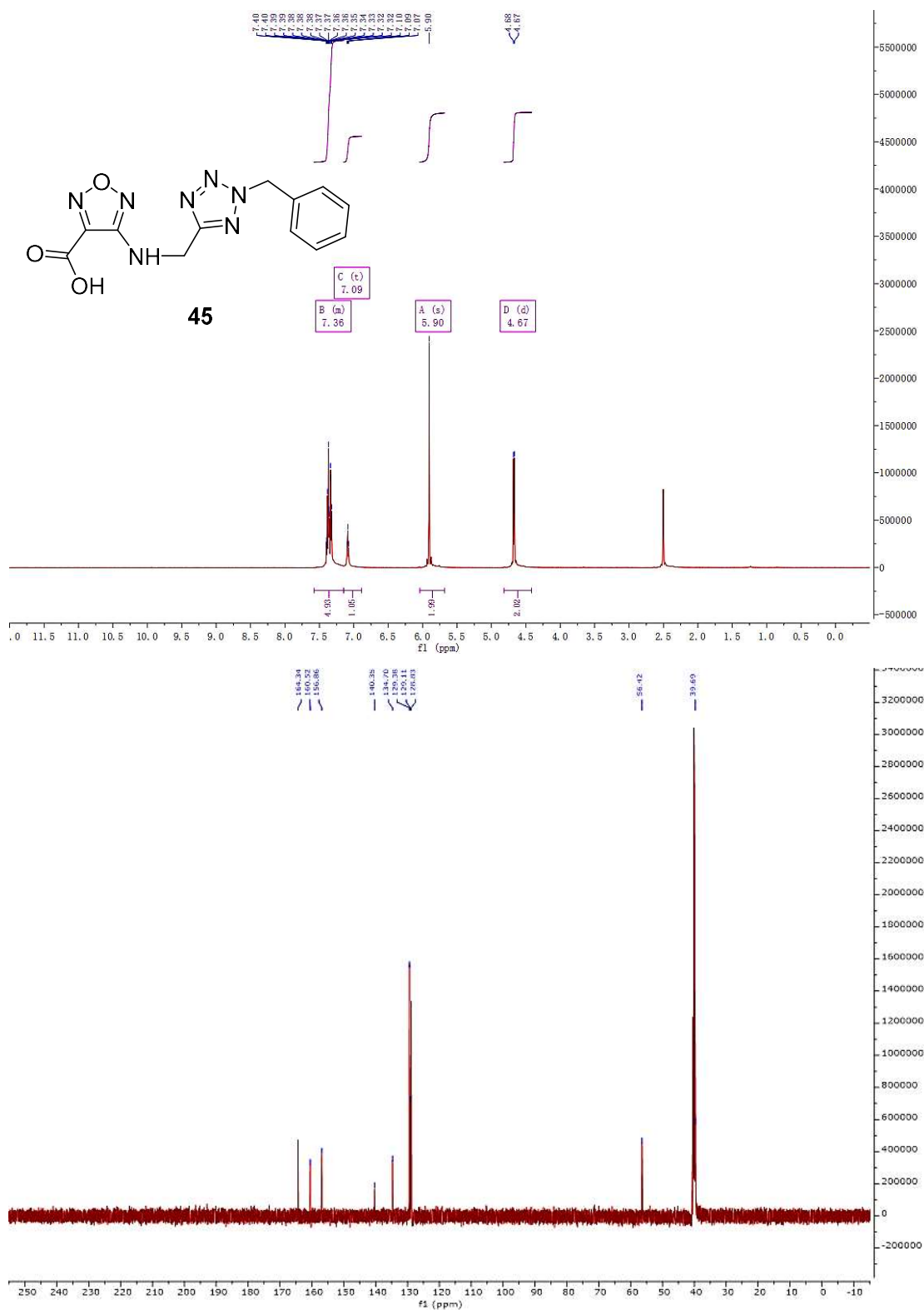^{1}H-NMR spectrum (500 MHz, DMSO-*d₆*) and ^{13}C-NMR spectrum (126 MHz, DMSO-*d₆*) of **41**
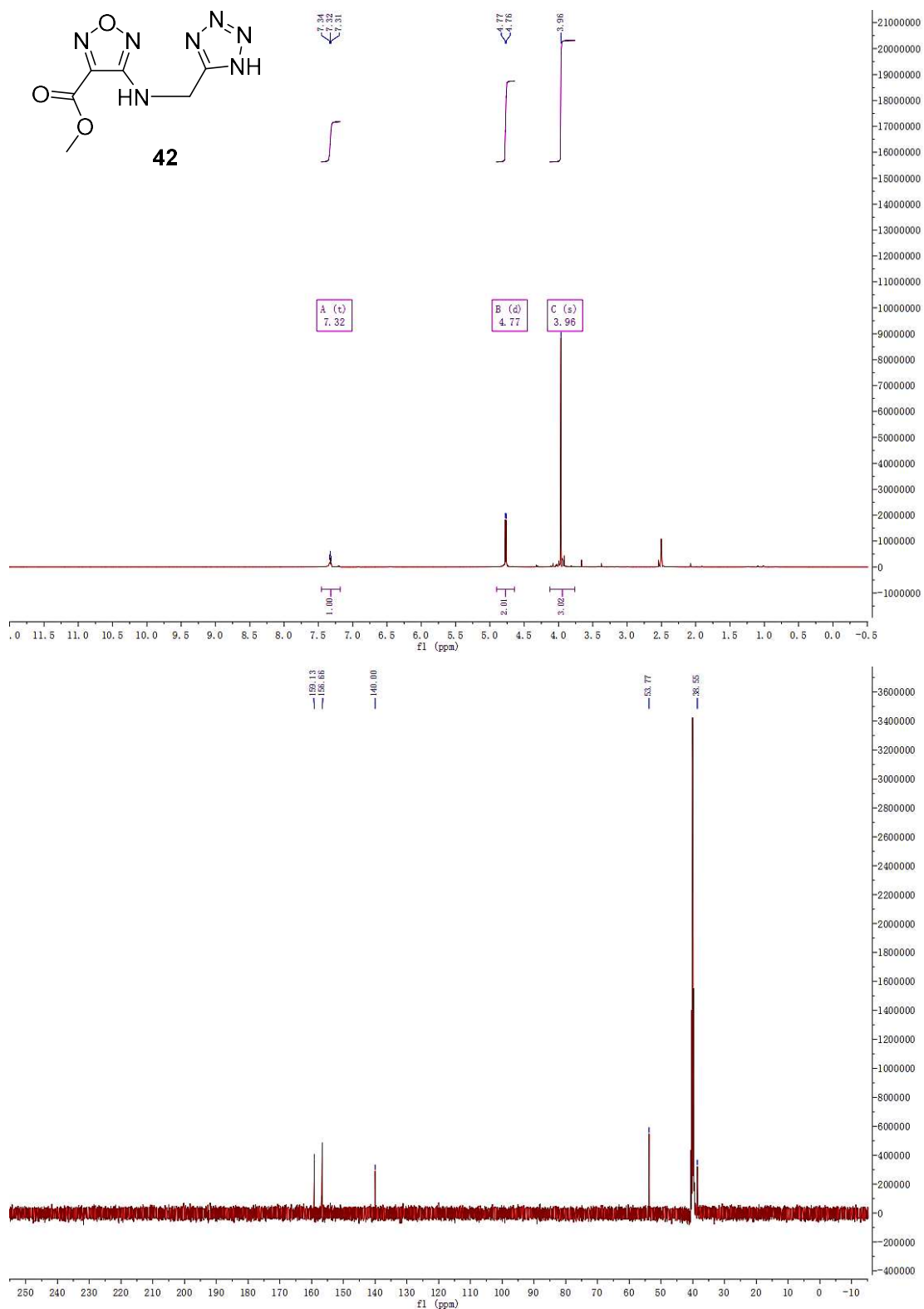
^{1}H-NMR spectrum (500 MHz, DMSO-d_6) and ^{13}C-NMR spectrum (126 MHz, DMSO-d_6) of **42**

^{1}H-NMR spectrum (500 MHz, DMSO-d_6) and ^{13}C-NMR spectrum (126 MHz, DMSO-d_6) of **43**
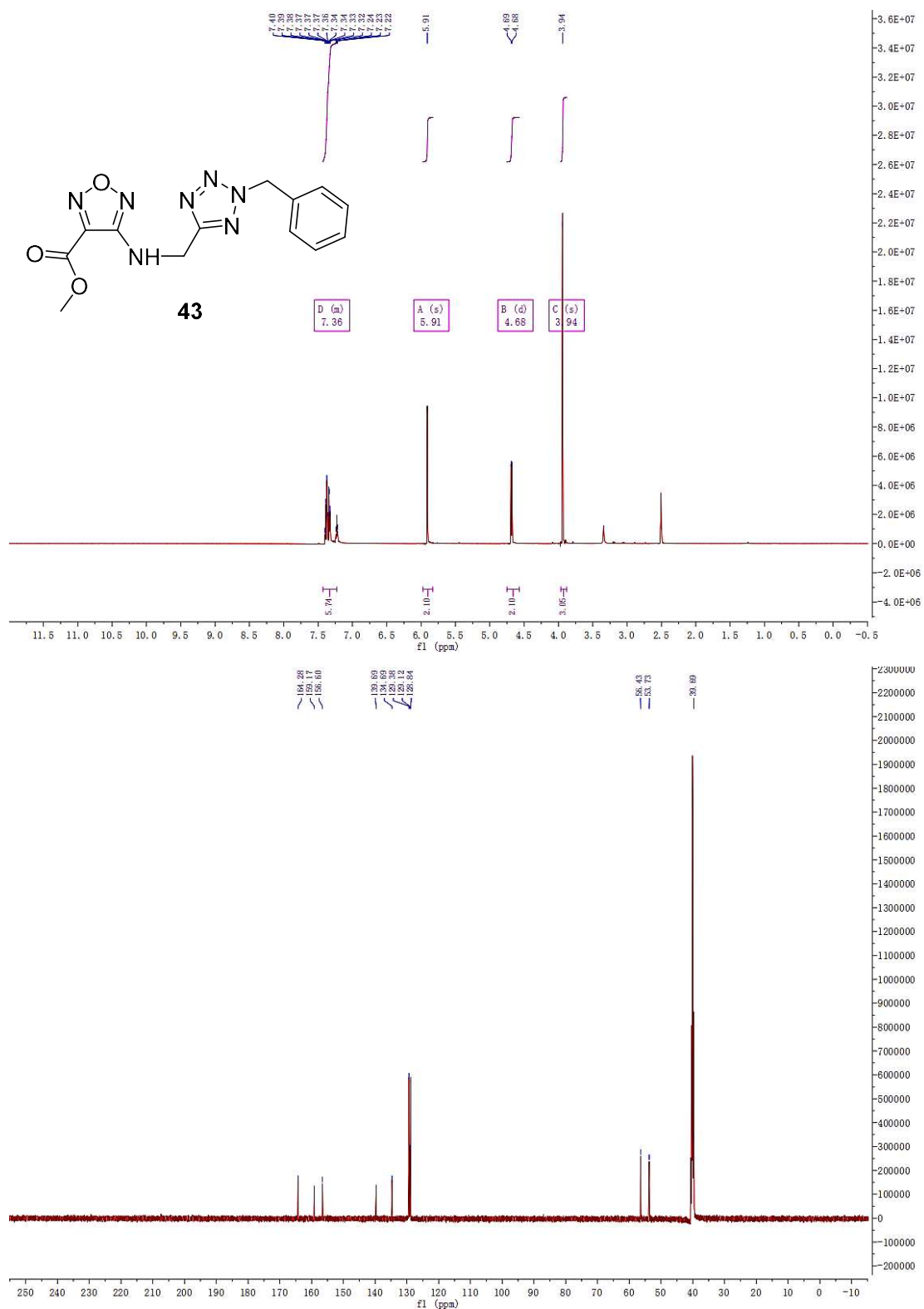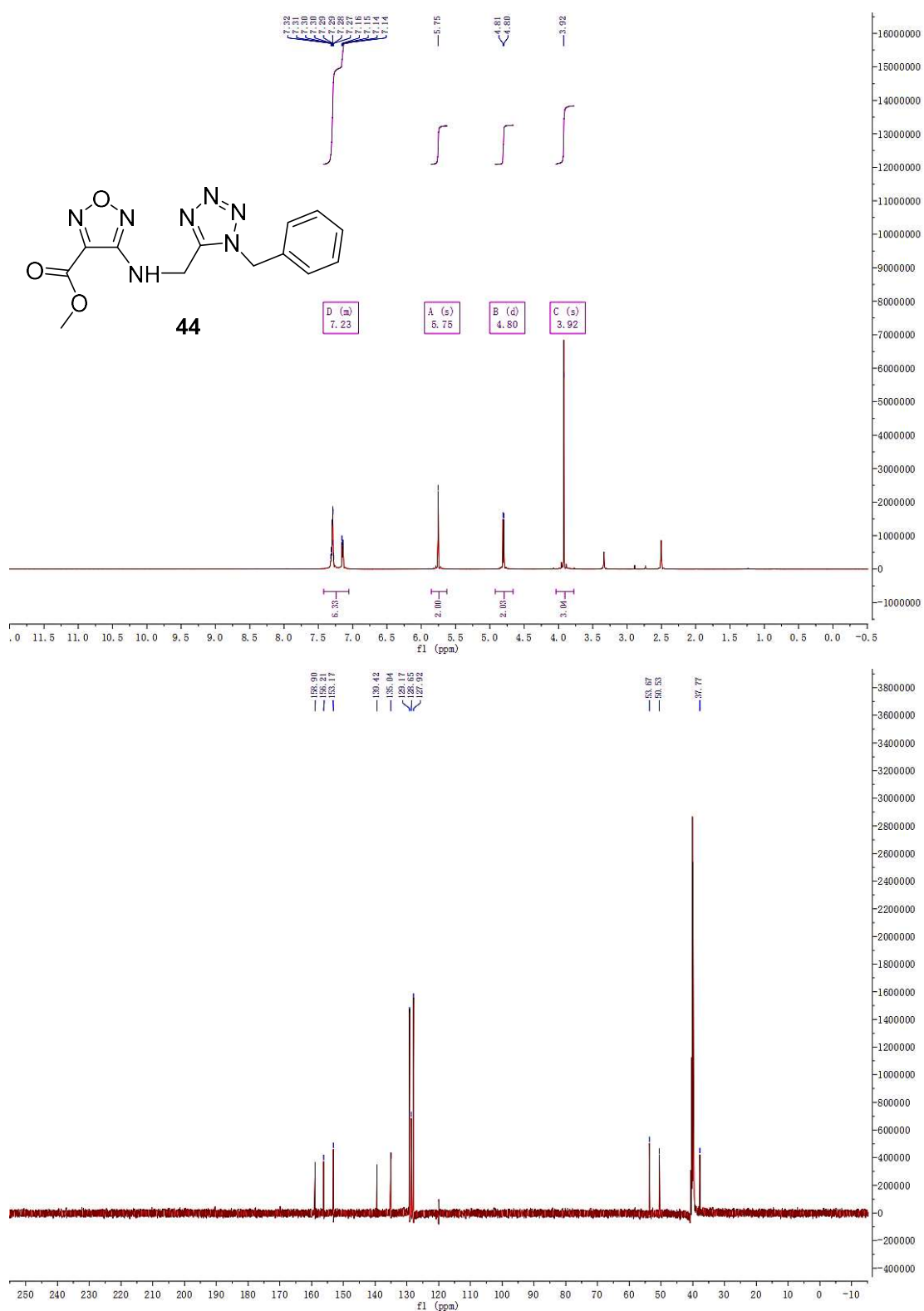
^{1}H-NMR spectrum (500 MHz, DMSO-d_6) and ^{13}C-NMR spectrum (126 MHz, DMSO-d_6) of **44**

^{1}H-NMR spectrum (500 MHz, DMSO-d_6) and ^{13}C-NMR spectrum (126 MHz, DMSO-d_6) of **45**

^{1}H-NMR spectrum (500 MHz, DMSO-d_6) and ^{13}C-NMR spectrum (126 MHz, DMSO-d_6) of **46**